# Numerical Study of Boundary Layer Flow with Variable Properties

By

*Farzana*

**Department of Mathematics**
**Quaid-i-Azam University**
**Islamabad, Pakistan**
**2016**

# Numerical Study of Boundary Layer Flow with Variable Properties

By

*Farzana*

Supervised By

*Prof. Dr. Malik Muhammad Yousaf*

**Department of Mathematics
Quaid-i-Azam University
Islamabad, Pakistan
2016**

# Numerical Study of Boundary Layer Flow with Variable Properties

By

*Farzana*

*A Dissertation Submitted in the Partial Fulfillment of*

*the requirements for the degree of*

DOCTOR OF PHILOSOPHY

IN

MATHEMATICS

Supervised By

*Prof. Dr. Malik Muhammad Yousaf*

## Department of Mathematics
## Quaid-i-Azam University
## Islamabad, Pakistan
## 2016

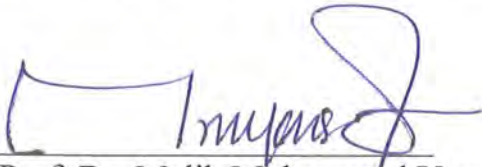# Numerical Study of Boundary Layer Flow with Variable Properties
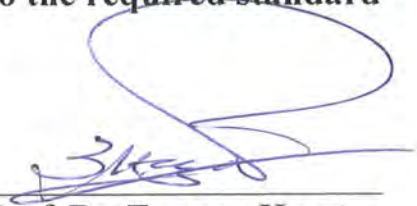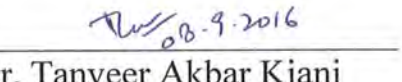
## By

## Farzana

## CERTIFICATE

A DISSERTATION SUBMITTED IN THE PARTIAL FULFILLMENT OF THE REQUIREMENTS FOR THE DEGREE OF THE DOCTOR OF PHILOSOPHY

**We accept this dissertation as conforming to the required standard**

1. _____
Prof. Dr. Malik Muhammad Yousaf
(Supervisor)

2. _____
Prof. Dr. Tasawar Hayat
(Chairman)

3. _____
Dr. Rahmat Ellahi
(External Examiner)

4. _____
Dr. Tanveer Akbar Kiani
(External Examiner)

# Department of Mathematics
# Quaid-I-Azam University
# Islamabad, Pakistan
# 2016

*Dedicated to my*

*Husband*

*And*

*Children*

*(Shayan and Abrish)*

# Acknowledgment

All appreciation to Almighty **ALLAH**, without whose will and consent we cannot proceed a single step. His blessings holds me through all the barrier of goal attainment.

I express my deepest and heart-felt gratitude to my supervisor, **Prof. Dr Muhammad Yousaf Malik** for his cooperation, knowledgeable discussions, guidance and inexhaustible inspiration throughout my research time. His sympathetic attitude broadened my vision of the subject and also increases my capabilities of research and hard work. May **ALLAH** bless him with long and healthy life.

I am great full to the chairman  department of Mathematics **Prof. Dr Tasawar Hayat**, all faculty members and administrative staff for their kind behavior throughout my academic period. I cannot put aside **Higher Education Commission (HEC) of Pakistan** for financial support during my PhD degree. I also would like to acknowledge my juniors for their moral support.

My Family has always taken care of me, their love, affection, moral support and prayers made me able to achieve my goals. The generous support from my husband **Asim** my parents **Qamar baz khan, M.javed Hussan Baha, Rai Naz** my brothers **Adnan , Rizwan , Farooq, Nasir** and my younger sister **Namika**  are always source of inspiration for me. Last but not least I cannot imagine my current position without constant source of love and cooperation  from my son **Shayan** and daughter **Abrish**.

*Farzana*

dominated by viscosity and creating the majority of drag experienced by the boundary body and one outside the boundary layer, where viscosity can be neglected without significant effects on the solution. This allows a closed-form solution for the flow in both areas, a significant simplification of the full Navier–Stokes equations. The majority of the heat transfer to and from a body also takes place within the boundary layer, again allowing the equations to be simplified in the flow field outside the boundary layer. The pressure distribution throughout the boundary layer in the direction normal to the surface (such as an airfoil) remains constant throughout the boundary layer, and is the same as on the surface itself. The field of boundary layer flow in the presence of stagnation point flow over surface and the several combinations of additional effects on the stretching problems are important in many practical applications, such as polymer sheet or filament extrusion from a dye or long thread between feed roll or wind-up roll, glass fiber and paper production, drawing of plastic films, liquid films in condensation process. Due to the high applicability of this problem in such industrial phenomena, it has attracted many researchers and one of the pioneering studies has been done by Sakiadis. Numerous investigations have been conducted on the magnetohydrodynamic (MHD) flows and heat transfer. The study of MHD boundary layer flow on a continuous stretching sheet has got considerable attention during the last few decades due to its numerous applications. The study of heat transfer and flow field is necessary for determining the quality of the final products of such processes. Both the kinematics of stretching and the simultaneous heating or cooling during such processes has a decisive influence on the quality of the final products. A broad review of the prevailing literature reveals that much commitment is absorbed to the fluid flow having phase slip solution. Heat transfer phenomena for flow of two dimensional viscous fluids after using MHD, variable thermal conductivity, heat generation/absorption, slip conditions is not being addressed comprehensively along with numerical solutions. Consideration of convective surface adds further complexities in the modelling. Specially, applications of numerical techniques for justification of the obtained approximate solutions of such type of highly non-linear models are not addressed in detail. We intend to discuss such issues in this thesis.

In the view of above mentioned discussion, this thesis is structured in the following forms:

**Chapter 1** is devoted to introduction and literature survey.

**Chapter 2** deals with the phase slip solution of boundary layer magnetic modulated flow.

We numerically investigate Taylor-Couette flow in a wide-gap configuration. The fluid is taken to be electrically conducting. As the Reynolds number measuring the rotation rate is increased, the initial onset of vortices involves phase slip events. Subsequent bifurcations lead to a variety of other solutions, including ones both symmetric and asymmetric about the mid-plane. For even larger Reynolds number a different type of phase slip arises, in which vortices form at the outer edges of the pattern and drift inward, disappearing abruptly at a

certain point. These solutions can also be symmetric or asymmetric about the mid-plane, and co-exist at the same Reynolds number **"Published in Acta Mech.**

**Chapter 3** deals with free convection boundary layer flow over a stretching flat plate with variable thermal conductivity and radiation. This work addresses the behavior of viscous fluid over a stretching flat plate with variable thermal conductivity. The effects of radiation are also encountered. Thermal conductivity is considered as a linear function of temperature. Approximate solutions through Homotopy Analysis Method (HAM) are obtained. The effects of different physical parameters on velocity and temperature fields are shown through tables and graphs. Numerical solution by using Runge-Kutta-Fehlberg method is computed for comparison which shows good agreement with the HAM solution **"Published in International Journal of Pure and Applied Mathematics.**

**Chapter 4** deals with Stagnation point flow over a stretching cylinder with variable thermal conductivity and slip condition. In this chapter we will discuss the behavior of viscous fluid near stagnation point over a stretching cylinder with variable thermal conductivity. The effects of slip conditions are also encountered in this work. Thermal conductivity is considered as a linear function of temperature. Numerical solutions of momentum and energy equations obtained through Homotopy Analysis Method (HAM) and shooting method are compared through tables. The effects of variation in physical parameters upon velocity and temperature field are also presented graphically. Skin friction and local Nusselt number are computed for further analysis **"Accepted in International Journal of Pure and Applied Mathematics".**

**Chapter 5** deals MHD Stagnation point over a stretching cylinder with variable thermal conductivity. This chapter addresses the behavior of viscous fluid near stagnation point over a stretching cylinder with variable thermal conductivity. The effects of heat generation/absorption are also encountered. Here thermal conductivity is considered as a linear function of temperature. Numerical solution obtained through Shooting method in conjunction with Runge-Kutta-Fehlberg method is compared with solution computed by HAM. The effect of variation in different physical parameters on velocity and temperature fields are shown graphically. Skin friction and Nusselt number are computed at the surface of cylinder to examine the behavior of fluid flow on boundary **"Submitted in Int. J. Fluid Mechanics".**

**In Chapter 6** Stagnation point flow over a stretching cylinder with variable viscosity and heat generation/absorption is presented. In the study of stagnation point flow over a stretching cylinder, variable viscosity and heat generation/absorption are considered. The problem is solved numerically by using Shooting method along with fifth order Runge-Kutta Fehlberg method and the obtained results are compared with the solutions computed through Homotopy Analysis Method. Behavior of velocity and temperature profiles on varying values of physical parameters is reflected through graphs. Skin friction and Nusselt number are computed at the surface of cylinder to study the flow behavior of the fluid on its boundary **"Submitted in Journal of Computational and Applied Mathematics"**.

**Chapter 7** is dedicated to observe the MHD stagnation point flow over a stretching cylinder with variable viscosity and joule heating effect. The problem is solved through HAM and Shooting method, and the computed results are compared graphically. Skin friction coefficient and local Nusselt number are calculated to see the effects of fluid flow due to the surface of cylinder. Also, behavior of velocity and temperature profiles on varying values of physical parameters is studied graphically **"Accepted in OMICS Group-Engineering journals.**

**In Chapter 8** Mixed convection stagnation point flow over a stretching cylinder with variable thermal conductivity and heat generation/absorption is presented. This article addresses the behavior of viscous fluid near stagnation point over a stretching cylinder with variable thermal conductivity. The effects of heat generation/absorption are also encountered. Comparison between solutions through HAM and shooting method is presented **"Submitted in Thermal Sciences for publications"**.

# Contents

# Chapter 1

# Introduction

Basically a boundary layer is a thin region of fluid near a wall where viscous effects are important to determine the flow field. Focus on study of boundary layer flow is to allow an inviscid flow solution that satisfies the no-slip condition at the wall surface. On the surface of object molecules stick to the surface when fluid moves upon it which slow down the flow just above them. Molecules farther away from surface of object, the fewer the collission. This ultimately creates the thin layer of fluid close the surface where velocity changes from zero on the surface to the free stream velocity far away from the surface. This type of layer is known as boundary layer of the fluid.

This chapter comprises the literature survey of the previous work related to the boundary layer flow, stagnation point flow, combined heat and mass transfer, mixed convection flow, phase slip solutions, Newtonian heating and melting heat transfer, boundary layer, slip conditions.

Hayat et al. [1] discussed the influence of thermal radiation by taking an exponentially stretching sheet upon the boundary layer flow. Nadeem [2] considered three dimensional boundary layer flow of Casson nanofluid past a linearly stretching sheet with convective boundary conditions. Malik [3] discussed the boundary layer flow of hyperbolic tangent fluid over a vertical exponentially stretching cylinder. Boundary layer flow of rotating two phase nanofluid over a stretching surface has been discussed by Nadeem et al. [4]. Sadia et al. [5] solved mixed convection boundary layer flow model over a vertical flat plate with radiative heat transfer. Non-similarity thermal boundary layer flow over a stretching flat plate is discussed in [6].

The flow between differentially rotating cylinders, known as Taylor-Couette flow (TC flow),

is one of the oldest problem in fluid dynamics, but continues to attract considerable experimental [11-12] as well as numerical [7-10] interest. Another indication of its continuing relevance is the number of distinct branches it has spawned. Two of these are: (a) ramped TC flow, where the inner and/or outer radii of the cylinders are not uniform, but vary along the axial direction, and (b) magnetic TC flow, where the fluid is taken to be electrically conducting, and magnetic fields are externally applied. In this work we combine these two branches, by using magnetic fields to impose the axial modulation that is otherwise created by the geometrical ramping. We demonstrate that the phenomenon of phase slip, whereby pairs of Taylor vortices are either created or destroyed, carries over from geometrically to magnetically ramped TC flows. We suggest that magnetically modulated TC flow may be a more convenient system to numerically study some of the resulting pattern formation effects.

The configuration of greatest interest in ramped TC flow is when the radii of the cylinders gradually vary in such a way that parts of the domain can be above the critical Reynolds number for the onset of Taylor vortices while other parts are still below. [13-18] considered such subcritical ramps in a general pattern formation context, and showed that the usual Eckhaus-stable wave-number band instead collapses to a single wave-number. [19] applied this so-called phase-diffusion equation approach specifically to TC flows, and demonstrated that "there exist ramps which do not permit any static patterns but force them to drift. That is, once the wave-number is fixed, at the transition point(s) from locally subcritical to supercritical, that can force the wave-number in other parts of the supercritical region to be Eckhaus-unstable. The pattern responds with a phase slip event, essentially an attempt to move the wave-number toward Eckhaus stability. The resulting Taylor vortices drift away though, forcing a new phase slip, and so on indefinitely. (Note however that not all subcritically ramped systems necessarily lead to phase slip behaviour for reviews of various pattern-forming systems without phase slip [20].

Turning next to magnetic TC flow, the current focus of attention is primarily on the magnetorotational instability (MRI), whereby a magnetic field can destabilize a rotation profile that would otherwise be stable according to the Rayleigh criterion. First discovered in 1959 in TC flows the MRI lay largely dormant until it was suggested that it might play a crucial role in astrophysical accretion disks [19-20]. This discovery reignited interest in the MRI in TC

flows, and specifically the possibility of obtaining it [21] or variants of it [22] experimentally. The standard MRI has not yet been obtained [23]. A further recent magnetic TC experiment [24-26] has measured in the same direction.

Over the years researchers have considered uniform fluid flow over bodies of various geometries due to their numerous applications in industry and engineering. Due to the complexity and non-linearity of the modeled governing equations exact solutions were very difficult to obtain. Efforts by many researchers to obtain analytical solution as well as numerical solution has been made. In last few decades, the study of stagnation flow has gained tremendous research interest. In fluid dynamics. Stagnation points exist at the surface of objects in the flow field, where the fluid is brought to rest by the object. Stagnation flow is basically the fluid motion near the stagnation point. After including the effects of magnetic field Chandrasekhar et al. [27] analyzed the stability of viscous flow within rotating cylinders. Two dimensional MHD steady flow of an upper (convective) Maxwell fluid near a stagnation point over a stretching surface was addressed by [28]. Hayat et al. [29] used HAM to address two-dimensional steady flow on stagnation point with mixed convection of viscoelastic fluid around heated surfaces. They found that for the case of a Newtonian fluid, a reverse flow region was developed. Hayat et al. [30] obtained analytical solution by applying HAM on the steady two-dimensional stagnation point flow over stretching sheet to observe the effect of heat transfer of a Maxwell fluid. Hayat et al. [31] applied homotopy perturbation method to investigate axisymmetric flow upon stretching sheet.

For problems involving chemical reactions and dissociating fluids the study of heat generation or absorption have great importance. Therefore heat generation effects modify the temperature distribution. An unsteady mixed convection flow having incompressible fluid was studied by Malik [32]. Viscous fluid about a stagnation point on sheet stretched in the presence of a variable free stream velocity was assumed.

Hussain [33] discussed flow of a third grade fluid within coaxial cylinders with the assumption of variable viscosity. Both steady and transient stretching problems have been studied in [34-36] under various assumptions.

Since physical properties of fluid are temperature dependent thus on increasing temperature transport phenomena increases. Also, by minimizing the viscosity across the momentum

boundary layer heat transfer at the wall will be affected. Therefore, it is better to consider the viscosity variation for incompressible fluids. Gary et al. [37] and Mehra et al. [38] proved that, when this effect is included the flow characteristics may change substantially when compared with constant viscosity. Mukhopadhyay et al. [39] examined the boundary layer flow with MHD having variable fluid viscosity upon heated stretching sheet.

There are many application of stagnation point, some of them are cooling devices like fan to electronic circuits, cooling reactors. Hiemenz in 1911 initiated the study of a stagnation point flow in the direction of a solid surface in moving fluids. Hiemenz reduced the well known Navier–Stokes equations by using appropriate transformation to get non-linear ordinary differential equations in two-dimensional stagnation point flows. Since then many investigations have been made and extended this idea to solve different stagnation point flow problems. Mahapatra and Gupta [40] obtained numerical solution of a boundary layer flow, stagnation point flow and heat transfer over a stretching sheet for a two dimensional model. Wang [41] presented two dimensional axisymmetric stagnation point flow on a shrinking sheet.

Vajravelu and Nayfeh [42] observed that in some industrial problems which covers chemical reactions and dissociating fluids, heat generation/absorption. Sparrow and Cess [43] and Chamkha [44] also discussed the heat generation effects. Flow in porous media has got attention by researchers due to its important applications. The thermally driven flows in porous media have several applications in chemical and mechanical engineering for example electrochemistry, fibrous insulation etc [45-47]. The problem of porous medium and heat transfer driven by a linearly stretching surface is one of the fundamental problem. Further, B. K. Datta etal [48] study uniform heat flux over temperature field in the flow over a stretching sheet. [49-50] studied heat transfer over a stretching surface with variable surface heat flux and over an unsteady stretching surface. Also number of researchers [51-57] worked on heat transfer characteristic of a continuous stretching surfaces with variable temperature.

# Chapter 2

# Phase Slip Solution of Magnetic Modulated Boundary-Layer Flow

## 2.1 Introduction

In this chapter, we examine the numerical calculations of Taylor-Couette flow in a wide-gap configuration by considering inner cylinder rotating and the outer cylinder stationary. Magnetic field is externally imposed on the electrically conducting. Taylor vortices are created where the field is weak, but not where the field is strong. variety of bifurcated solutions occurs, including ones both symmetric and asymmetric about the midplane. These solutions can also be symmetric or asymmetric about the midplane. Many of the dynamics of these phase slip solutions are analogous to previous results in geometrically ramped Taylor-Couette flows.

## 2.2 Mathematical formulation

We consider the standard wide-gap Taylor-Couette configuration with radius $r_i$ and $r_o$ satisfying $\frac{r_i}{r_o} = \frac{1}{2}$. $\Omega$ is the rate of rotation of the inner cylinder, and the outer cylinder is stationary. The governing equations are

$$\rho \left[ \frac{\partial U}{\partial t} + (U \,.\triangledown)U \right] = -\nabla p + \rho.\nu. \triangledown^2 U - \mu^{-1}(\nabla \times B) \times B, \tag{2.1}$$

$$\frac{\partial B}{\partial t} = \eta. \bigtriangledown^2 B + \bigtriangledown \times (U \times B), \tag{2.2}$$

Should up with the following equations

$$R_e(\frac{\partial U}{\partial t} + U. \bigtriangledown .U) = -\nabla p + \nabla^2 U + H_a^2.R_m^{-1}(\nabla \times B) \times B, \tag{2.3}$$

$$\frac{\partial B}{\partial t} = R_m^{-1} \bigtriangledown^2 B + \bigtriangledown \times (U \times B), \tag{2.4}$$

where the nondimensional parameters are

$$R_m = \frac{\Omega r_i^2}{\eta}. \tag{2.5}$$

Magnetic field is given as

$$B_z \approx \frac{(1 + cos(\frac{2z}{z_0})}{2}, \tag{2.6}$$

which is applied externally having wavelength $z_0 = 50(r_0$- $r_i)$. In the so-called inductions limit, we can expand the magnetic field as

$$B = B_0 + R_m b, \tag{2.7}$$

where $B_0$ is the externally imposed field, and $R_m b$ is the induced field.

Using Eq. (2.7) in Eq. (2.3 − 2.4) , we get

$$Re(\frac{\partial U}{\partial t} + U. \bigtriangledown .U) = -\nabla p + \nabla^2 U + H_a^2.(\bigtriangledown \times b) \times (B_0 + R_m b), \tag{2.8}$$

$$R_m \frac{\partial b}{\partial t} = \bigtriangledown^2 b + \bigtriangledown \times [(U \times (B_0 + R_m b))] \tag{2.9}$$

Taking $R_m \longrightarrow 0$, we get the suitably scaled Navier-Stokes and magnetic induction equations

$$Re\frac{\partial U}{\partial t} = -\nabla p + \nabla^2 U - R_e U \cdot \nabla U + H_a^2(\nabla \times b) \times B_0 \tag{2.10}$$

9

$$\nabla^2 b = -\nabla \times (U \times B_0). \tag{2.11}$$

Length has been scaled by $r_i$, time by $\Omega^{-1}$, and $U$ by $\Omega r_i$. $B_0$ is the magnetic field, and $b$ the induced field. The two nondimensional parameters in these equations are the usual Reynolds number

$$R_e = \frac{\Omega r_i^2}{\nu} \tag{2.12}$$

measuring the inner cylinder's rotation rate, and the Hartmann number

$$H_a = \frac{B_0 r_i}{\sqrt{\mu \rho \nu \eta}} \tag{2.13}$$

measuring the strength of the imposed field. The quantities $\mu$, $\rho$, $\nu$, and $\eta$ are the fluid's permeability, density, viscosity, and magnetic diffusivity, respectively. See also for a more detailed derivation of these equations in the inductionless limit, in the context of magnetic spherical Couette flow.

## 2.3 Solution of the problem

The spatial structure of the imposed field $B_0$ is given by

$$B_0 = \frac{(1 + \cos(\kappa z) I_0(\kappa r))}{2} . \hat{\mathbf{e}}_z + \sin(\frac{(\kappa z) I_1(\kappa r)}{2}) . \hat{\mathbf{e}}_r, \tag{2.14}$$

where $\kappa = 2\pi/z_0$, and $I_0$ and $I_1$ are the modified Bessel functions. The wavelength $z_0$ is an adjustable parameter, but once fixed, the rest of the structure is completely determined by the requirements that $B_0$ be a potential field, and imposed from the region $r > r_o$ rather than $r < r_i$. That is, with a suitable array of external Helmholtz coils one could actually impose such a field, a point we will return to in the conclusion. Note finally that the $r$-dependent parts of $B_0$ are necessary to satisfy

$$\nabla \cdot B_0 = 0 \text{ and } \nabla \times B_0 = 0, \tag{2.15}$$

but are infact quite small. Using the asymptotic properties $I_0(\kappa r) \approx 1$ and $I_1(\kappa r) \ll 1$ for $\kappa r \ll 1$, one obtains

$$B_0 \approx [(1 + \cos\frac{(\kappa z)}{2})]\,\hat{\mathbf{e}}_{z},\tag{2.16}$$

as desired to create the magnetic ramping effect.

These Eqs. (2.10 − 2.11) together with boundary conditions no-slip for $U$ and perfectly conducting for $b$, were numerically solved using an axisymmetric, pseudo-spectral code . Very briefly, $U$ and $b$ are expanded as

$$U = \nabla \times (\psi\,\hat{\mathbf{e}}_\phi) + v\,\hat{\mathbf{e}}_\phi, \qquad b = \nabla \times (a\,\hat{\mathbf{e}}_\phi) + \vec{b}\,\hat{\mathbf{e}}_\phi,\tag{2.17}$$

then $\psi$, $v$, $a$ and $b$ are further expanded in terms of Chebyshev polynomials in $r$ and Fourier series in $z$. Typical resolutions used were $20 - 30$ Chebyshev polynomials and $200 - 300$ Fourier modes. The time-stepping of Eq. (2.10) is second-order Runge-Kutta, modified to treat the diffusive terms implicitly. Eq. (2.11) is directly inverted for $b$ at each time-step of Eq. (2.10). Typical time-steps used were $0.02 - 0.05$.

After preliminary scans in the range $z_0 = 20 - 80$ yielded qualitatively similar phase slip solutions, the axial length was fixed at $z_0 = 50$. For comparison, the spatially ramped experiment most closely related to our magnetic case had a nondimensional length of 29. Again after some preliminary scans, it was found that Hartmann numbers in the range $2 - 10$ also yielded similar solutions, so only $H_a = 5$ was investigated in further detail. The single remaining parameter, the Reynolds number, was then varied throughout the interval $R_e = 67 - 85$. The upper limit was chosen partly because enough interesting things had already happened by then, and partly because the calculations become more time-consuming beyond that point. Eventually of course one would also expect the solutions to become three-dimensional, although in the non-magnetic problem at least non-axisymmetric instabilities do not arise until much larger Reynolds numbers, around three times supercritical versus less than 30% supercriticaly considered here.

Finally that at least some of the cases required extremely long integration times before periodic solutions emerged. This is a natural consequence of having $z_0 \gg 1$: the diffusive time-scale between two points separated by the maximum possible distance $\frac{z_0}{2}$ is $R_e(\frac{z_0}{2})^2 = O(10^5)$, so very long time-scales are almost inevitable.

## 2.4  Results and discussion

The flow at $R_e = 67$, still below the onset of Taylor vortices. There is infact already a deviation from the ideal Couette profile, most noticeably in the meridional circulation $\psi$, which is identically zero in the ideal basic state, but now consists of four large circulation cells centered on the midplane $z = 25$. These cells already appear for all $R_e > 0$, and are analogous to the Ekman cells obtained in cylinders with top and bottom endplates. In this case they are caused by the $r$-dependent parts of $B_0$; if the imposed field were exactly $B_z = \frac{(1+\cos(\kappa z)}{2})$, then the ideal Couette profile

$$v = C_1 r + \frac{C_2}{r} \tag{2.18}$$

By taking $z_0$ to be sufficiently large, these deviations from the ideal profile can thus be made as small as desired. Geometrically ramped TC flows also have deviations from the ideal Couette profile, caused by similar dynamics as the endplate-induced Ekman cells. These deviations from the ideal profile are not crucial though to any of the phase equation results, including the existence of drifting patterns .
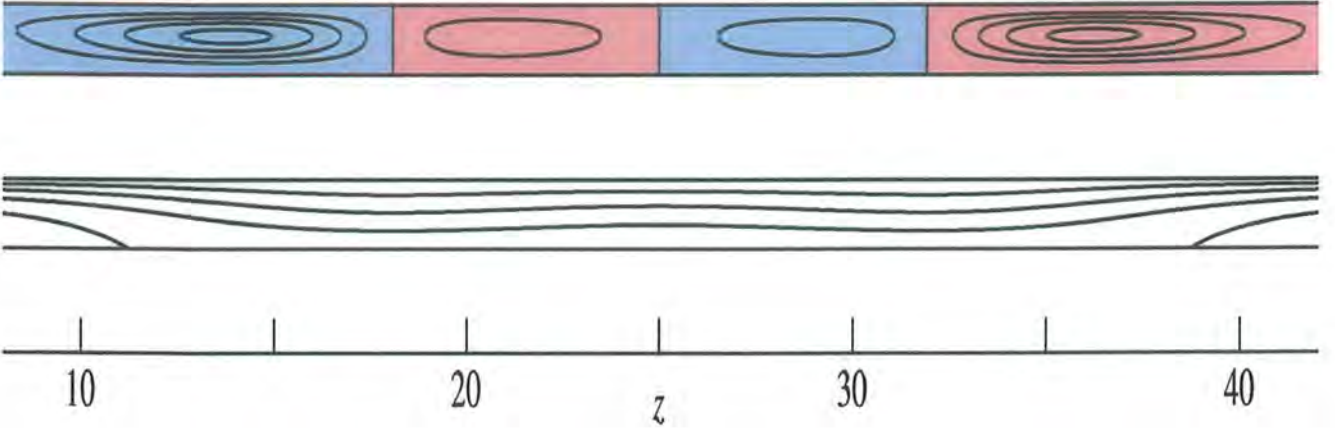


Fig 2.1: The solution at $R_e = 67$, $\psi$ with contour $10^{-3}$.
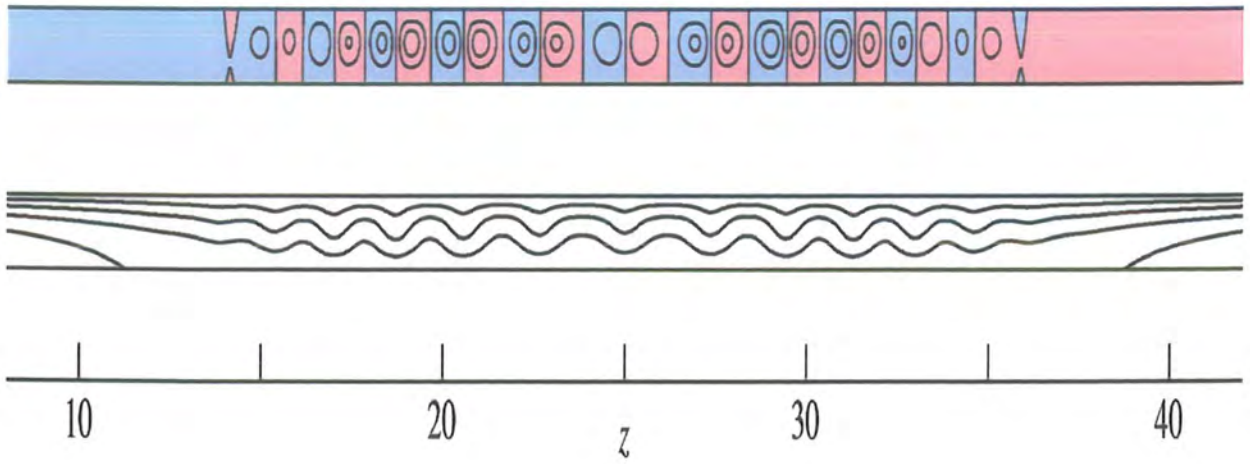
**Fig 2.2:** The solution at $R_e = 67.2$, $\psi$ with contour 0.01.
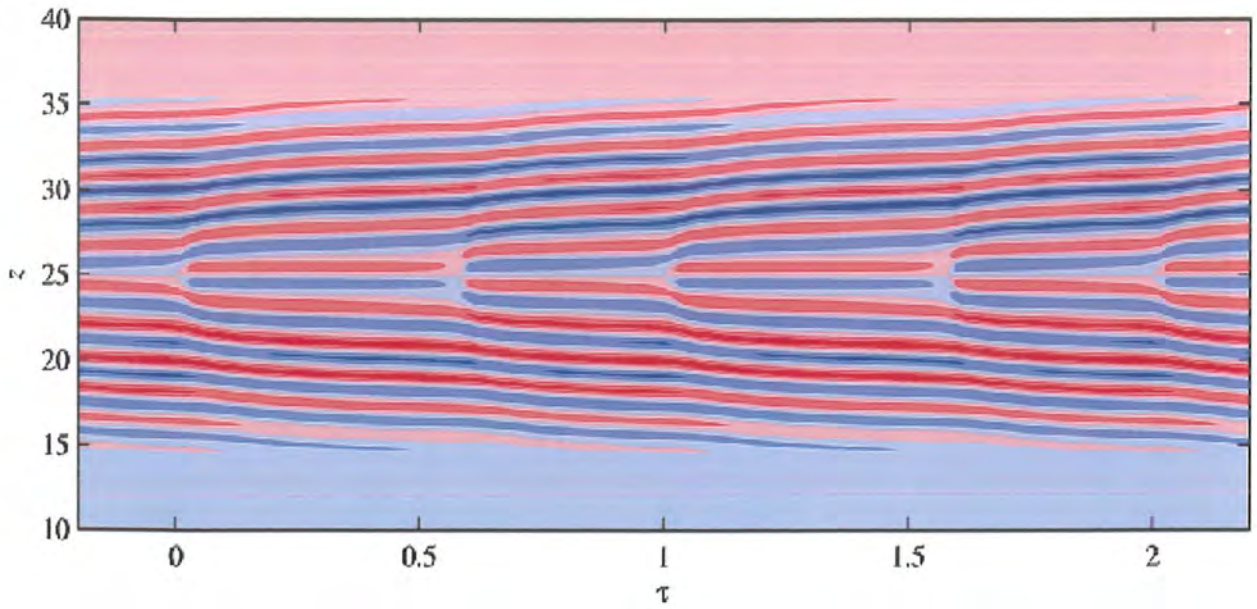


**Fig 2.3:** Contour plots of $\psi(t; z; 1.5)$ at $R_e = 74.5$, with a contour interval of 0.01 and $T = 4393$.

13
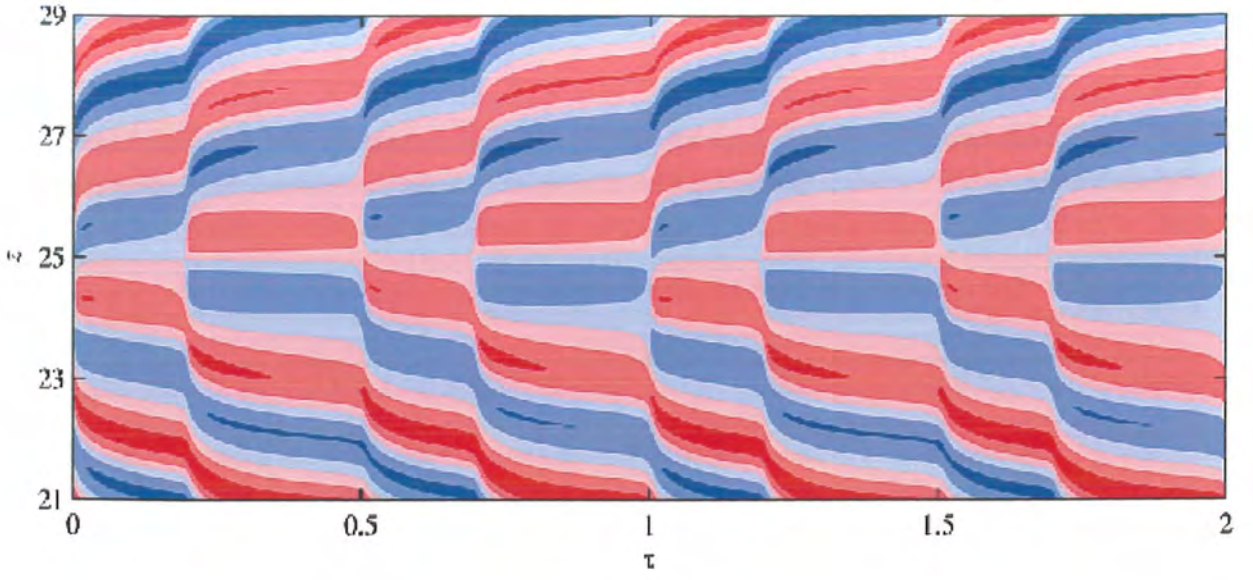
**Fig 2.4:** The solution at $R_e = 75.5$, where the period $T = 13334$.
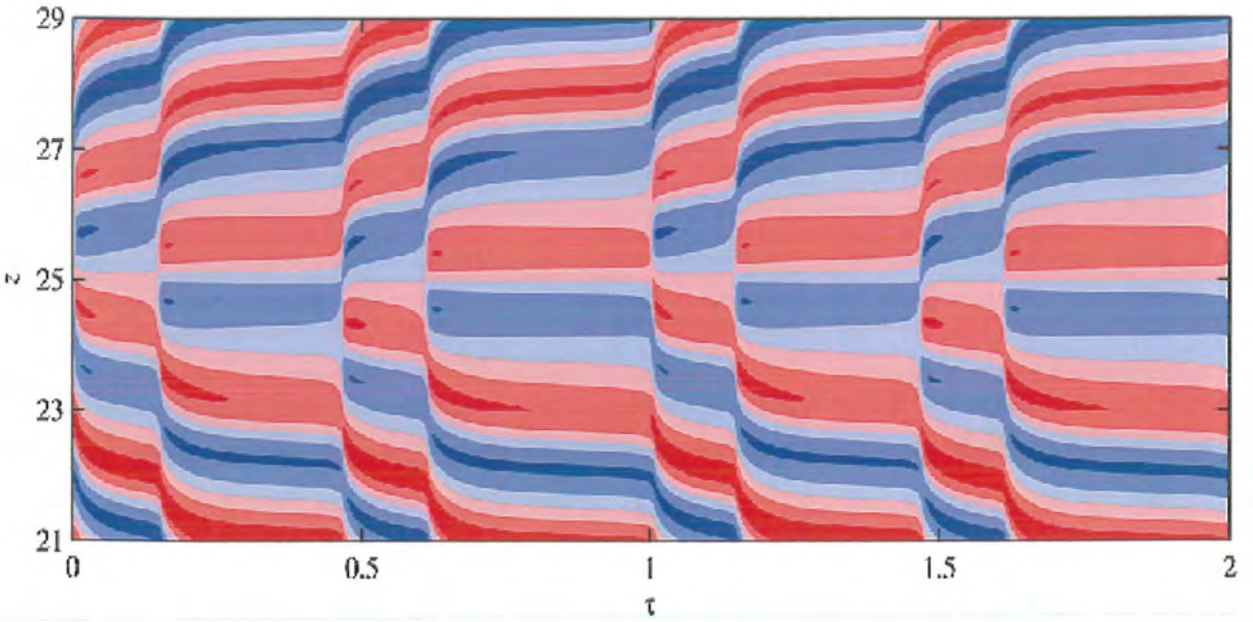


**Fig 2.5:** The solution at $R_e = 75.5$, where the period $T = 13334$.

14
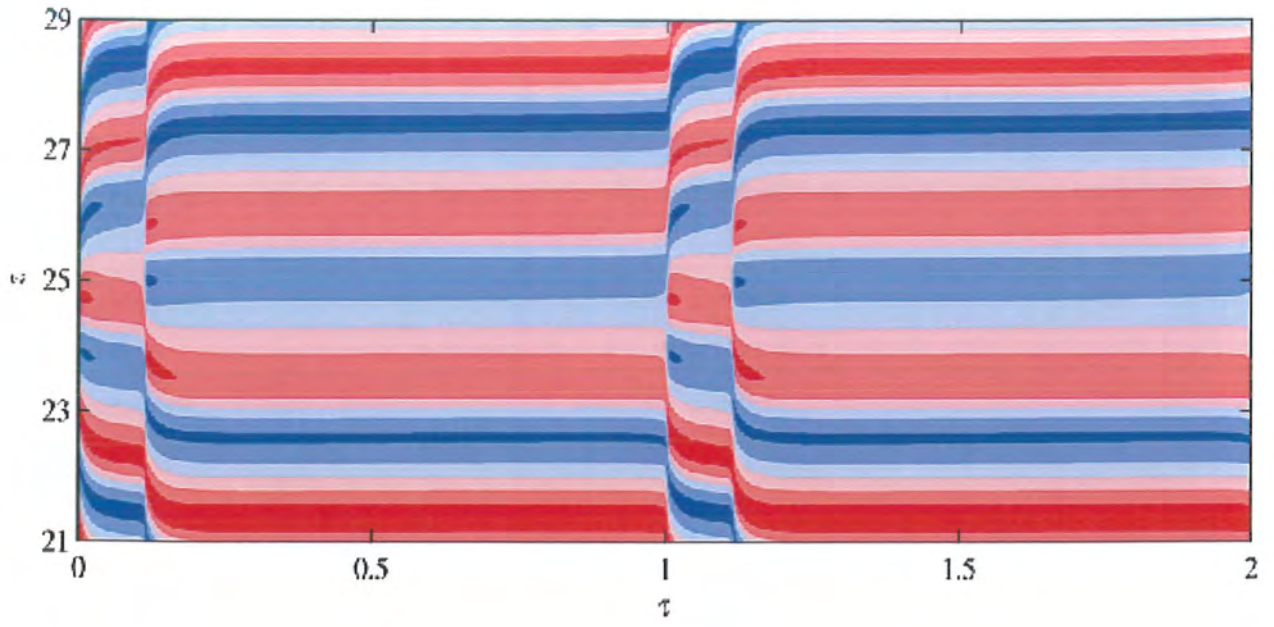
**Fig 2.6:** The solution at $R_e = 76.5$ where the period $T = 54388$.
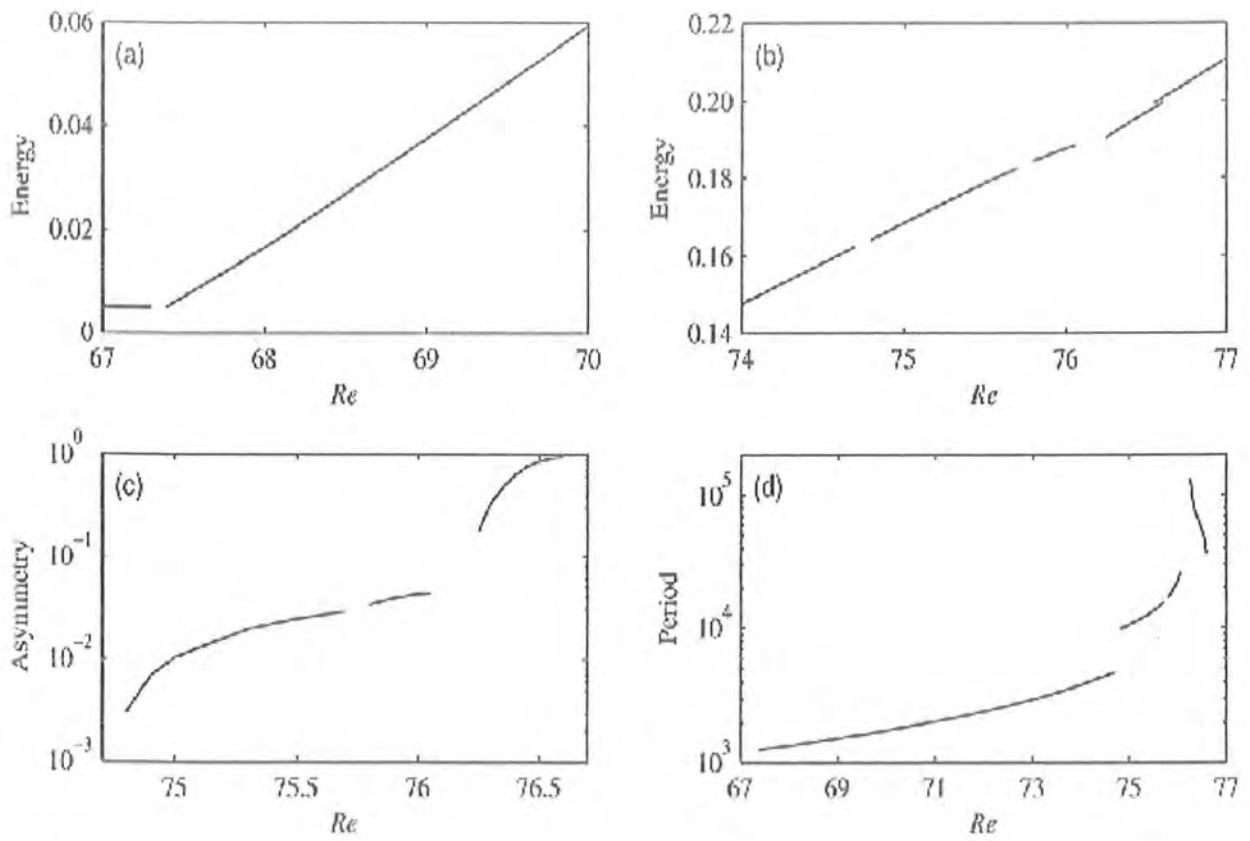
**Fig 2.7:** (a) and (b) both show the kinetic energy in the meridional circulation (c) shows the fraction of the energy that is contained in the asymmetric component. (d) shows the extreme variation over more than two orders of magnitude.
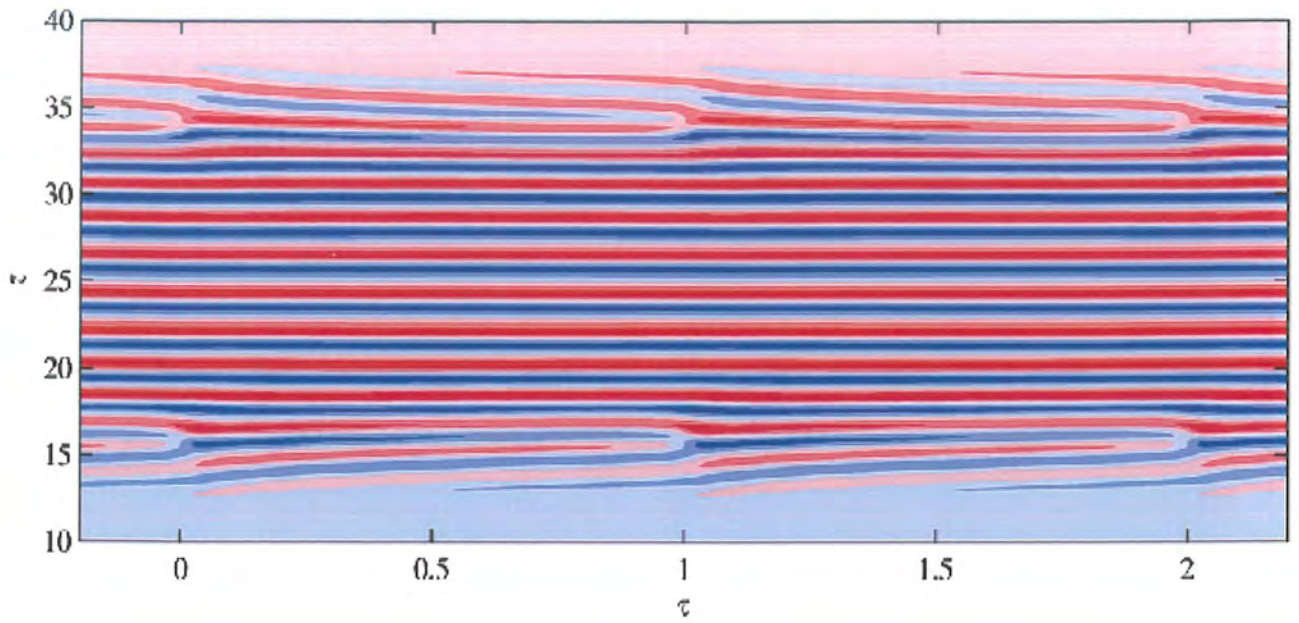
**Fig 2.8:** The solution at $R_e = 85$ where the period $T = 638$.
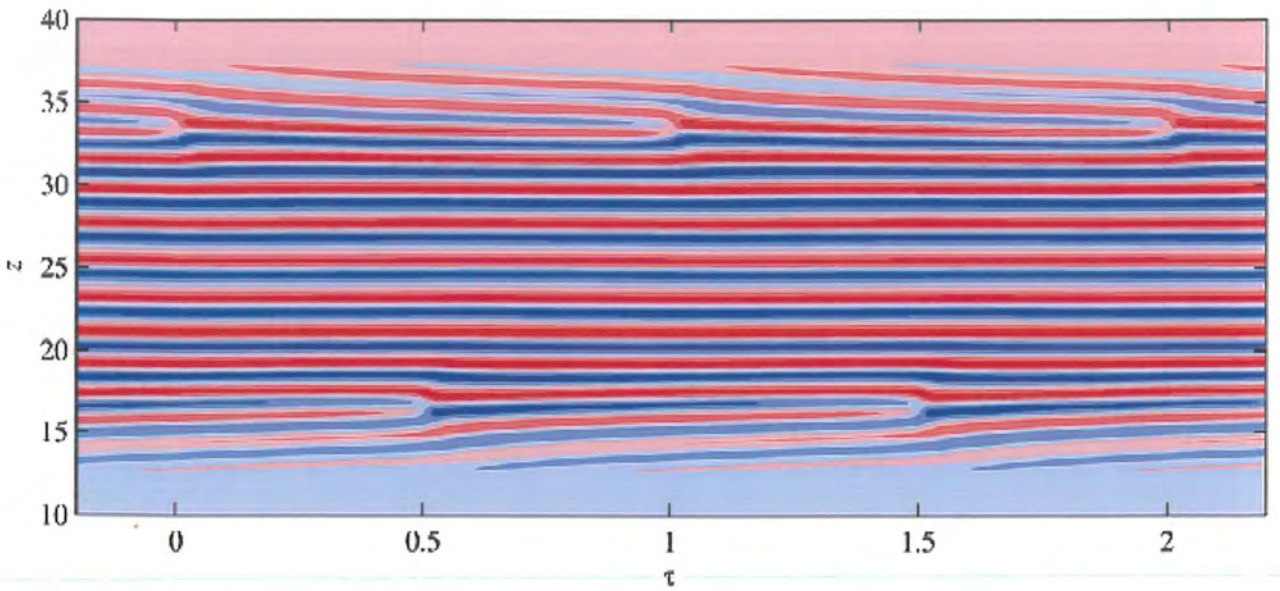


**Fig 2.9:** The solution at $R_e = 85$ where the period $T = 755$.

17

As expected in Fig. 2.1 we find Taylor vortices in the middle, where the imposed field is weak, but not near the ends, where it is strong. This solution is in fact steady, without either drift or phase slip events. However, it is also not the initial onset of Taylor vortices; instead, these solutions exist only in the range $76.5 < R_e \leq 81.3$. This background circulation is still present even here, but is overwhelmed by the Taylor vortices, with the result that clockwise and counter-clockwise vortices are almost the same strength. In Fig. 2.2 The bifurcation point occurs at $R_e = 67.4$, via a supercritical Hopf bifurcation, that is, a drifting pattern. Two further comments are also in order regarding this initial bifurcation. First, the slight reduction from $R_e = 68.2$ in the non-magnetic case to $R_e = 67.4$ here is caused by the presence of the background cells, and does not indicate a subcritical bifurcation. Second, as a transition from a steady to a periodic solution, it is a true bifurcation. This is different from TC flows with endplates, where the background Ekman cells cause the bifurcation to be imperfect, from one steady pattern to another, but without any true bifurcation. To best illustrate the full time-dependence of the drifting pattern, including the phase slip events that form a crucial part of it, we begin by noting that the radial structure of the vortices is relatively straightforward, $\psi = 0$ at either boundary, and in between is positive/negative for clockwise/counter-clockwise vortices. Simply focusing on the middle $r = 1.5$ will therefore capture all the essential features. Contour plots of $\psi(t, z, 1.5)$ will then reveal the structure in both time and length along the cylinder. As illustrated in Fig. 2.3 , the solution consists of a series of phase slips at the midplane $z = 25$. The newly created Taylor vortices drift outward, eventually fading away at $|z - 25| \approx 10$, where the magnetic field becomes too strong for them to persist. The period of these solutions gradually increases from $T = 1243$ at $R_e = 67.4$ to $T = 4393$ at $R_e = 74.5$, the value shown in Fig. 2.3. The next two bifurcations occur at $R_e = 74.8$ and $R_e = 75.8$. The first one breaks the midplane symmetry $\psi(t, z) = -\psi(t, 50 - z)$ seen in Fig. 2.3, but still preserves the shift-and-reflect symmetry $\psi(t, z) = -\psi(t + T/2, 50 - z)$. Correspondingly, the average value of the asymmetric component over a period is still zero. The second one breaks the shift-and-reflect symmetry as well. There are thus two solutions, with average asymmetric components of either sign (just as in a pitchfork bifurcation). Figs. 2.4 and 2.5 show examples of these solutions, at $R_e = 75.5$ and $R_e = 76$. The first bifurcation already causes the period to double, since it now takes two of the original cycles for the asymmetry to occur first in one

18

half and then in the other. Beyond that, the periods still continue increasing, from $T = 13334$ at $R_e = 75.5$ to $T = 22616$ at $R_e = 76$. Both of these symmetry-breaking bifurcations are also supercritical, with no hysteresis if $R_e$ is reduced again. Fig. 2.6 shows the pattern at $R_e = 76.5$. We notice two differences in comparison with figure 2.5. First, the asymmetry is considerably greater, with the pattern shifted so much in $z$ that there is now a Taylor vortex sitting right on the midpoint $z = 25$. Fig. 2.7 compares the entire range $67 \leq R_e \leq 77$, and quantifies items such as how the strength of the Taylor vortices gradually increases, how the degree of asymmetry increases, and how the period varies.

The second difference is that the pattern in Fig. 2.6 has only two phase slip events per period, whereas in Fig. 2.5 there are four per period. The most natural way to connect the two therefore would be to have a period-doubling bifurcation as $R_e$ is reduced from 76.5 back toward 76. Pinning down exactly where this bifurcation occurs was unfortunately not possible. For $R_e \leq 76.05$ the solutions have four phase slips per period, and for $R_e \geq 76.25$ they have two per period. However, between 76.05 and 76.25 they not only have very long cycle times (see Fig. 2.6), but even after integrating to $t = 10^6$ the solutions still had not settled into a precise periodicity. It is possible of course that the solutions in this narrow gap really are chaotic, and bifurcate to a four-cycle at one end and a two-cycle at the other.

Finally, on the steady, symmetric Fig. 2.2 branch, what happens if $R_e$ is increased rather than decreased? At $R_e = 81.4$ a Hopf bifurcation occurs, or rather two essentially simultaneously, corresponding to symmetric and asymmetric perturbations. As a result, attempting to unravel the full details of the bifurcation diagram proved fruitless. The underlying dynamics are quite straightforward though. Figs. 2.8 and 2.9 show two solutions that both exist at $R_e = 85$. We note first that they are very different from the previous phase slip solutions. Rather than having pairs of vortices created in the middle and then drifting outward, we now have vortices moving in from the edges, and then being abruptly destroyed when $|z - 25|$ is around Fig. 2.8 or Fig. 2.9. Based on the local value of the field, the flow should be linearly unstable to Taylor vortices in the region $11 < z < 39$. All of these dynamics are thus happening within the expected region, but it is not clear what singles out the particular location where the phase slips occur.

Comparing Figs. 2.8 and 2.9, the most obvious difference between them is that Fig. 2.8 is

19

symmetric, whereas Fig. 2.9 is asymmetric. That is, in Fig. 2.8 the phase slips in the top and bottom halves are in phase in time, whereas in Fig. 2.9 they are exactly half a period out of phase. This pattern presumably also explains why the two perturbation types both arose at virtually the same critical Reynolds number. This very weak coupling between the two regions also means that very long runs were required in some cases before a definite phase relationship emerged. Indeed, there may also be some Reynolds numbers where no definite relationship ever arises, resulting in some type of quasi-periodic solution. These difficulties lead us to concentrate on the single value $R_e = 85$, rather than attempt to map out a full bifurcation diagram over the range $R_e \geq 81.4$.

## 2.5  Conclusions

We have seen in this work

- How a magnetically ramped Taylor-Couette system can yield qualitatively similar phase slip dynamics as in the more familiar geometrically ramped system. It would be of considerable interest to make the comparison more quantitative, by deriving the equivalent of the Riecke & Paap phase-diffusion equation, and seeing whether it can indeed explain the results presented here.

- Future numerical extensions of this work include a systematic search for the spatiotemporal chaos. This will likely require imposing fields consisting of harmonics $\kappa$, $2\kappa$, etc., analogous to the special choices of ramps.

- Also of interest is the magnetorotational instability mentioned in the introduction, where the magnetic field has a destabilizing rather than stabilizing influence; we would then expect to find Taylor vortices where the field is strong rather than weak.

- More generally, it is noteworthy that there do not appear to be any direct numerical simulations of any of the geometrically ramped experiments mentioned in the introduction. The only related numerical work is n, who did not address subcritical ramping though.

- The most likely reason for this almost complete absence of numerical work in geometrically

ramped TC flows is that the geometry then becomes too complicated to allow the very long integration times that are required for equilibrated solutions to emerge.

# Chapter 3

# Free Convection Boundary Layer Flow over a Flat Plate with Variable Thermal Conductivity and Radiation

## 3.1 Introduction

In this chapter we address the behavior of viscous fluid upon a flat plate having variable thermal conductivity. Effects of radiation are also encountered. Approximate solutions through Homotopy Analysis Method (HAM) are obtained. Tables and graphs are shown of the involved parameters on velocity field and temperature field. Using Runge-Kutta-Fehlberg method to compare numerical solutions.

## 3.2 Mathematical formulation

Here we are taking steady, incompressible and boundary layer of two-dimension viscous fluid for free convection flows upon a flat plate. Also we are considering the influence of variable

22

thermal conductivity along with radiation. The governing equations are

$$\frac{\partial u}{\partial \bar{x}} + \frac{\partial v}{\partial \bar{y}} = 0, \tag{3.1}$$

$$u\frac{\partial u}{\partial \bar{x}} + v\frac{\partial u}{\partial \bar{y}} = \nu \frac{\partial^2 u}{\partial \bar{y}^2} + g\beta\left(T - T_\infty\right), \tag{3.2}$$

$$u\frac{\partial T}{\partial \bar{x}} + v\frac{\partial T}{\partial \bar{y}} = \frac{1}{\rho c_p}\frac{\partial}{\partial \bar{y}}(\alpha\frac{\partial T}{\partial \bar{y}}) - \frac{1}{\rho c_p}\frac{\partial q_r}{\partial y}, \tag{3.3}$$

imposing the boundary conditions

$$u = 0, \quad v = 0, \quad T = T_w\left(x\right), \frac{\partial T}{\partial y} = -\frac{q_w(x)}{k} \quad \text{at} \ \ \bar{y} = 0, \tag{3.4}$$

$$u = 0, v = 0, T = T_\infty \quad \text{as} \ \bar{y} \to \infty. \tag{3.5}$$

In the above expressions $q_r$ is the radiative heat flux, $\nu$ represent kinematic viscosity, $\rho$ represent density, $c_p$ represent specific heat, $\alpha = \alpha_\infty(1 + \epsilon\theta)$ is the variable thermal conductivity, $T$ and $T_\infty$ are the temperatures of the fluid and surroundings respectively.

The radiative heat flux is simplified as

$$q_r = -\frac{4\sigma^*}{3k^*}\frac{\partial T^4}{\partial y}. \tag{3.6}$$

Temperature difference within the flow is assumed to be sufficiently small such as the term $T^4$ can be written as a linear function of temperature. Using Taylor series to expand $T^4$ about $T_\infty$ and neglecting higher-order terms, we get

$$T^4 = T_\infty^4 + 4(T - T_\infty)T_\infty^3. \tag{3.7}$$

Using the similarity transformations

$$\begin{aligned}
\Psi &= x^{\frac{3}{4}}(T_w(x))^{\frac{1}{4}}f(x,\eta), \\
T &= T_w(x)\theta(x,\eta), \ \eta = [T_w(x)]^{1/4}\frac{\bar{y}}{x^{\frac{1}{4}}}.
\end{aligned} \tag{3.8}$$

23

Equation (3.1) is satisfied while Eqs. (3.2 − 3.4) takes the form

$$f''' + \frac{(3 + P(x))}{4} f f'' - \frac{1}{2}(1 + P(x))f'^2 + \theta = x\left(f'\frac{\partial f'}{\partial x} - f''\frac{\partial f}{\partial x}\right), \qquad (3.9)$$

$$\frac{1}{\Pr}(1 + \epsilon\theta + R)\theta'' + \frac{3 + P(x)}{4} f\theta' - P(x)f'\theta + \frac{1}{\Pr}\epsilon\theta'^2 = x\left(f'\frac{\partial \theta}{\partial x} - \theta'\frac{\partial f}{\partial x}\right), \qquad (3.10)$$

$$x\frac{\partial f}{\partial x}(x,0) + \frac{1}{4}[3 + P(x)]f(x,0) = -M(x), \quad f'(x,0) = 0, \quad f'(x,\infty) = 0, \qquad (3.11)$$

$$\theta(x,0) = 1, \quad \theta(x,\infty) = 0. \qquad (3.12)$$

with $P(x) = \frac{x}{T_w(x)}\frac{dT_w}{dx}$. We consider the case of an impermeable flat plate ($M(x) = 0$) with a wall temperature distribution of the form

$$T_w(x) = x^m, \qquad (3.13)$$

where $m$ is a constant. In this case $P(x) = m$. $Eq.(3.9) − (3.12)$ reduces to the similarity form

$$f''' + \frac{(3 + m)}{4} f f'' - \frac{1}{2}(1 + m)f'^2 + \theta = 0, \qquad (3.14)$$

$$\frac{1}{\Pr}(1 + \epsilon\theta + R)\theta'' + \frac{1}{4}(3 + m)f\theta' - mf'\theta + \frac{1}{\Pr}\epsilon\theta'^2 = 0, \qquad (3.15)$$

$$\begin{aligned}
f(0) &= 0, \quad f'(0) = 0, \quad f'(\infty) = 0, \\
\theta(0) &= 1, \quad \theta(\infty) = 0,
\end{aligned} \qquad (3.16)$$

where Pr, $R$ and $\epsilon$ denotes the Prandtl number, radiation parameter and thermal conductivity parameter respectively. Such that

$$\Pr = \frac{\mu c_p}{\alpha_\infty} \text{ and } R = \frac{16\sigma^* T_\infty^3}{3K^*\alpha_\infty}. \qquad (3.17)$$

24

## 3.3 Homotopic solutions

Homotopy analysis method depends upon the initial guesses $(f_0(\eta),\ \theta_0(\eta))$ and linear operators $(L_f,\ L_\theta)$ which are chosen in the forms

$$f_0(\eta) = 0, \quad \theta_0(\eta) = \exp(-\eta), \tag{3.18}$$

$$L_f = \frac{d^3 f}{d\eta^3} - \frac{df}{d\eta}, \quad L_\theta = \frac{d^2\theta}{d\eta^2} - \theta, \tag{3.19}$$

with

$$L_f[C_1 + C_2 * \exp(-\eta)] = 0, \tag{3.20}$$

$$L_\theta[C_3 * \exp(-\eta)] = 0, \tag{3.21}$$

where $C_i\ (i = 1 - 3)$ are the arbitrary constants.

### 3.3.1 Zeroth-order problem

$$(1-p)\,L_f[\hat{f}(\eta;p) - \hat{f}_0(\eta)] = p\hbar_f N_f[\hat{f}(\eta;p), \hat{\theta}(\eta;p)] \tag{3.22}$$

$$(1-p)\,L_\theta[\hat{\theta}(\eta;p) - \hat{\theta}_0(\eta)] = p\hbar_\theta N_\theta[\hat{f}(\eta;p), \hat{\theta}(\eta;p)] \tag{3.23}$$

$$\hat{f}(0;p) = 0, \quad \hat{f'}(0;p) = 0, \quad \hat{f'}(\infty;p) = 0, \tag{3.24}$$

$$\hat{\theta}(0;p) = 1, \quad \hat{\theta}(\infty;p) = 0, \tag{3.25}$$

$$N_f[\hat{f}(\eta;p), \hat{\theta}(\eta;p)] = \frac{\partial^3 \hat{f}(\eta;p)}{\partial\eta^3} + (\frac{3+M}{4})\hat{f}(\eta;p)\frac{\partial^2 \hat{f}(\eta;p)}{\partial\eta^2} - (\frac{1+M}{2})\left(\frac{\partial\hat{f}(\eta;p)}{\partial\eta}\right)^2 + \theta \tag{3.26}$$

$$\begin{aligned}
N_\theta\left[\hat{\theta}(\eta;p), \hat{f}(\eta;p)\right] &= \frac{1}{\Pr}\left(1 + \epsilon\hat{\theta}(\eta,p) + R\right)\frac{\partial^2\hat{\theta}(\eta,p)}{\partial\eta^2} + \frac{\epsilon}{\Pr}\left(\frac{\partial\hat{\theta}(\eta;p)}{\partial\eta}\right)^2 \\
&\quad + \left((\frac{3+M}{4})\hat{f}(\eta;p)\frac{\partial\hat{\theta}(\eta;p)}{\partial\eta} - (M)\frac{\partial\hat{f}(\eta;p)}{\partial\eta}\hat{\theta}(\eta;p)\right) \tag{3.27}
\end{aligned}$$

where $p \in [0,1]$ is embedding parameter $\hbar_f$ and $\hbar_\theta$ are the non-zero auxiliary parameters.

### 3.3.2 $m$th-order deformation problems

$$L_f \left[ f_m \left( \eta \right) - \chi_m f_{m-1} \left( \eta \right) \right] = \hbar R_m^f \left( \eta \right), \tag{3.28}$$

$$L_\theta \left[ \theta_m \left( \eta \right) - \chi_m \theta_{m-1} \left( \eta \right) \right] = \hbar_\theta R_m^\theta \left( \eta \right), \tag{3.29}$$

$$f_m \left( 0 \right) = 0, \ f_m' \left( 0 \right) = 0, \ f_m' \left( \infty \right) = 0, \tag{3.30}$$

$$\theta_m \left( 0 \right) = 1, \quad \theta_m \left( \infty \right) = 0, \tag{3.31}$$

$$R_m^f \left( \eta \right) = f_{m-1}''' + \left( \frac{3+M}{4} \right) \sum_{k=0}^{m-1} f_k f_{m-1-k}'' - \left( \frac{1+M}{2} \right) \sum_{k=0}^{m-1} f_k' f_{m-1-k}' + \theta_{m-1}, \tag{3.32}$$

$$
\begin{aligned}
R_m^\theta(\eta) &= \frac{1}{\mathrm{Pr}}(1 + R + \epsilon\theta)\theta_{m-1}'' + \frac{1}{\mathrm{Pr}}\epsilon\theta_{m-1}'^2 + \left( \frac{3+M}{4} \right) \sum_{k=0}^{m-1} f_k \theta_{m-1-k}' \\
&\quad - M \sum_{k=0}^{m-1} \theta_k f_{m-1-k}',
\end{aligned}
\tag{3.33}
$$

$$\chi_m = \begin{cases} 0, & m \le 1 \\ 1, & m > 1 \end{cases}. \tag{3.34}$$

For $p = 0$ and $p = 1$, we can write

$$\widehat{f} \left( \eta; 0 \right) = f_0 \left( \eta \right), \quad \widehat{f} \left( \eta; 1 \right) = f \left( \eta \right), \tag{3.35}$$

$$\widehat{\theta} \left( \eta; 0 \right) = \theta_0 \left( \eta \right), \quad \widehat{\theta} \left( \eta; 1 \right) = \theta \left( \eta \right) \tag{3.36}$$

and with the variation of $p$ from 0 to 1, $\widehat{f} \left( \eta; p \right)$ and $\widehat{\theta} \left( \eta; p \right)$ varies from the initial solutions $f_0 \left( \eta \right)$ and $\theta_0(\eta)$ to the final solutions $f \left( \eta \right)$ and $\theta(\eta)$ respectively. By Taylor's series we have

$$\widehat{f} \left( \eta; p \right) = f_0 \left( \eta \right) + \sum_{m=1}^{\infty} f_m \left( \eta \right) p^m, \quad f_m \left( \eta \right) = \frac{1}{m!} \frac{\partial^m \widehat{f} \left( \eta; p \right)}{\partial p^m} \bigg|_{p=0} \tag{3.37}$$

$$\widehat{\theta} \left( \eta; p \right) = \theta_0 \left( \eta \right) + \sum_{m=1}^{\infty} \theta_m \left( \eta \right) p^m, \quad \theta_m \left( \eta \right) = \frac{1}{m!} \frac{\partial^m \widehat{\theta} \left( \eta; p \right)}{\partial p^m} \bigg|_{p=0}. \tag{3.38}$$

26

The value of auxiliary parameter is chosen so properly that the series (3.37) and (3.38) converges at $p = 1$ i.e.

$$f(\eta) = f_0(\eta) + \sum_{m=1}^{\infty} f_m(\eta), \tag{3.39}$$

$$\theta(\eta) = \theta_0(\eta) + \sum_{m=1}^{\infty} \theta_m(\eta). \tag{3.40}$$

The general solutions are given by

$$f_m(\eta) = f_m^*(\eta) + C_1 + C_2 * \exp(-\eta), \tag{3.41}$$

$$\theta_m(\eta) = \theta_m^*(\eta) + C_3 * \exp(-\eta), \tag{3.42}$$

where the constants $C_1$, $C_2$ and $C_3$ can be calculated by using Eqs. (3.30) and (3.31) $C_f$ Skin friction and $Nu_x$ local Nusselt number are defined as

$$C_f = \frac{\tau_w}{\rho u_w^2}, \qquad Nu_x = \frac{x q_w}{k(T_w - T_\infty)}, \tag{3.43}$$

where

$$\tau_w = \mu \left( \frac{\partial u}{\partial y} \right)_{y=0}, \qquad q_w = -k \left( \frac{\partial T}{\partial y} \right)_{y=0}, \tag{3.44}$$

$$C_f \operatorname{Re}_x^{1/2} = f''(0), \quad Nu_x \operatorname{Re}_x^{-1/2} = -\theta'(0). \tag{3.45}$$

Where $\operatorname{Re}_x = x \sqrt{\frac{a}{\nu}}$.

## 3.4 Convergence of the homotopy solutions

Homotopy analysis method is used to get the criteria of convergence for desired solution of given equations. The convergence control parameter $\hbar$ is involved in the series solution. HAM solution depends upon this parameter which basically control the convergence region and rate of approximation. Here the $40^{th}$-order of approximations for $\hbar_f$ and $\hbar_\theta$ have been made for the desirable range. The convergence **Table 3.1** is prepared for each of the function up to $40^{th}$ order of approximation.

| Order of convergence | $-f''(0)$ | $-\theta'(0)$ |
|---|---|---|
| 1 | 0.5500 | 0.6097 |
| 5 | 0.2686 | 0.5922 |
| 10 | 0.2238 | 0.5894 |
| 15 | 0.2139 | 0.5900 |
| 20 | 0.2109 | 0.5909 |
| 25 | 0.2097 | 0.5916 |
| 30 | 0.2092 | 0.5921 |
| 35 | 0.2091 | 0.5925 |
| 39 | 0.2090 | 0.5924 |
| 40 | 0.2090 | 0.5924 |

**Table 3.1** Convergence table for velocity profile $f(\eta)$ and temperature profile $\theta(\eta)$.

## 3.5   Shooting method

Shooting method is a numerical technique by which one can find an approximate solution of a boundary value problem. It is like a cannonball which is fired from origin to hit a given target. Here we are considering constant horizontal but the vertical distance (height of the ball) depends on the gravitation.

The theme of the shooting method basically the replacement of the given boundary value problem by some initial value problem. If we consider the nonlinear differential equation

$$u''(\eta) = f(\eta, u(\eta), u'(\eta)), \quad a \leq \eta < \infty \tag{3.46}$$

subject to the conditions

$$u(a) = \alpha, \quad u(\infty) = \beta. \tag{3.47}$$

We assume that $u'(a) = s$ and solve the initial value problem

$$u''(\eta) = f(\eta, u(\eta), u'(\eta)), \quad a \leq \eta < \infty \tag{3.48}$$

subject to the conditions

$$u(a) = \alpha, \quad u'(\infty) = s, \tag{3.49}$$

upto $\eta \to \infty$ using any numerical technique. Make sure that solution obtained from initial value problem $u(\infty, s)$ must satisfy the boundary condition $u(\infty) = \beta$. We define $\phi(s) = u(\infty, s) - \beta$. Here the problem is to find $s$ such that $\phi(s) = 0$ which can be computed using any iterative method. But in our case we have used Newton-Raphson method

$$s^{(k+1)} = s^{(k)} - \frac{\phi(s^{(k)})}{\phi'(s^{(k)})}, \tag{3.50}$$

due to its better accuracy. This technique gives a sequence of iterates $\{s^{(k)}\}$ and we choose one value of $s$ which satisfy the relation limit when k approaches to infinity $\phi(s^{(k)}) = 0$. Here the sub method Runge-Kutta-Fehlberg method of $5^{th}$ order is applied to solve the initial value problem.

To apply Shooting method first the given nonlinear ordinary differential equation is reduced to a system of first order ordinary differential equations. This system is transformed to initial value problems by replacing missing initial conditions with assumed slopes. Using end conditions (i.e. when $\eta \to \infty$) initial conditions are computed through Newton-Raphson method which meet the given target. We can rewrite the dimensionless governing $Eqs.$ $(3.12) - (3.13)$ in the following form:

$$f''' = -\frac{3+M}{4}ff'' + \frac{1}{2}(1+M)f'^2 - \theta \tag{3.51}$$

$$\theta'' = \frac{\Pr}{(1+\epsilon\theta+R)}\left[-\frac{3+M}{4}f\theta' + Mf'\theta - \frac{1}{\Pr}\epsilon\theta'^2\right] \tag{3.52}$$

29

We define a set of new variables

$$y_1 = f, \quad y_2 = f', \quad y_3 = f'', \quad y_4 = \theta \text{ and } y_5 = \theta'. \tag{3.53}$$

Using these variables:

$$y_1' = y_2, \tag{3.54}$$

$$y_2' = y_3, \tag{3.55}$$

$$y_3' = -\frac{3+M}{4} y_1 y_3 + \frac{1}{2}(1+M) y_2^2 - y_4, \tag{3.56}$$

$$y_4' = y_5, \tag{3.57}$$

$$y_5' = \frac{\text{Pr}}{(1 + \epsilon y_4 + R)} \left[ -\frac{3+M}{4} y_1 y_5 + M y_2 y_4 - \frac{\epsilon}{\text{Pr}} y_5^2 \right]. \tag{3.58}$$

In this system of ordinary differential equations prime denotes derivatives w.r.t. $\eta$. The initial conditions are modified to

$y_1(0) = 0, \quad y_2(0) = 0, \quad y_4(0) = 1,$

and the end conditions takes the form $y_2(\eta) \to 0, \quad y_4(\eta) \to 0$ when $\eta \to \infty$.

In the above system there are five ordinary differential equations with three initial conditions and two end conditions. To solve this system by Runge-Kutta-Fehlberg method five initial conditions are required to solve five unknowns appearing in the solution. Three of them are given while two initial guesses are still required. These two conditions are given for $\eta \to \infty$. An important step is to find the value of $\eta$ at $\infty$ (i.e. $\eta_\infty$) where end conditions are satisfied. The solution procedure starts with initial guess (e.g. $f'(0) = s$) and solve the system to determine the appropriate value of $f''(0)$ and $\theta'(0)$. The process is continued (using Newton-Raphson method) with revised value of $s$ until two success values of $f''(0)$ and $\theta'(0)$ differ only after the specific number of significant digits. The final value of $\eta$ is considered as $\eta_\infty$ that can be

used to calculate the fluid velocity $f'$ and the temperature field $\theta$. This initial value problem is solved numerically by employing the fifth order Runge-Kutta-Fehlberg method with shooting technique using MATLAB software.

## 3.6 Results and discussion

Here graphical behavior are discussed for velocity and temperature fields after variation of different physical parameters. The influence of radiation parameter $R$ on velocity field is showing in Fig 3.1. We can see that velocity increases by increasing radiation parameter $R$. The behavior of $\epsilon$ on velocity field is plotted in Fig. 3.2. This figure identify that fluid velocity increases by increasing variable thermal conductivity parameter. The effects of variation in temperature parameter $M$ on temperature field and velocity profile are sketched in Figs. (3.3) and (3.4) respectively. By increasing temperature parameter temperature profile decreases. It is quite obvious because $M$ is inversely proportional to wall temperature. Fig. 3.5 is plotted to see the effects of Pr on temperature profile. This figure clearly shows that by increasing Prandtl number viscosity increases as a result temperature profile decreases. Fig. 3.6 is plotted to observe the effects of variation in radiation parameter $R$ on temperature field. Here increase in radiation parameter increases the temperature profile.
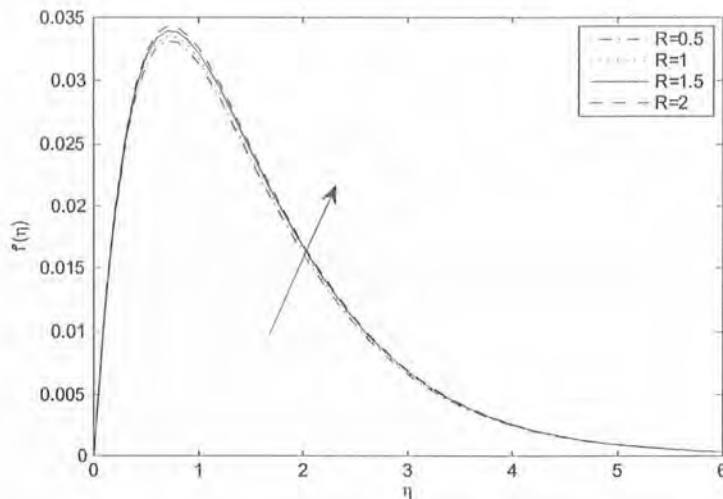


**Fig 3.1**: Effect of $R$ on velocity profile $f'(\eta)$ with $M = 1, Pr = 2, \epsilon = 0.2$.
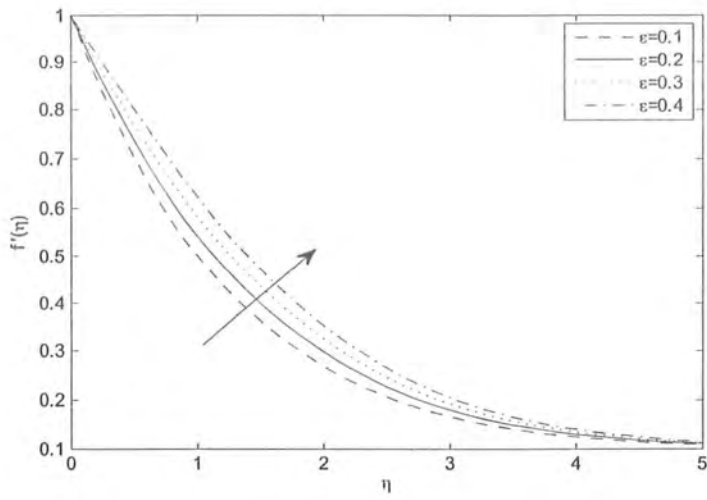
**Fig 3.2**: Effect of $\epsilon$ on velocity profile $f'(\eta)$ with $M = 1, Pr = 2, R = 0.2$
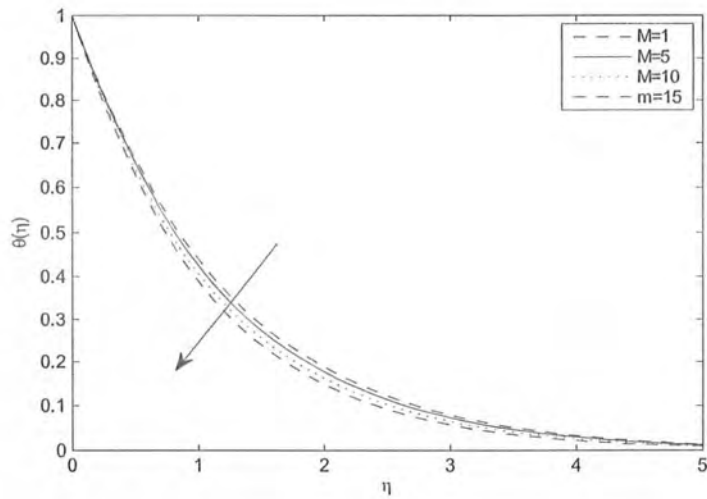


**Fig 3.3**: Effect of $M$ on temperature profile $\theta(\eta)$ with $R = 1, Pr = 2, \epsilon = 0.2$
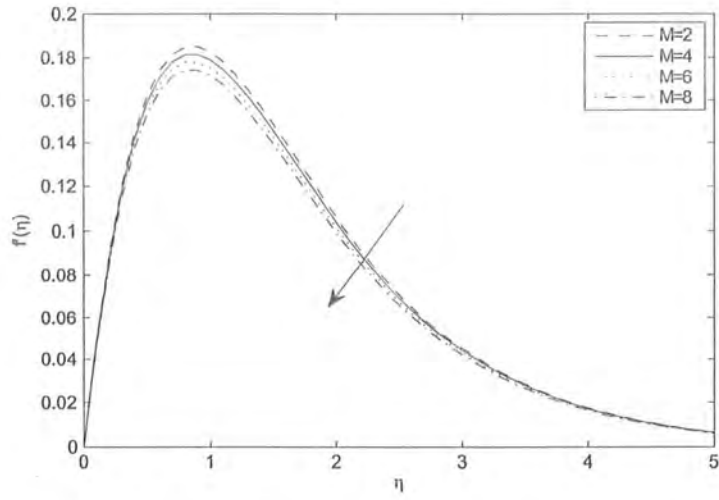
**Fig 3.4:** Effect of $M$ on velocity profile $f'(\eta)$ with $R = 1$, Pr$= 2$, $\epsilon = 0.2$
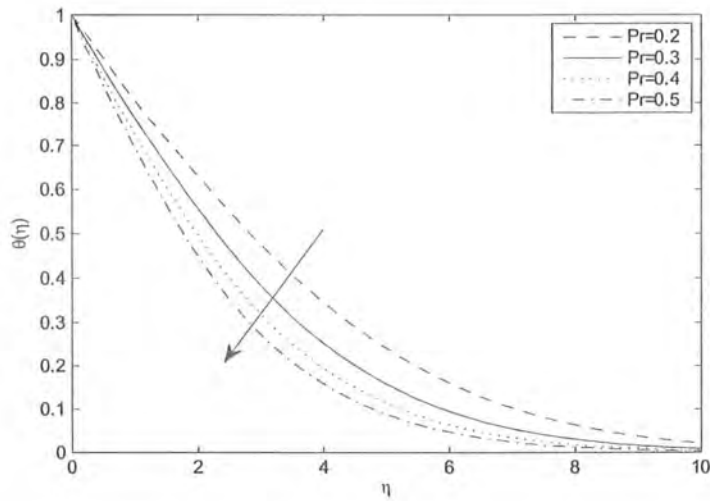


**Fig 3.5:** Effect of Pr on temperature profile $\theta(\eta)$ with $R = 1$, $M = 0.2$, $\epsilon = 0.2$
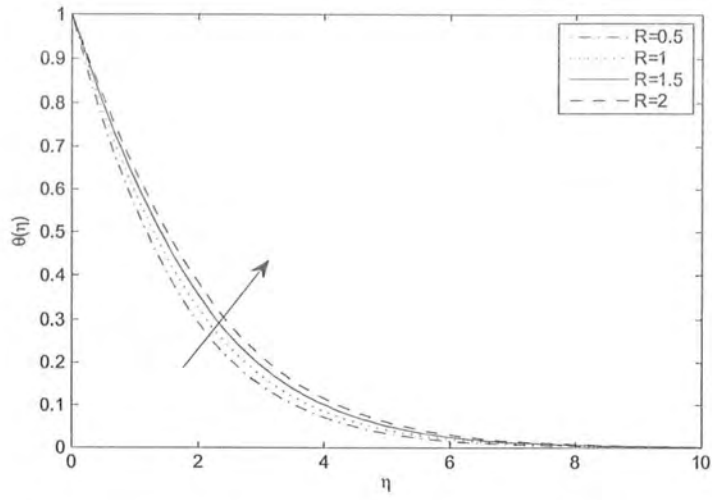
**Fig 3.6**: Effect of $R$ on temperature profile $\theta(\eta)$ with $M = 1$, Pr= 2, $\epsilon = 0.2$.

| $M$ | Pr | $\epsilon$ | $R$ | $f''(0)$ |
|-----|-----|-----|-----|-----|
| 0.1 | 2 | 1 | 1 | 0.781798 |
| 0.3 | | | | 0.774325 |
| 0.5 | | | | 0.766929 |
| 0.7 | | | | 0.759609 |

**Table 3.2**: The variation of $f''(0)$ with respect to $M$.

| $M$ | $Pr$ | $\epsilon$ | $R$ | $-\theta'(0)$ |
|---|---|---|---|---|
| 1 | 1 | 1 | 1 | 0.600000 |
| 2 | | | | 0.630000 |
| 3 | | | | 0.677000 |
| 1 | 0.1 | | | 0.404400 |
| | 0.2 | | | 0.408019 |
| | 0.3 | | | 0.493589 |
| | 1 | 0.2 | | 0.391581 |
| | | 0.3 | | 0.362597 |
| | | 0.4 | | 0.357245 |
| | | 1 | 0.1 | 0.391758 |
| | | | 0.2 | 0.444500 |
| | | | 0.3 | 0.457632 |

**Table 3.3:** Temperature gradient $-\theta'(0)$ at the outside surface of plate for different values of $\epsilon$, $Pr$ and $R$.

| | $M = 1$ | | $M = 2$ | |
|---|---|---|---|---|
| $\epsilon$ | $HAM$ | $Shooting\ Method$ | $HAM$ | $Shooting\ Method$ |
| 2 | 0.8730 | 0.87301 | 0.78432 | 0.78471 |
| 4 | 0.8834 | 0.88368 | 0.79522 | 0.79511 |
| 6 | 0.8938 | 0.89287 | 0.8043 | 0.80413 |
| 8 | 0.9025 | 0.90093 | 0.81209 | 0.81209 |

**Table 3.4.** Comparison of velocity values $f'(\eta)$ obtained through HAM and Shooting

method.

| | $Pr = 1$ | | $Pr = 2$ | |
|---|---|---|---|---|
| $R$ | $HAM$ | $Shooting\ Method$ | $HAM$ | $Shooting\ Method$ |
| 0.5 | 0.8572 | 0.8555 | 0.7731 | 0.7724 |
| 1 | 0.8780 | 0.8772 | 0.7978 | 0.79969 |
| 1.5 | 0.8897 | 0.8891 | 0.8165 | 0.8158 |
| 2 | 0.9041 | 0.9032 | 0.8333 | 0.8325 |

**Table 3.5.** Comparison of temperature values obtained through HAM and Shooting method.

**Table 3.1** Represents the order of convergence for velocity profile $f(\eta)$ and temperature profile $\theta(\eta)$. In **Table 3.2** we see that $C_f \propto \mathrm{Re}_x^{-\frac{1}{2}}$ thus, as Reynold number increases, decreases $|C_f|$. Viscous forces start reducing by increasing $\mathrm{Re}_x$, causing $|C_f|$ reduces. Again by increasing temperature parameter $M$ the $|C_f \mathrm{Re}_x|$ decreases.

The effects of variation in temperature parameter $M$, Prandtl number Pr, thermal variable parameter $\epsilon$ and radiation parameter $R$ on temperature gradient $\theta'(0)$ are reflected in **Table 3.3**. We see that $Nu_x^2 \propto \mathrm{Re}_x$ thus as $\mathrm{Re}_x = \frac{Ux}{v}$ increases the viscosity goes down. We can see that rate of convectional heat transfer growing by decreasing viscosity. The influence of coefficient of convectional heat transfer is tabulated in **Table 3.4**. By increasing value of Prandtl number, viscosity increases because it is ratio between momentum diffusitivity and thermal diffusivity. Therefore Nusselt number increases as Reynolds number decreases.

## 3.7 Conclusions

Main findings of present analysis are listed below:

- The influence of velocity and temperature fields are same for radiation parameter $R$ i.e. by increasing radiation parameter $R$ both velocity and temperature fields increases.

- By increasing temperature parameter $M$ temperature field and velocity field decreases.

- On increasing Prandtl number Pr result in decreasing Therma boundary layer.

# Chapter 4

# Effect of Variable Thermal Conductivity and Slip Conditions over a Stretching Cylinder

## 4.1 Introduction

In this chapter we discuss the behavior of viscous fluid close to stagnation point over a stretching cylinder by taking variable thermal conductivity. The effects of slip conditions are also encountered in this work. Numerical results of momentum equation and energy equation obtained through Homotopy Analysis Method (HAM) and Shooting method are compared through table. Graphical results of variation in physical parameters upon velocity and temperature fields are also presented.

## 4.2 Mathematical formulation

Here we are taking steady, incompressible and boundary layer of two-dimension viscous fluid upon a stretching cylinder in the vecinity of stagnation point. Also we are considering the influence of with heat generation/absorption. The governing equations are

$$\frac{\partial (ru)}{\partial x} + \frac{\partial (rv)}{\partial r} = 0, \tag{4.1}$$

37

$$u\frac{\partial u}{\partial x} + v\frac{\partial u}{\partial r} = U_e\frac{dU_e}{\partial x} + \nu\left(\frac{\partial^2 u}{\partial r^2} + \frac{1}{r}\frac{\partial u}{\partial r}\right), \tag{4.2}$$

$$u\frac{\partial T}{\partial x} + v\frac{\partial T}{\partial r} = \frac{1}{\rho c_p}\frac{\partial}{\partial r}\left(k\left(T\right)r\frac{\partial T}{\partial r}\right) + \frac{Q}{\rho c_p}(T - T_\infty). \tag{4.3}$$

There is a proportional relation of velocity slip to the local shear stress,

$$u = U_w(x) + \frac{2 - \sigma_v}{\sigma_v}\lambda_0\frac{\partial u}{\partial r}, \quad v = 0, \quad T = T_w \quad \text{at } r = R, \tag{4.4}$$

$$u \to U_e = bx, \quad T \to T_\infty \quad \text{as } r \to \infty. \tag{4.5}$$

In the above expressions $\sigma_v$ is the tangential momentum accommodation coefficient, $\lambda_0$ is the mean free path, $Q$ represent heat added or removed from the fluid, $\nu$ represent kinematic viscosity, $\rho$ represent density, $c_p$ represent specific heat, $k\left(T\right)$ represent variable thermal conductivity, $T$ is the temperature of the fluid and $T_\infty$ is the temperature of the surrounding fluid, $U_w(x)$ represent stretching velocity, $U_e$ represent free stream velocity.

Using the transformations of the form

$$\eta = \sqrt{\frac{a}{\nu}}\left(\frac{r^2 - R^2}{2R}\right), \quad \psi = \sqrt{\nu a}xRf\left(\eta\right), \tag{4.6}$$

$$u = axf'\left(\eta\right), \ v = -\sqrt{\nu a}\frac{R}{r}f\left(\eta\right), \tag{4.7}$$

$$\theta\left(\eta\right) = \frac{T - T_\infty}{T_w - T_\infty}. \tag{4.8}$$

Equation (4.1) is identically satisfied while Eqs. (4.2) to (4.4) take the form

$$(1 + 2K\eta)f''' + ff'' - \left(f'\right)^2 + 2Kf'' + A^2 = 0, \tag{4.9}$$

$$(1 + \epsilon\theta)\left(1 + 2K\eta\right)\theta'' + \epsilon\left(1 + 2K\eta\right)\theta'^2 + 2\left(1 + \epsilon\theta\right)K\theta' + \Pr f\theta' + \beta\theta = 0 \tag{4.10}$$

Imposing the boundary conditions

$$f(0) = 0, \quad f'(0) = 1 + \lambda f''(0), \ f'(\infty) = A, \tag{4.11}$$

38

$$\theta\left(0\right) = 1, \quad \theta\left(\infty\right) = 0, \tag{4.12}$$

where $K$ , $A$, $\beta$, $\epsilon$, $\lambda$ and Pr denotes curvature parameter, stretching ratio parameter, heat generation/absorption, small temperature parameter, velocity slip parameter and Prandtl number which are given by

$$K = \frac{1}{R}\sqrt{\frac{\nu}{a}}, \ \ \mathrm{Pr} = \frac{\mu c_p}{k_\infty}, \tag{4.13}$$

$$A = \frac{b}{a}, \ \ \lambda = \frac{2 - \sigma_v}{\sigma_v}\lambda_0\sqrt{\frac{a}{\nu}}, \beta = \frac{Q}{\rho c_p a}. \tag{4.14}$$

## 4.3   Homotopic solutions

Homotopy analysis method depends upon the initial guesses $(f_0, \theta_0)$ and linear operators $(L_f, L_\theta)$ which are given in the forms

$$f_0\left(\eta\right) = \frac{1}{1 + \lambda}(A - 1)(\exp\left(-\eta\right) - 1) + A\eta, \ \ \ \theta_0\left(\eta\right) = \exp\left(-\eta\right), \tag{4.15}$$

$$L_f\left(\eta\right) = \frac{d^3 f}{d\eta^3} - \frac{df}{d\eta}, \ \ L_\theta\left(\eta\right) = \frac{d^2\theta}{d\eta^2} - \theta, \tag{4.16}$$

with

$$L_f[C_1 + C_2 * \exp\left(-\eta\right)] = 0, \tag{4.17}$$

$$L_\theta[C_3 * \exp\left(-\eta\right)] = 0, \tag{4.18}$$

where $C_i$ $(i = 1 - 3)$ are the arbitrary constants.

### 4.3.1   Zeroth-order problem

$$(1 - p)L_f\left[\widehat{f}\left(\eta;p\right) - f_0\left(\eta\right)\right] = p\hbar_f N_f\left[\widehat{f}\left(\eta;p\right)\right], \tag{4.19}$$

$$(1 - p)L_\theta\left[\widehat{\theta}\left(\eta;p\right) - \theta_0\left(\eta\right)\right] = p\hbar_\theta N_\theta\left[\widehat{\theta}\left(\eta;p\right), \widehat{f}\left(\eta;p\right)\right], \tag{4.20}$$

$$\widehat{f}\left(0;p\right) = 0, \ \ \ \widehat{f'}\left(0;p\right) = 1 + \lambda\widehat{f''}\left(0;p\right), \ \ \ \widehat{f'}\left(\infty;p\right) = A, \tag{4.21}$$

39

$$\widehat{\theta}\left(0;p\right)=1, \qquad \widehat{\theta}\left(\infty;p\right)=0, \tag{4.22}$$

$$N_f\left[\widehat{f}\left(\eta,p\right)\right]=(1+2K\eta)\frac{\partial^3\widehat{f}(\eta;p)}{\partial\eta^3}+\widehat{f}\left(\eta;p\right)\frac{\partial^2\widehat{f}(\eta;p)}{\partial\eta^2}-\left(\frac{\partial\widehat{f}(\eta;p)}{\partial\eta}\right)^2+2K\frac{\partial^2\widehat{f}(\eta;p)}{\partial\eta^2}+A^2, \tag{4.23}$$

$$\begin{aligned}
N_\theta\left[\widehat{\theta}\left(\eta;p\right),\widehat{f}\left(\eta;p\right)\right] &= \left(1+\epsilon\widehat{\theta}(\eta,p)\right)(1+2K\eta)\frac{\partial^2\widehat{\theta}(\eta,p)}{\partial\eta^2}\\
&\quad +\epsilon\left(1+2K\eta\right)\left(\frac{\partial\widehat{\theta}(\eta,p)}{\partial\eta}\right)^2+2K\frac{\partial\widehat{\theta}(\eta,p)}{\partial\eta}\left(1+\epsilon\widehat{\theta}(\eta,p)\right)\\
&\quad +\Pr\left(\widehat{f}\left(\eta;p\right)\frac{\partial\widehat{\theta}\left(\eta;p\right)}{\partial\eta}+\beta\widehat{\theta}(\eta,p).\right)
\end{aligned} \tag{4.24}$$

where $p\in[0,1]$.

### 4.3.2   mth-order deformation problems

$$L_f\left[f_m\left(\eta\right)-\chi_m f_{m-1}\left(\eta\right)\right]=\hbar_f R_m^f\left(\eta\right), \tag{4.25}$$

$$L_\theta\left[\theta_m\left(\eta\right)-\chi_m\theta_{m-1}\left(\eta\right)\right]=\hbar_\theta R_m^\theta\left(\eta\right), \tag{4.26}$$

$$f_m\left(0\right)=0, \ f_m'(0)=\lambda\ f_m''(0), \ f_m'\left(\infty\right)=0, \tag{4.27}$$

$$\theta_m\left(0\right)=\theta_m\left(\infty\right)=0, \tag{4.29}$$

$$R_m^f\left(\eta\right)=(1+2K\eta)f_{m-1}'''\left(\eta\right)+2Kf_{m-1}''+\sum_{k=0}^{m-1}\left[f_{m-1-k}f_k''-f_{m-1-k}'f_k'\right]+A^2\left(1-\chi_m\right), \tag{4.30}$$

$$\begin{aligned}
R_m^\theta\left(\eta\right) &= (1+2K\eta)\left(\theta_{m-1}''+\epsilon\sum_{k=0}^{m-1}\theta_{m-1-k}\theta_k''\right)+\epsilon\left(1+2K\eta\right)\sum_{k=0}^{m-1}\theta_{m-1-k}'\theta_k'\\
&\quad +2K\left(\theta_{m-1}'+\epsilon\sum_{k=0}^{m-1}\theta_{m-1-k}\theta_k'\right)+\Pr\left(\sum_{k=0}^{m-1}f_{m-1-k}\theta_k'+\beta\theta_{m-1}\right),
\end{aligned} \tag{4.31}$$

40

$$\chi_m = \begin{cases} 0, & m \leq 1 \\ 1, & m > 1 \end{cases} \tag{4.32}$$

For $p = 0,1$, we can write

$$\widehat{f}(\eta;0) = f_0(\eta), \quad \widehat{f}(\eta;1) = f(\eta), \tag{4.33}$$

$$\widehat{\theta}(\eta;0) = \theta_0(\eta), \quad \widehat{\theta}(\eta;1) = \theta(\eta) \tag{4.34}$$

By Taylor's series we have

$$\widehat{f}(\eta;p) = f_0(\eta) + \sum_{m=1}^{\infty} f_m(\eta) p^m, \quad f_m(\eta) = \frac{1}{m!} \frac{\partial^m \widehat{f}(\eta;p)}{\partial p^m}\bigg|_{p=0} \tag{4.35}$$

$$\widehat{\theta}(\eta;p) = \theta_0(\eta) + \sum_{m=1}^{\infty} \theta_m(\eta) p^m, \quad \theta_m(\eta) = \frac{1}{m!} \frac{\partial^m \widehat{\theta}(\eta;p)}{\partial p^m}\bigg|_{p=0}. \tag{4.36}$$

Auxiliary parameter is chosen so properly so series (4.35) and (4.36) converge at $p = 1$ i.e.

$$f(\eta) = f_0(\eta) + \sum_{m=1}^{\infty} f_m(\eta), \tag{4.37}$$

$$\theta(\eta) = \theta_0(\eta) + \sum_{m=1}^{\infty} \theta_m(\eta). \tag{4.38}$$

In terms of special solutions $(f_m^*, \theta_m^*)$ are given by

$$f_m(\eta) = f_m^*(\eta) + C_1 + C_2 e^{-\eta}, \tag{4.39}$$

$$\theta_m(\eta) = \theta_m^*(\eta) + C_3 e^{-\eta}, \tag{4.40}$$

## 4.4 Convergence of HAM solutions

Homotopy analysis method is applied to find the convergence of the equations. The convergence of the series solutions depend upon the auxiliary parameter $\hbar$. A table is constructed to get

41

the series solution.

| Order of approximations | $-f''(0)$ | $-\theta'(0)$ |
|---|---|---|
| 1 | 0.68210 | 0.51574 |
| 5 | 0.65162 | 0.39681 |
| 10 | 0.65113 | 0.38029 |
| 15 | 0.65111 | 0.37788 |
| 20 | 0.65111 | 0.37746 |
| 21 | 0.65111 | 0.37744 |
| 23 | 0.65111 | 0.37741 |
| 25 | 0.65111 | 0.37739 |
| 26 | 0.65111 | 0.37739 |

**Table 4.1.** Convergence of series solutions for different order of approximations when $K = 0.2$, $\beta = 0.1$, $A = 0.1$, $\epsilon = 0.1$, $\lambda = 0.1$ and $\Pr = 2.0$.

## 4.5 Shooting method

For the numerical solution by Shooting method the given nonlinear ordinary differential equations are converted to a system of first order ordinary differential equations. The system is transformed to initial value problems by replacing missing initial conditions with slopes. Using end conditions (i.e. when $\eta \to \infty$) initial conditions are computed through Newton-Raphson method which meets the given target. We can rewrite the dimensionless governing Eqns. $(4.9) - (4.10)$ in the form:

$$f''' = \frac{1}{(1 + 2K\eta)}[(f')^2 - ff'' - 2Kf'' - A^2] \tag{4.41}$$

$$\theta'' = \frac{1}{(1 + \epsilon\theta)(1 + 2K\eta)}\left[-\epsilon(1 + 2K\eta)\theta'^2 - 2(1 + \epsilon\theta)K\theta' - \Pr f\theta' - \beta\theta\right]. \tag{4.42}$$

Define a set of new variables

$$y_1 = f, \; y_2 = f', y_3 = f'',$$ (4.43)

$$y_4 = \theta \;\; \text{and} \;\; y_5 = \theta'.$$ (4.44)

These variables modify the above ordinary differential equations to the system of first order ordinary differential equations:

$$y_1' = y_2,$$ (4.45)

$$y_2' = y_3,$$ (4.46)

$$y_3' = \frac{1}{(1 + 2K\eta)}[(y_2)^2 - y_1 y_3 - 2K y_2' - A^2],$$ (4.47)

$$y_4' = y_5,$$ (4.48)

$$y_5' = \frac{1}{(1 + \epsilon y_4)(1 + 2K\eta)} \left[ -\epsilon (1 + 2K\eta) y_4^2 - 2(1 + \epsilon\theta) K y_5 - \Pr y_1 \, y_5 - \beta y_4 \right].$$ (4.49)

In this system of ordinary differential equations prime denotes derivatives w.r.t. $\eta$. The initial conditions are modified to

$y_1(0) = 0, \quad y_2(0) = 1 + \lambda y_3(0), \quad y_4(0) = 1,$

and the end conditions takes the form $y_2(\eta) \rightarrow A, \quad y_4(\eta) \rightarrow 0$ when $\eta \rightarrow \infty$.

In the above system there are five ordinary differential equations with three initial conditions and two end conditions. To solve this system by Runge-Kutta-Fehlberg (RKF) method five initial conditions are required to solve five unknowns that appear in the solutions. Three of them are given while two initial guesses are still required for application of the RKF method.

43

The other two conditions are given for $\eta \to \infty$. An important step is to find the value of $\eta$ at $\infty$ (i.e. $\eta_\infty$) where end conditions are satisfied. The solution procedure starts with initial guess (e.g. $f'(0) = s$) and solving the system to determine the appropriate value of $f''(0)$ and $\theta'(0)$. The process is continued (using Newton-Raphson method) with revised value of $s$ until two successive values of $f''(0)$ and $\theta'(0)$ differ only after the specific number of significant digits. The final value of $\eta$ is considered as $\eta_\infty$ that can be used to calculate the fluid velocity $f'(\eta)$ and the temperature field $\theta(\eta)$ in the boundary layer for set of physical parameters. Numerical solution is getting by employing the fifth order Runge-Kutta-Fehlberg method with shooting technique using MATLAB software.

## 4.6   Comparison of HAM and Shooting method

Comparison between numerical solutions obtained through homotopy analysis method and shooting method are presented in Tables $(4.2 - 4.3)$. In the solution computed by homotopy analysis method 26 order of approximations has been achieved (see Table 4.1). For shooting method solution is obtained in conjunction with Fehlberg method. In Table 4.2 both solutions are computed for two values of stretching parameter $A=0.1$ and 0.5 when curvature parameter $K=0$, 0.2, 0.5 and 0.8.

| | $A = 0.1$ | | $A = 0.5$ | |
|---|---|---|---|---|
| $K$ | $HAM$ | $Shooting\ Method$ | $HAM$ | $Shooting\ Method$ |
| 0 | 0.2242 | 0.2248 | 0.7792 | 0.7798 |
| 0.2 | 0.2261 | 0.2265 | 0.7707 | 0.7710 |
| 0.5 | 0.2041 | 0.2043 | 0.7511 | 0.7516 |
| 0.8 | 0.1419 | 0.1421 | 0.6860 | 0.6865 |

Table 4.2 Comparison of HAM solution and numerical solution obtained by using shooting method for velocity profile $f'(\eta)$ against stretching parameter $A$ and curvature parameter $K$ when $\mathrm{Pr} = 0.1$, $\beta = 0.1$, $\epsilon = 0.1$.

44

In Table 4.3 the solutions are calculated for two values of curvature parameter $K$=0.1 and 0.5 when Prandtl number Pr=0, 0.2, 0.5 and 0.8. On comparing both solutions it is observed that they have good agreement.

| | $K = 0.1$ | | $K = 0.5$ | |
|---|---|---|---|---|
| Pr | $HAM$ | $Shooting\ Method$ | $HAM$ | $Shooting\ Method$ |
| 0 | -0.1133 | -0.1133 | -0.2781 | -0.2781 |
| 0.2 | -0.1873 | -0.1877 | -0.3304 | -0.3307 |
| 0.5 | -0.3023 | -0.3028 | -0.4108 | -0.4110 |
| 0.8 | -0.4094 | -0.4096 | -0.4900 | -0.4903 |

**Table 4.3** Comparison of HAM solution and numerical solution obtained by using shooting method for temperature $\theta(\eta)$ against Prandtl Number Pr and curvature parameter $K$ when $\beta = 0.1$, $\epsilon = 0.1$, $A = 0.1$.

## 4.7 Results and discussion

Here the graphical results of velocity and temperature fields for different values of physical parameters are discussed. The influence of curvature parameter $K$ on temperature field are plotted in Fig. 4.1. From this figure we can see that increase in curvature parameter $K$ temperature decreases. Fig. 4.2 is the behaviour of slip parameter $\lambda$ on temperature field. From this figure we can see that by increasing slip parameter temperature of the fluid increases. The variation of stretching ratio parameter $A$ on temperature is sketched in Fig. 4.3 which clarify that on increasing $A$ temperature decreases. The influence of stretching ratio parameter $A$ on velocity field is plotted in Fig. 4.4. It can be seen that velocity field increases with an increase in stretching ratio parameter $A$. Fig. 4.5 is the behavior of small parameter $\epsilon$ on temperature field. It is observed that temperature decreases as we increase the small parameter $\epsilon$. The behavior of Prandtl number Pr upon temperature field is shown in Fig. 4.6. From the graph we can see that increasing Prandtl number Pr temperature and thermal boundary layer decrease. Fig. 4.7 and 4.8 reflects the behaviour of temperature profile for positive and negative values of heat generation/absorption parameter $\beta$ respectively. The temperature and boundary layer

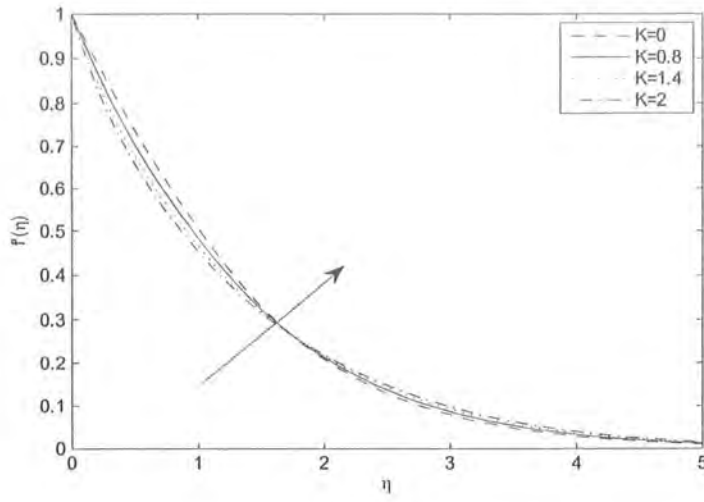increases on increasing $\beta$ (i.e. either negative or positive values of $\beta$).



**Fig. 4.1:** Effects of $K$ on velocity profile when $\beta = 0.1$, $A = 0.1$, $\epsilon = 0.1, \lambda = 0.1$ and $\mathrm{Pr} = 2.0$.
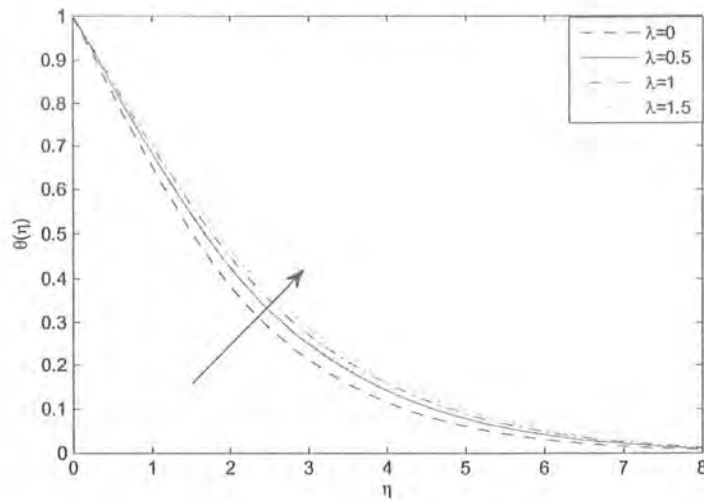


**Fig. 4.2:** Effect of $\lambda$ on temperature profile where $\beta = 0.1$, $A = 0.1$, $\epsilon = 0.1, K = 0.1$ and $\mathrm{Pr} = 2.0$.
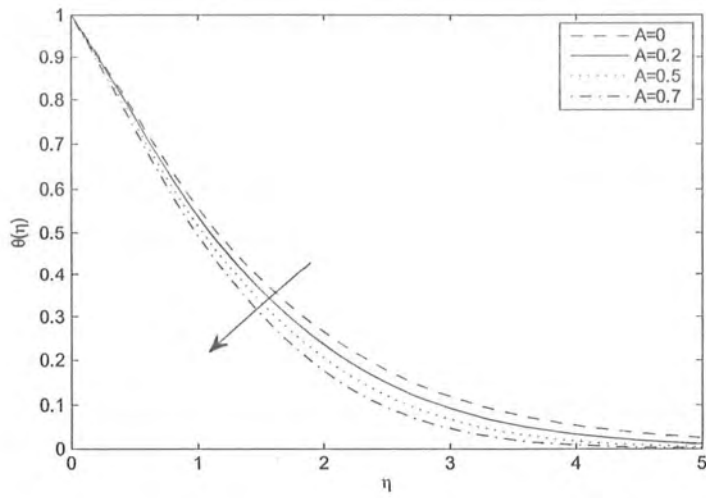
46

**Fig. 4.3**: Effect of $A$ on temperature profile where $\beta = 0.1, \lambda = 0.1$, $\epsilon = 0.1, K = 0.1$ and $\mathrm{Pr} = 2.0$.



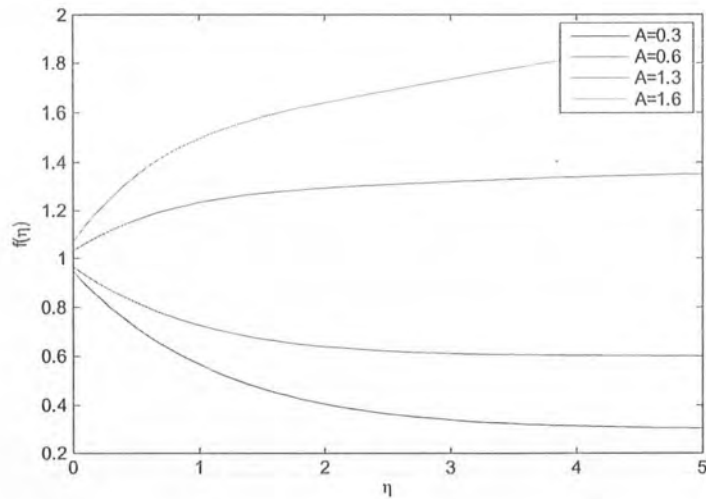**Fig. 4.4**: Effect of $A$ on velocity profile where $\beta = 0.1, \lambda = 0.1$, $\epsilon = 0.1, K = 0.1$ and $\mathrm{Pr} = 2.0$.
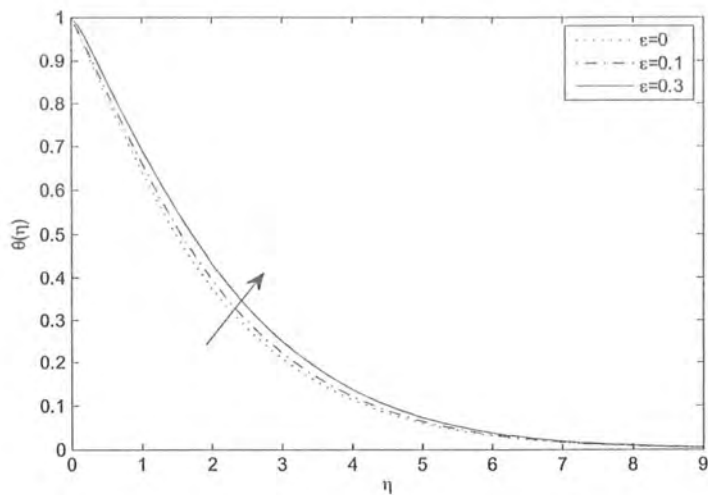
**Fig. 4.5:** Effect of $\epsilon$ on temperature profile where $\beta = 0.1$, $\lambda = 0.1$, $A = 0.1$, $K = 0.1$ and $\mathrm{Pr} = 2.0$.
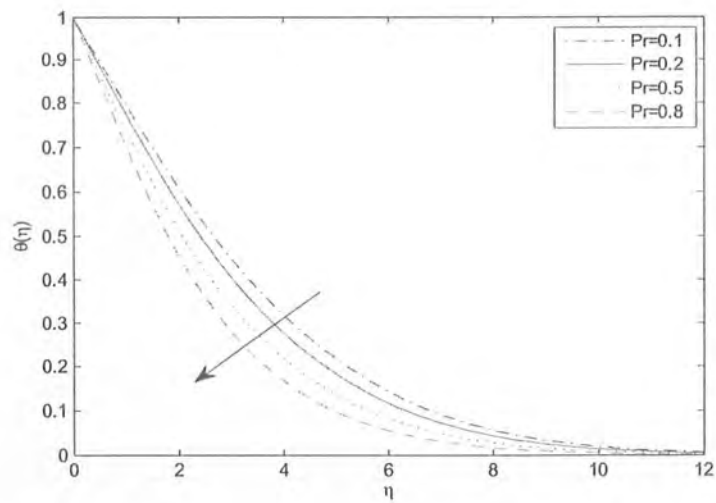


**Fig. 4.6:** Effect of Pr on temperature profile where $\lambda = 0.1$, $A = 0.1$, $K = 0.1$ and $\beta = 0.1$.

**Fig. 4.7**: Effect of $\beta$ on temperature profile where $\lambda = 0.1$, $A = 0.1$, $K = 0.1$ and $\mathrm{Pr} = 2.0$.
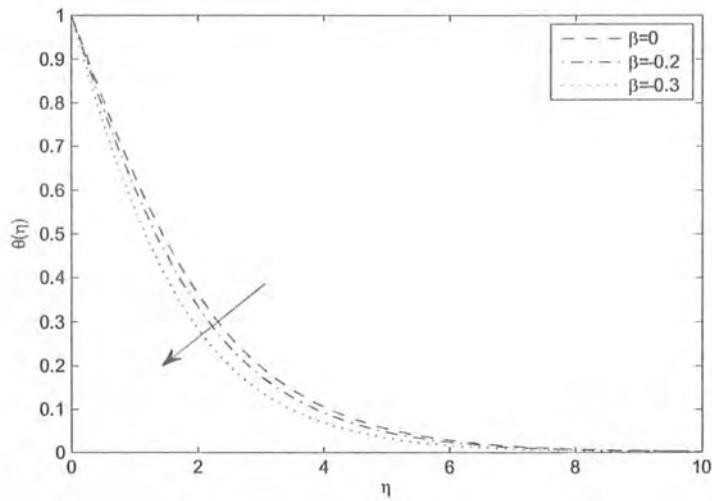


**Fig. 4.8**: Effect of $\beta$ on temperature profile where $\lambda = 0.1$, $A = 0.1$, $K = 0.1$ and $\mathrm{Pr} = 0.2$.
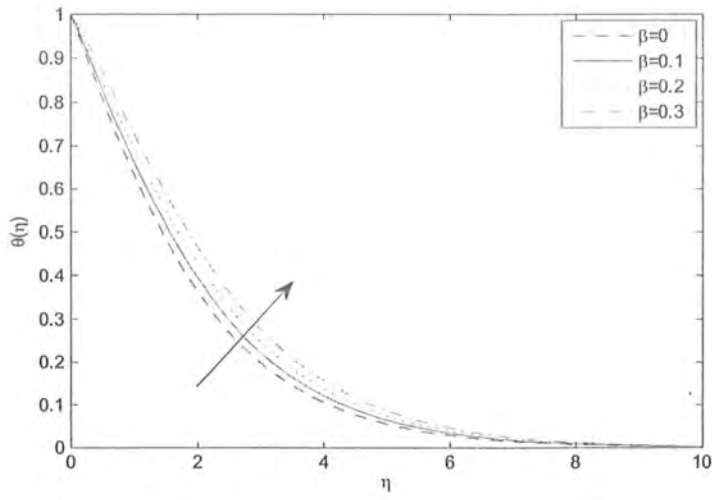
| $\lambda$ | $K$ | $A$ | $-f''(0)$ |
|---|---|---|---|
| 0.1 | 0.1 | 0.1 | 0.63610 |
| | 0.2 | | 0.65112 |
| | 0.3 | | 0.66586 |
| | 0.1 | 0.2 | 0.60201 |
| | | 0.3 | 0.55639 |
| | | 0.4 | 0.50060 |
| 0.2 | | 0.1 | 0.58368 |
| 0.3 | | | 0.53708 |
| 0.4 | | | 0.49936 |

Table 4.4: The variation of $\frac{1}{2}C_f\sqrt{\mathrm{Re}_x}$ with respect to $K$, $A$ and $\lambda$ .

| Pr | $\beta$ | $\epsilon$ | $-\theta'(0)$ |
|---|---|---|---|
| 1 | 0.1 | 0.1 | 0.4044 |
| 1.5 | | | 0.5077 |
| 1.7 | | | 0.5444 |
| 1 | 0.2 | | 0.3523 |
| | 0.4 | | 0.2292 |
| | 0.5 | | 0.1539 |
| | 0.1 | 0.2 | 0.3806 |
| | | 0.4 | 0.3425 |
| | | 0.5 | 0.3267 |

Table 4.5: Temperature gradient $-\theta'(0)$ at the outside surface of cylinder for different values of $\epsilon$, Pr and $\beta$.

$$u\frac{\partial u}{\partial x} + v\frac{\partial u}{\partial r} = U_e\frac{\partial U_e}{\partial x} + \nu\left(\frac{\partial^2 u}{\partial r^2} + \frac{1}{r}\frac{\partial u}{\partial r}\right) - \frac{\sigma B_0^2 u}{\rho}, \tag{5.2}$$

$$u\frac{\partial T}{\partial x} + v\frac{\partial T}{\partial r} = \frac{1}{\rho c_p}\frac{\partial}{\partial r}\left(k\left(T\right)r\frac{\partial T}{\partial r}\right) + \frac{Q}{\rho c_p}(T - T_\infty), \tag{5.3}$$

By inserting boundary layer conditions

$$u = U_w = ax, \quad v = 0, \quad T = T_w \quad \text{at } r = R, \tag{5.4}$$

$$u \to U_e = bx, \quad T \to T_\infty \quad \text{as } r \to \infty. \tag{5.5}$$

In the above equations $\beta_T$ represent thermal expansion coefficient, $Q$ represent heat added or removed from the fluid, $\nu$ represent kinematic viscosity, $\rho$ represent density, $c_p$ represent specific heat, $k\left(T\right)$ represent variable thermal conductivity, $T$ and $T_\infty$ are the temperatures of the fluid and surroundings respectively.

Using the similarity transformations

$$\eta = \sqrt{\frac{a}{\nu}}\left(\frac{r^2 - R^2}{2R}\right), \quad \psi = \sqrt{\nu a}xRf\left(\eta\right), \tag{5.6}$$

$$u = axf'\left(\eta\right), \quad v = -\sqrt{\nu a}\frac{R}{r}f\left(\eta\right), \quad \theta\left(\eta\right) = \frac{T - T_\infty}{T_w - T_\infty}. \tag{5.7}$$

Equation (5.1) is identically satisfied while Eqs. $(5.2 - 5.3)$ take the form

$$(1 + 2K\eta)f''' + ff'' - \left(f'\right)^2 + 2Kf'' + A^2 + H_a^2(A - f') + \beta\theta = 0, \tag{5.8}$$

$$(1 + \epsilon\theta)\left(1 + 2K\eta\right)\theta'' + \epsilon\left(1 + 2K\eta\right)\theta'^2 + 2\left(1 + \epsilon\theta\right)K\theta' + \Pr f\theta' + \Pr\beta\theta = 0, \tag{5.9}$$

and the boundary conditions $(5.4 - 5.5)$ are modified to

$$f(0) = 0, \quad f'(0) = 1, \quad f'(\infty) = A, \tag{5.10}$$

$$\theta\left(0\right) = 1, \quad \theta\left(\infty\right) = 0, \tag{5.11}$$

Where $K$, $A$, $\beta$, $\epsilon$, $H_a$ and Pr denotes curvature parameter, stretching ratio parameter, heat generation/absorption, small temperature parameter, Hartmann number and Prandtl number which are given by

$$K = \frac{1}{R}\sqrt{\frac{\nu}{a}}, \ \ \mathrm{Pr} = \frac{\mu c_p}{k_\infty}, \ A = \frac{b}{a}, \tag{5.12}$$

$$\beta = \frac{Q}{\rho c_p U_0}, \ H_a^2 = \frac{\sigma B_0^2}{\rho a}. \tag{5.13}$$

## 5.3   Homotopic solutions

Homotopy analysis method depend upon the initial guesses ($f_0$, $\theta_0$) and linear operators ($L_f$, $L_\theta$) which are given as

$$f_0(\eta) = A\eta + (1-A)(1-\exp(-\eta)), \quad \theta_0(\eta) = \exp(-\eta), \tag{5.14}$$

$$L_f(\eta) = \frac{d^3 f}{d\eta^3} - \frac{df}{d\eta}, \quad L_\theta(\eta) = \frac{d^2\theta}{d\eta^2} - \theta, \tag{5.15}$$

with

$$L_f[C_1 + C_2 * \exp(-\eta)] = 0, \tag{5.16}$$

$$L_\theta[C_3 * \exp(-\eta)] = 0, \tag{5.17}$$

where $C_i$ ($i = 1 - 3$) are the arbitrary constants.

### 5.3.1   Zeroth-order problem

$$(1-p) L_f \left[ \widehat{f}(\eta; p) - f_0(\eta) \right] = p\hbar_f N_f \left[ \widehat{f}(\eta; p) \right], \tag{5.18}$$

$$(1-p) L_\theta \left[ \widehat{\theta}(\eta; p) - \theta_0(\eta) \right] = p\hbar_\theta N_\theta \left[ \widehat{\theta}(\eta; p), \widehat{f}(\eta; p) \right], \tag{5.19}$$

$$\widehat{f}(0; p) = 0, \quad \widehat{f}'(0; p) = 1, \quad \widehat{f}'(\infty; p) = A, \tag{5.20}$$

$$\widehat{\theta}(0; p) = 1, \quad \widehat{\theta}(\infty; p) = 0, \tag{5.21}$$

$$N_f\left[\widehat{f}(\eta,p)\right] = (1+2K\eta)\frac{\partial^3\widehat{f}(\eta;p)}{\partial\eta^3} + \widehat{f}(\eta;p)\frac{\partial^2\widehat{f}(\eta;p)}{\partial\eta^2} - \left(\frac{\partial\widehat{f}(\eta;p)}{\partial\eta}\right)^2$$
$$+2K\frac{\partial^2\widehat{f}(\eta;p)}{\partial\eta^2} + H^2a(A - \frac{\partial\widehat{f}(\eta;p)}{\partial\eta}) + A^2, \tag{5.22}$$

$$N_\theta\left[\widehat{\theta}(\eta;p),\widehat{f}(\eta;p)\right] = \left(1+\epsilon\widehat{\theta}(\eta,p)\right)(1+2K\eta)\frac{\partial^2\widehat{\theta}(\eta,p)}{\partial\eta^2}$$
$$+\epsilon(1+2K\eta)\left(\frac{\partial\widehat{\theta}(\eta,p)}{\partial\eta}\right)^2 + 2\left(1+\epsilon\widehat{\theta}(\eta,p)\right)K\frac{\partial\widehat{\theta}(\eta,p)}{\partial\eta}$$
$$+\Pr\left(\widehat{f}(\eta;p)\frac{\partial\widehat{\theta}(\eta;p)}{\partial\eta} + \beta\widehat{\theta}(\eta,p)\right) \tag{5.23}$$

where $p \in [0,1]$ .

### 5.3.2  mth-order deformation problems

$$L_f\left[f_m(\eta) - \chi_m f_{m-1}(\eta)\right] = \hbar_f\mathcal{R}_m^f(\eta), \tag{5.24}$$

$$L_\theta\left[\theta_m(\eta) - \chi_m\theta_{m-1}(\eta)\right] = \hbar_\theta\mathcal{R}_m^\theta(\eta), \tag{5.25}$$

$$f_m(0) = f_m'(0) = f_m'(\infty) = 0, \tag{5.26}$$

$$\theta_m(0) = \theta_m(\infty) = 0, \tag{5.27}$$

$$\mathcal{R}_m^f(\eta) = (1+2K\eta)f_{m-1}'''(\eta) + 2Kf_{m-1}'' + \sum_{k=0}^{m-1}\left[f_{m-1-k}f_k'' - f_{m-1-k}'f_k'\right]$$
$$+Ha^2(1-\chi_m)\left(A(1-\chi_m) - f_{m-1}'\right) + A^2(1-\chi_m), \tag{5.28}$$

$$\mathcal{R}_m^\theta(\eta) = (1+2K\eta)\left(\theta_{m-1}'' + \epsilon\sum_{k=0}^{m-1}\theta_{m-1-k}\theta_k''\right) + \epsilon(2+2K\eta)\sum_{k=0}^{m-1}\theta_{m-1-k}'\theta_k'$$
$$+2K\left(\theta_{m-1}' + \epsilon\sum_{k=0}^{m-1}\theta_{m-1-k}\theta_k'\right) + \Pr\left(\sum_{k=0}^{m-1}f_{m-1-k}\theta_k' + \beta\theta_{m-1}\right), \tag{5.29}$$

$$\chi_m = \begin{cases} 0, & m \leq 1 \\ 1, & m > 1 \end{cases}. \tag{5.30}$$

For $p = 0$, 1, we can write

$$\widehat{f}(\eta; 0) = f_0(\eta), \quad \widehat{f}(\eta; 1) = f(\eta), \tag{5.31}$$

$$\widehat{\theta}(\eta; 0) = \theta_0(\eta), \quad \widehat{\theta}(\eta; 1) = \theta(\eta) \tag{5.32}$$

By Taylor's series we have

$$\widehat{f}(\eta; p) = f_0(\eta) + \sum_{m=1}^{\infty} f_m(\eta) p^m, \quad f_m(\eta) = \frac{1}{m!} \frac{\partial^m \widehat{f}(\eta; p)}{\partial p^m} \bigg|_{p=0}, \tag{5.33}$$

$$\widehat{\theta}(\eta; p) = \theta_0(\eta) + \sum_{m=1}^{\infty} \theta_m(\eta) p^m, \quad \theta_m(\eta) = \frac{1}{m!} \frac{\partial^m \widehat{\theta}(\eta; p)}{\partial p^m} \bigg|_{p=0}. \tag{5.34}$$

The value of auxiliary parameter is chosen so properly such that series (5.33) and (5.34) converge at $p = 1$ i.e.

$$f(\eta) = f_0(\eta) + \sum_{m=1}^{\infty} f_m(\eta), \tag{5.35}$$

$$\theta(\eta) = \theta_0(\eta) + \sum_{m=1}^{\infty} \theta_m(\eta). \tag{5.36}$$

The general solutions are given by

$$f_m(\eta) = f_m^{\star}(\eta) + C_1 + C_2 e^{-\eta}, \tag{5.37}$$

$$\theta_m(\eta) = \theta_m^{\star}(\eta) + C_3 e^{-\eta}, \tag{5.38}$$

$C_f$ Skin friction and $Nu_x$ local Nusselt number can be defined as

$$C_f = \frac{\tau_w}{\rho u_w^2}, \qquad Nu_x = \frac{x q_w}{k(T_f - T_\infty)}, \tag{5.39}$$

$$\tau_w = \mu \left( \frac{\partial u}{\partial r} \right)_{r=R}, \qquad q_w = -k \left( \frac{\partial T}{\partial r} \right)_{r=R}, \tag{5.40}$$

56

$$C_f \operatorname{Re}_x^{1/2} = f''(0), \qquad Nu_x \operatorname{Re}_x^{-1/2} = -\theta'(0).\tag{5.41}$$

Where $\operatorname{Re}_x = x\sqrt{\frac{a}{\nu}}$.

## 5.4 Convergence of HAM solutions

Homotopy analysis method is applied to find the convergence of desired equations. The convergence of the series solutions depend upon the auxiliary parameter $\hbar$.

| Order of approximations | $-f''(0)$ | $-\theta'(0)$ |
|---|---|---|
| 1 | 0.7287 | 0.5259 |
| 5 | 0.6825 | 0.4174 |
| 7 | 0.6813 | 0.4102 |
| 10 | 0.6808 | 0.4075 |
| 11 | 0.6808 | 0.4073 |
| 12 | 0.6808 | 0.4072 |
| 14 | 0.6808 | 0.4072 |
| 15 | 0.6808 | 0.4073 |
| 16 | 0.6808 | 0.4073 |

Table 5.1. Convergence table when $K = 0.2$, $\beta = 0.1$, $A = 0.1$, $\epsilon = 0.1$, $\lambda = 0.1$ and $\Pr = 2.0$.

## 5.5 Shooting method

In this section Shooting method is applied to obtain numerical solution of given governing differential equations. First the given nonlinear ordinary differential equations are reduced to a system of first order ordinary differential equations. This system is transformed to initial value problems by replacing missing initial conditions with assumed slopes. Using end conditions (i.e. when $\eta \to \infty$) initial conditions are computed through Newton-Raphson method which hit the given target. We can rewrite the dimensionless governing *Eqns.* (5.8) − (5.9) in the form:

$$f''' = \frac{1}{(1 + 2K\eta)}[(f')^2 - ff'' - 2Kf'' - A^2 - H_a^2(A - f')], \quad (5.43)$$

$$\theta'' = \frac{1}{(1 + \epsilon\theta)(1 + 2K\eta)}\left[-\epsilon(1 + 2K\eta)\theta'^2 - 2(1 + \epsilon\theta)K\theta' - \Pr f\theta' - \beta\theta\right]. \quad (5.44)$$

Define a set of new variables

$$y_1 = f, \; y_2 = f', y_3 = f'', y_4 = \theta \; \text{ and } \; y_5 = \theta'. \quad (5.45)$$

By assuming these variables we get:

$$y_1' = y_2, \quad (5.46)$$

$$y_2' = y_3, \quad (5.47)$$

$$y_3' = \frac{1}{(1 + 2K\eta)}[y_2^2 - y_1 y_3 - 2K y_2' - A^2 - H_a^2(A - y_2)], \quad (5.48)$$

$$y_4' = y_5, \quad (5.49)$$

$$y_5' = \frac{1}{(1 + \epsilon y_4)(1 + 2K\eta)}\left[-\epsilon(1 + 2K\eta)y_4^2 - 2(1 + \epsilon\theta)K y_5 - \Pr y_1\, y_5 - \beta y_4\right]. \quad (5.50)$$

In this system of ordinary differential equations prime denotes derivatives w.r.t. $\eta$. The initial conditions are modified to

$y_1(0) = 0, \quad y_2(0) = 1, \quad y_4(0) = 1,$

and the end conditions takes the form $y_2(\eta) \to A, \quad y_4(\eta) \to 0$ when $\eta \to \infty$.

In the above system there are five ordinary differential equations with three initial conditions

and two end conditions. To solve this system by Runge-Kutta-Fehlberg method five initial conditions are required to solve five unknowns that appears in the solution. Three of them are given while two initial guesses are still required. The other two conditions are given for $\eta \to \infty$. An important step is to find the value of $\eta$ at $\infty$ (i.e. $\eta_\infty$) where end conditions are satisfied. The solution procedure starts with initial guess (e.g. $f'(0) = s$) and solve the system of equations to determine the appropriate value of $f''(0)$ and $\theta'(0)$. The process is continued (using Newton-Raphson method) with revised value of $s$ until two successive values of $f''(0)$ and $\theta'(0)$ differ only after the specific number of significant digits. The final value of $\eta$ is considered as $\eta_\infty$ that can be used to calculate the fluid velocity $f'$ and the temperature field $\theta$ for a set of physical parameters. Numerical solution is getting by employing the fifth order Runge-Kutta-Fehlberg method with shooting technique using MATLAB software.

## 5.6 Comparison of HAM and Shooting method

Comparison between numerical solutions obtained through homotopy analysis method and shooting method are presented in tables $(5.2 - 5.3)$. In the solution computed by homotopy analysis method 16 order of approximations has been achieved (see table 5.1). For shooting method solution is obtained in conjunction with Fehlberg method.

| | $H_a = 0.3$ | | $H_a = 0.6$ | | $H_a = 0.8$ | |
|---|---|---|---|---|---|---|
| $K$ | $HAM$ | $Shooting\ method$ | $HAM$ | $Shooting\ method$ | $HAM$ | $Shooting\ method$ |
| 0.1 | 0.731 | 0.730 | 0.806 | 0.804 | 0.876 | 0.872 |
| 0.2 | 0.748 | 0.749 | 0.823 | 0.822 | 0.892 | 0.892 |
| 0.3 | 0.767 | 0.768 | 0.841 | 0.841 | 0.911 | 0.911 |
| 0.4 | 0.785 | 0.786 | 0.861 | 0.860 | 0.931 | 0.931 |
| 0.5 | 0.805 | 0.805 | 0.879 | 0.879 | 0.994 | 0.990 |

Table 5.2: Comparison of HAM solution and numerical solution obtained by using shooting method for MHD parameter $H_a$ when $\Pr = 1$, $\beta = 0.2$, $A = 1.1$, and $\epsilon = 0.1$.

In table 5.2 the solutions are calculated for values of curvature parameter $H_a$=0.3, 0.6 and 0.5 when curvature parameter $K$=0.1, 0.2, 0.3, 0.4 and 0.5. On comparing both solutions it is observed that they have good agreement.

| | Pr = 0 | | Pr = 0.5 | | Pr = 0.7 | |
|---|---|---|---|---|---|---|
| $K$ | *HAM* | *Shooting method* | *HAM* | *Shooting method* | *HAM* | *Shooting method* |
| 0.1 | 1.000 | 1.000 | 1.000 | 1.000 | 1.000 | 1.000 |
| 0.2 | 0.960 | 0.955 | 0.960 | 0.955 | 0.958 | 0.945 |
| 0.3 | 0.922 | 0.922 | 0.922 | 0.953 | 0.918 | 0.925 |
| 0.4 | 0.885 | 0.865 | 0.885 | 0.851 | 0.880 | 0.858 |
| 0.5 | 0.850 | 0.825 | 0.850 | 0.815 | 0.842 | 0.804 |

**Table 5.3:** Comparison of HAM solution and numerical solution obtained by using shooting method for Prandtl number parameter Pr when $K = 0.2$, $\lambda = 0.1$, $\beta = 0.2$, $A = 0.1$ and $\epsilon = 0.1$.

In table 5.3 the solutions are calculated for two values of curvature parameter Pr=0, 0.5 and 0.7 when curvature parameter $K$=0.1, 0.2, 0.3, 0.4 and 0.5. On comparing both solutions it is observed that they have good agreeme

## 5.7  Results and discussion

The graphical results of velocity field and temperature field are discussed by taking variation in involved physical parameters. Fig. 5.1 is plotted to see the behavior of velocity on varying curvature parameter $K$. It can be seen that with the increase of curvature parameter $K$ velocity decreases near the plate while increases far away from the plate. Because by increasing curvature parameter $K$, radius of curvature decreases which implies that the area of cylinder decreases. Thus less resistance is offered by the cylinder therefore velocity of the fluid increases. Fig. 5.2 is plotted to observe the behaviour of velocity field when MHD parameter $H_a$ varies. On increasing MHD parameter $H_a$ velocity of the fluid increases. The effect of variation of stretching ratio parameter $A$ on velocity is sketched in Fig. 5.3. Fig. 5.4 is dedicated to see the effects of

variation of curvature parameter $K$ on $f'$. It is observed that temperature increases with an increase in curvature parameter. Fig. 5.5 sketched to notice the influence of stretching ratio parameter $A$ on temperature field. On increasing stretching ratio parameter $A$ temperature field decreases. Fig. 5.6 shows the behavior of small parameter $\epsilon$ on temperature field which clarify that temperature increases as we increase the small parameter $\epsilon$. The contribution of Prandtl number Pr on temperature field is sketched through Fig. 5.7, which clarify that on increasing Prandtl number Pr temperature decreases. Fig. 5.8 is plotted to see the bahaviour of heat generation/absorption parameter $\beta$ on temperature field and observed that temperature and thermal boundary layer increase with an increase in heat generation/absorption $\beta$.
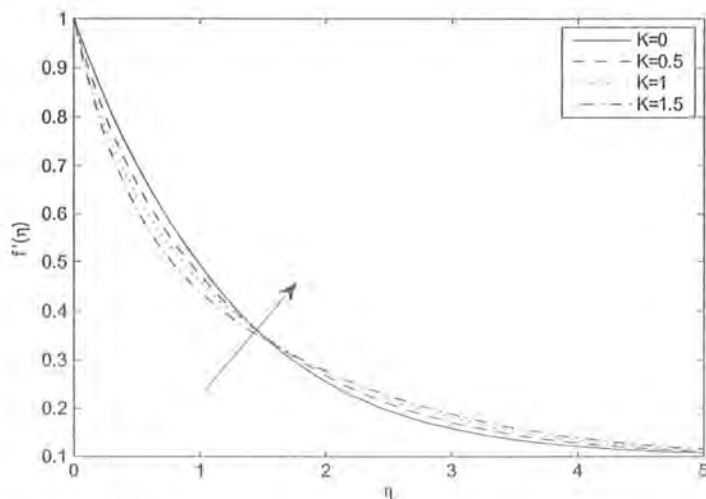


Fig 5.1: Effect of $K$ on velocity profile where $A = 0.1$, $\beta = 0.2$, $H_a = 0.1$, $\epsilon = 0.1$ and Pr $= 1$.
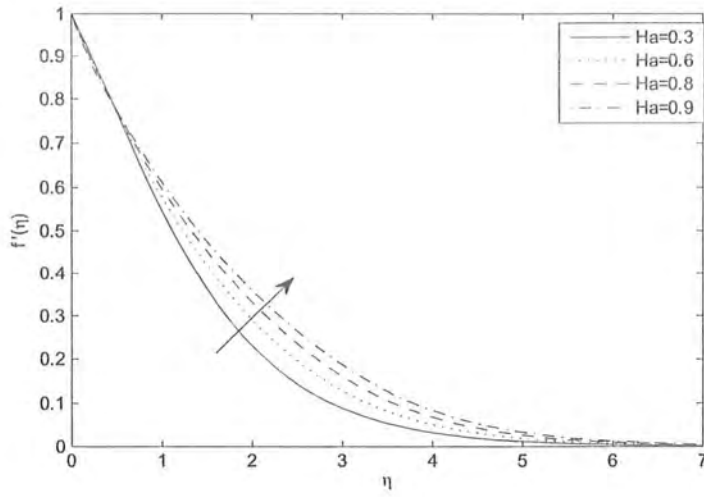
**Fig 5.2:** Effect of $H_a$ on velocity profile where $K = 0.1$, $\beta = 0.2$, $A = 0.1$, $\epsilon = 0.1$ and $\Pr = 1$.
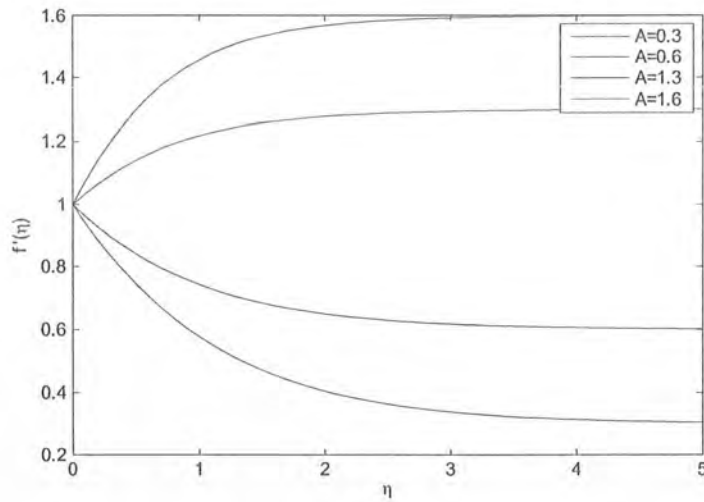


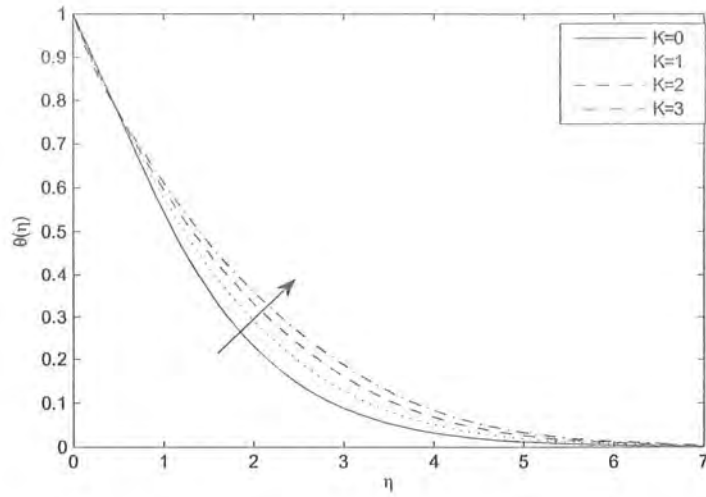**Fig 5.3**: Effect of $A$ on velocity profile where $K = 0.1$, $\beta = 0.2$, $H_a = 0.1$, $\epsilon = 0.1$ and $\Pr = 2.0$.

62

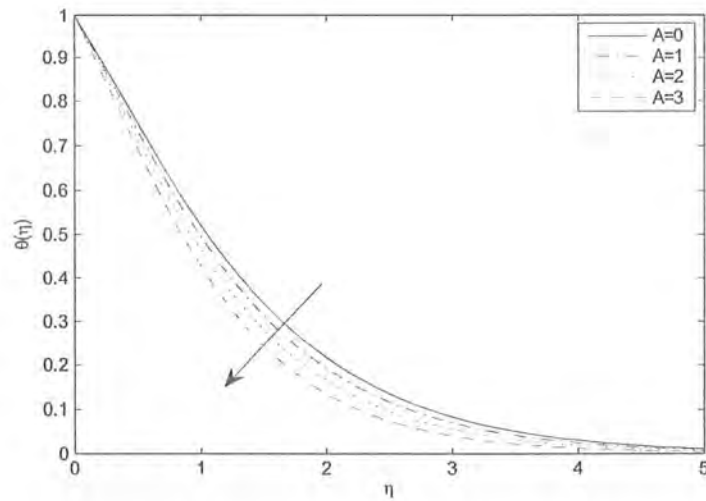**Fig 5.4**: Effect of $K$ on temperature profile where $A = 0.1$, $\beta = 0.2$, $H_a = 0.1$, $\epsilon = 0.1$ and $\mathrm{Pr} = 1$.



**Fig 5.5**: Effect of $A$ on temperature profile where $K = 0.1$, $\beta = 0.2$, $H_a = 0.1$, $\epsilon = 0.1$ and $\mathrm{Pr} = 1$.

63

**Fig 5.6**: Effect of $\epsilon$ on temperature profile where $K = 0.1$, $\beta = 0.2$, $H_a = 0.1$, $A = 0.1$ and $\text{Pr} = 1$.



**Fig 5.7**: Effect of Pr on temperature profile where $K = 0.1$, $\beta = 0.2$, $H_a = 0.1$, $\epsilon = 0.1$ and $A = 0.1$.
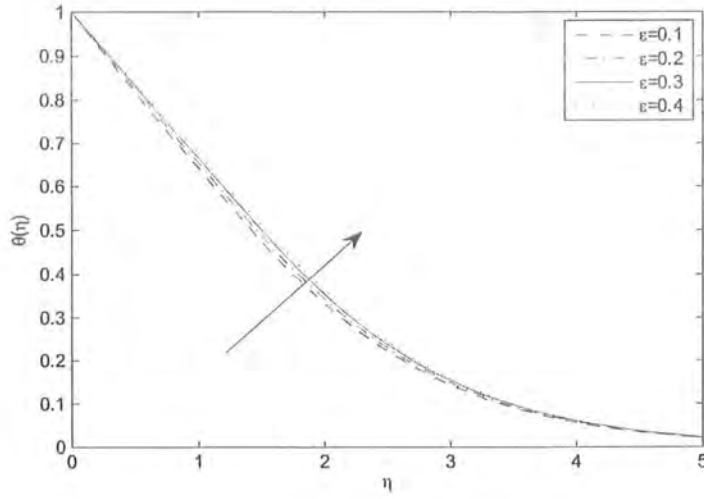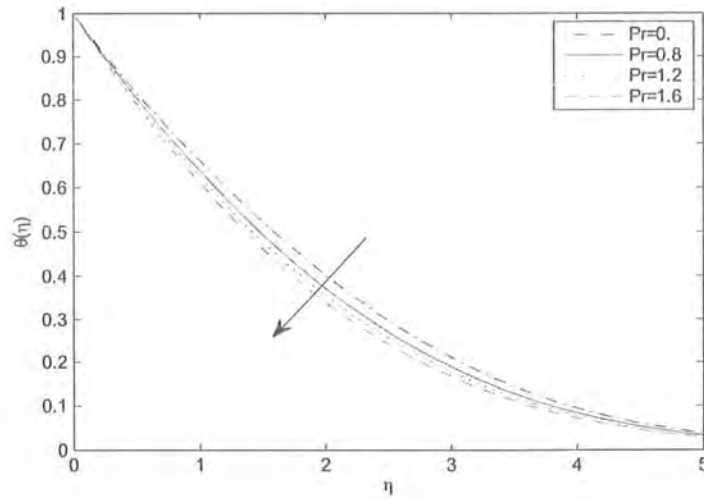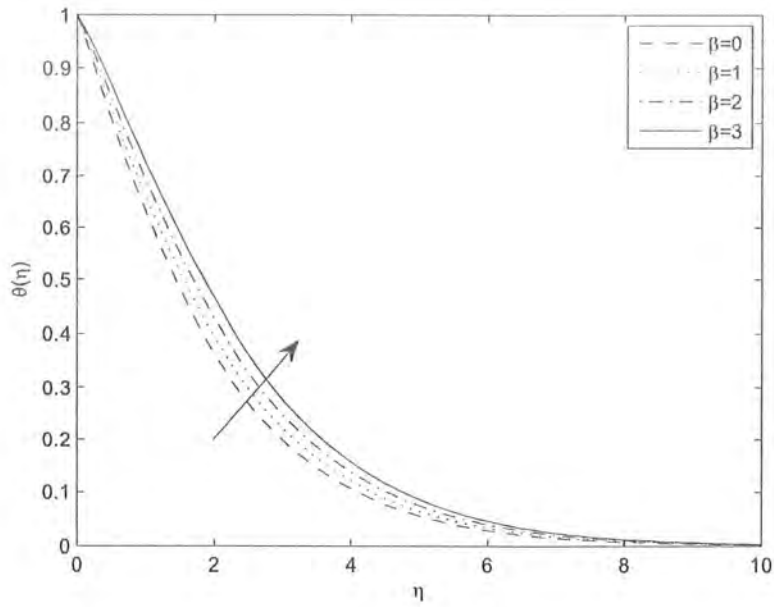
**Fig 5.8:** Effect of $\beta$ on temperature profile where $K = 0.1$, $A = 0.1$, $H_a = 0.1$, $\epsilon = 0.1$ and $\Pr = 1$.

| $H_a$ | $A$ | $K$ | $-f''(0)$ |
|-------|-----|-----|-----------|
| 0.3 | 0.1 | 0.1 | 0.6162 |
| 0.6 |     |     | 0.7415 |
| 0.8 |     |     | 0.8712 |
| 0.5 | 0.2 |     | 0.6559 |
|     | 0.3 |     | 0.6108 |
|     | 0.4 |     | 0.5551 |
|     | 0.1 | 0.2 | 0.7714 |
|     |     | 0.3 | 0.8577 |
|     |     | 0.4 | 0.9490 |

**Table 5.4:** The Skin friction $\frac{1}{2}C_f\sqrt{\mathrm{Re}_x}$ when $K$, $A$ and $H_a$ varies.

65

| Pr | $\epsilon$ | $\beta$ | $-\theta'(0)$ |
|----|----|----|----|
| 1 | 0.1 | 0.2 | 0.4895 |
| | | 0.3 | 0.4606 |
| | | 0.4 | 0.4313 |
| 1.2 | | 0.1 | 0.5276 |
| 1.3 | | | 0.5325 |
| 1.4 | | | 0.5374 |
| 1 | 0.2 | | 0.4747 |
| | 0.3 | | 0.4197 |
| | 0.4 | | 0.3461 |

**Table 5.5:** Temperature gradient $-\theta'(0)$ at the outside surface of cylinder for different values of $\epsilon$, $Pr$ and $\beta$.

Reading the **Table 5.4** the Reynold number increases, $|C_f|$ decreases. We know that increases the $Re_x$ viscous forces start reducing so $|C_f|$ reduces. Here we increase the MHD parameter $H_a$ the $|C_f Re_x|$ decreases. As we increase the stretching ratio parameter $A$ the skin friction $|C_f Re_x|$ decreases. But in the case of curvature parameter $K$ the $|C_f Re_x|$ increases.

Reading the **Table 5.5**, we conclude that decreasing viscosity is due to increase in Reynolds number. For the case of stretching cylinder decreasing viscosity causing increase in rate of convectional heat transfer.

## 5.8 Concluding remarks

The main analysis

- The effect of curvature parameter $K$ on velocity and temperature fields are same i.e on increasing curvature parameter both velocity field and temperature field increase .

- Temperature field increases for the positive number of $\beta$ and decreases for the negative values of $\beta$.

- Increase of small parameter $\epsilon$ causes increase in temperature field.

- Effects of stretching ratio parameter $A$ on velocity and temperature fields are opposite.

# Chapter 6

# Stagnation Point Flow over a Stretching Cylinder with Variable Viscosity and Heat Generation/absorption

## 6.1 Introduction

In this chapter we discuss the behavior of viscous fluid close to stagnation point over a stretching cylinder by taking variable thermal viscosity. The effects of heat generation/absorption are also encountered in this work. Numerical results of momentum equation and energy equation obtained through Homotopy Analysis Method (HAM) and Shooting method are compared through table. Graphical results of variation in physical parameters upon velocity and temperature fields are also presented.

## 6.2 Mathematical formulation

By taking steady, incompressiable and two-dimensional boundary layer flow with variable viscosity over a stretching cylinder in the area of stagnation point with heat generation/absorptions.

The governing equations are

$$\frac{\partial (ru)}{\partial x} + \frac{\partial (rv)}{\partial r} = 0, \tag{6.1}$$

$$u\frac{\partial u}{\partial x} + v\frac{\partial u}{\partial r} = U_e\frac{\partial U_e}{\partial x} + \frac{1}{r\rho_0}\frac{\partial}{\partial r}(\mu r\frac{\partial u}{\partial r}), \tag{6.2}$$

$$u\frac{\partial T}{\partial x} + v\frac{\partial T}{\partial r} = \frac{\alpha}{r\rho c_p}\frac{\partial}{\partial r}\left(r\frac{\partial T}{\partial r}\right) + \frac{Q}{\rho c_p}(T - T_\infty), \tag{6.3}$$

subjected to the boundary conditions

$$u = U_w = ax, \quad v = 0, \quad T = T_w \quad \text{at } r = R, \tag{6.4}$$

$$u \to U_e = bx, \quad T \to T_\infty \quad \text{as } r \to \infty. \tag{6.5}$$

In the above expressions $Q$ represent heat added or removed from the fluid, $\nu$ represent kinematic viscosity, $\rho$ represent density, $c_p$ represent specific heat, $\alpha$ represent thermal conductivity, $T$ and $T_\infty$ are the temperature of the fluid and surroundings respectively, $U_w$ is the stretching velocity, $U_e$ is the free stream velocity.

Variation of the viscosity are assumed to be in the form:

$$\mu = \mu_0 e^{-\xi(T - T_0)}, \tag{6.6}$$

where $\mu_0$ is viscosity at slit temperature $T_0$.

Using the following similarity transformation

$$\eta = \sqrt{\frac{a}{\nu}}\left(\frac{r^2 - R^2}{2R}\right), \quad \psi = \sqrt{\nu a}xRf(\eta), \tag{6.7}$$

$$u = axf'(\eta), \quad v = -\sqrt{\nu a}\frac{R}{r}f(\eta), \quad \theta(\eta) = \frac{T - T_\infty}{T_w - T_\infty}. \tag{6.8}$$

Equation (6.1) satisfied identically while Eqs. (6.2) − (6.5 takes the following form

$$(1 - B\theta)[(1 + 2K\eta)f''' + 2Kf'' - (1 + 2K\eta)Bf''\theta'] + ff'' - (f')^2 + A^2 = 0, \tag{6.9}$$

$$(1 + 2K\eta)\theta'' + 2K\theta' + \Pr f\theta' + \Pr\beta\theta = 0, \tag{6.10}$$

69

$$f(0) = 0, \quad f'(0) = 1, \quad f'(\infty) = A, \tag{6.11}$$

$$\theta(0) = 1, \quad \theta(\infty) = 0. \tag{6.12}$$

where $K$, $A$, $\beta$, $B$ and Pr denotes curvature parameter, stretching ratio parameter, heat generation/absorption, variable viscosity and Prandtl number which are given by

$$K = \frac{1}{R}\sqrt{\frac{\nu}{a}}, \quad \Pr = \frac{\mu c_p}{\alpha}, \quad A = \frac{b}{a}, \tag{6.13}$$

$$B = -\xi(T_w - T_0), \quad \beta = \frac{Q}{\rho c_p a}. \tag{6.14}$$

## 6.3   Homotopic solutions

Homotopy analysis method depends upon the initial guesses ($f_0$, $\theta_0$) and linear operators ($L_f$, $L_\theta$) which are given in the forms

$$f_0(\eta) = A\eta + (1-A)(1 - \exp(-\eta)), \quad \theta_0(\eta) = \exp(-\eta), \tag{6.15}$$

$$L_f(\eta) = \frac{d^3 f}{d\eta^3} - \frac{df}{d\eta}, \quad L_\theta(\eta) = \frac{d^2\theta}{d\eta^2} - \theta, \tag{6.16}$$

with

$$L_f[C_1 + C_2 \exp(-\eta)] = 0, \quad L_\theta[C_3 * \exp(-\eta)] = 0, \tag{6.17}$$

where $C_i$ ($i = 1 - 3$) are the arbitrary constants.

### 6.3.1   Zeroth-order problem

$$(1-p) L_f \left[\widehat{f}(\eta; p) - f_0(\eta)\right] = p\hbar_f N_f \left[\widehat{f}(\eta; p)\right], \tag{6.18}$$

$$(1-p) L_\theta \left[\widehat{\theta}(\eta; p) - \theta_0(\eta)\right] = p\hbar_\theta N_\theta \left[\widehat{\theta}(\eta; p), \widehat{f}(\eta; p)\right], \tag{6.19}$$

$$\widehat{f}(0; p) = 0, \quad \widehat{f}'(0; p) = 1, \quad \widehat{f}'(\infty; p) = A, \tag{6.20}$$

70

$$\widehat{\theta}(0;p) = 1, \qquad \widehat{\theta}(\infty;p) = 0, \tag{6.21}$$

$$\begin{aligned}
\dot{N_f}\left[\widehat{f}(\eta,p)\right] &= (1 - B\widehat{\theta}(\eta;p))[(1+2K\eta)\frac{\partial^3 \widehat{f}(\eta;p)}{\partial\eta^3} + 2K\frac{\partial^2 \widehat{f}(\eta;p)}{\partial\eta^2} - (1+2K\eta)B\frac{\partial^2 \widehat{f}(\eta;p)}{\partial\eta^2}\frac{\partial\widehat{\theta}(\eta,p)}{\partial\eta}] \\
&\quad + \widehat{f}(\eta;p)\frac{\partial^2 \widehat{f}(\eta;p)}{\partial\eta^2} - \left(\frac{\partial\widehat{f}(\eta;p)}{\partial\eta}\right)^2 + A^2,
\end{aligned} \tag{6.22}$$

$$N_\theta\left[\widehat{\theta}(\eta;p),\widehat{f}(\eta;p)\right] = (1+2K\eta)\frac{\partial^2\widehat{\theta}(\eta,p)}{\partial\eta^2} + 2K\frac{\partial\widehat{\theta}(\eta,p)}{\partial\eta} + \text{Pr}\begin{pmatrix} \widehat{f}(\eta;p)\frac{\partial\widehat{\theta}(\eta;p)}{\partial\eta} + \\ \beta\widehat{\theta}(\eta,p). \end{pmatrix} \tag{6.23}$$

where $p \in [0,1]$.

### 6.3.2 mth-order deformation problems

$$L_f\left[f_m(\eta) - \chi_m f_{m-1}(\eta)\right] = \hbar_f \mathcal{R}_m^f(\eta), \tag{6.24}$$

$$L_\theta\left[\theta_m(\eta) - \chi_m \theta_{m-1}(\eta)\right] = \hbar_\theta \mathcal{R}_m^\theta(\eta), \tag{6.25}$$

$$f_m(0) = f'_m(0) = f'_m(\infty) = 0, \quad \theta_m(0) = \theta_m(\infty) = 0, \tag{6.26}$$

$$\begin{aligned}
\mathcal{R}_m^f(\eta) &= (1+2K\eta)f_{m-1}'''(\eta) + 2Kf_{m-1}'' - (1+2K\eta)B\sum_{k=0}^{m-1}f_{m-1-k}''\theta_k' - B(1+2Kx) \\
&\quad \sum_{k=0}^{m-1}f_{m-1-k}''\theta_k - 2KB\sum_{k=0}^{m-1}f_{m-1-k}''\theta_k + (1+2Kx)B^2\sum_{k=0}^{m-1}f_{m-1-k}''\theta_{m-1-k}'\theta_k \\
&\quad + \sum_{k=0}^{m-1}\left[f_{m-1-k}f_k'' - f_{m-1-k}'f_k'\right] + A^2(1-\chi_m),
\end{aligned} \tag{6.27}$$

71

$$\mathcal{R}_m^{\theta}(\eta) = (1 + 2K\eta)\left(\theta_{m-1}'' + \epsilon\sum_{k=0}^{m-1}\theta_{m-1-k}\theta_k''\right) + 2K\theta_{m-1}'$$
$$+ \Pr\left(\sum_{k=0}^{m-1} f_{m-1-k}\theta_k' + \beta\theta_{m-1}\right), \tag{6.28}$$

$$\chi_m = \begin{cases} 0, & m \le 1 \\ 1, & m > 1 \end{cases}. \tag{6.29}$$

For $p = 0,1$,

$$\widehat{f}(\eta;0) = f_0(\eta), \quad \widehat{f}(\eta;1) = f(\eta), \tag{6.30}$$

$$\widehat{\theta}(\eta;0) = \theta_0(\eta), \quad \widehat{\theta}(\eta;1) = \theta(\eta). \tag{6.31}$$

By Taylor's series, we have

$$\widehat{f}(\eta;p) = f_0(\eta) + \sum_{m=1}^{\infty} f_m(\eta)p^m, \quad f_m(\eta) = \frac{1}{m!}\frac{\partial^m \widehat{f}(\eta;p)}{\partial p^m}\bigg|_{p=0}, \tag{6.32}$$

$$\widehat{\theta}(\eta;p) = \theta_0(\eta) + \sum_{m=1}^{\infty} \theta_m(\eta)p^m, \quad \theta_m(\eta) = \frac{1}{m!}\frac{\partial^m \widehat{\theta}(\eta;p)}{\partial p^m}\bigg|_{p=0}. \tag{6.33}$$

Auxiliary parameter is chosen such that Eqs (6.32) and (6.33) converge at $p = 1$ i.e.

$$f(\eta) = f_0(\eta) + \sum_{m=1}^{\infty} f_m(\eta), \tag{6.34}$$

$$\theta(\eta) = \theta_0(\eta) + \sum_{m=1}^{\infty} \theta_m(\eta). \tag{6.35}$$

The general solutions are given by

$$f_m(\eta) = f_m^{\star}(\eta) + C_1 + C_2 e^{-\eta}, \tag{6.36}$$

$$\theta_m(\eta) = \theta_m^{\star}(\eta) + C_3 e^{-\eta}, \tag{6.37}$$

$C_f$ Skin friction and $Nu_x$ local Nusselt number can be defined as

$$C_f = \frac{\tau_w}{\rho U_w^2}, \qquad Nu_x = \frac{xq_w}{k(T_f - T_\infty)}, \qquad (6.38)$$

here

$$\tau_w = \mu \left(\frac{\partial u}{\partial r}\right)_{r=R}, \qquad q_w = -k \left(\frac{\partial T}{\partial r}\right)_{r=R}, \qquad (6.39)$$

$$C_f \operatorname{Re}_x^{1/2} = (1 - A\theta)f''(0), \qquad Nu_x \operatorname{Re}_x^{-1/2} = -\theta'(0). \qquad (6.40)$$

Where $\operatorname{Re}_x = x\sqrt{\frac{a}{\nu}}$.

## 6.4 Convergence of HAM solutions

Here Homotopy analysis method is used to get the criteria of convergence for desired solution of given equations. The convergence control parameter $\hbar$ is involved in the series solution. HAM solution depends upon this parameter which basically control the convergence region and rate of approximation. Fig $(6.1 - 6.2)$ are for the $\hbar$-curves $\hbar_f$ and $\hbar_\theta$ are between $-1 \leq \hbar_f \leq -0.2$ and $-1 \leq \hbar_\theta \leq -0.2$.
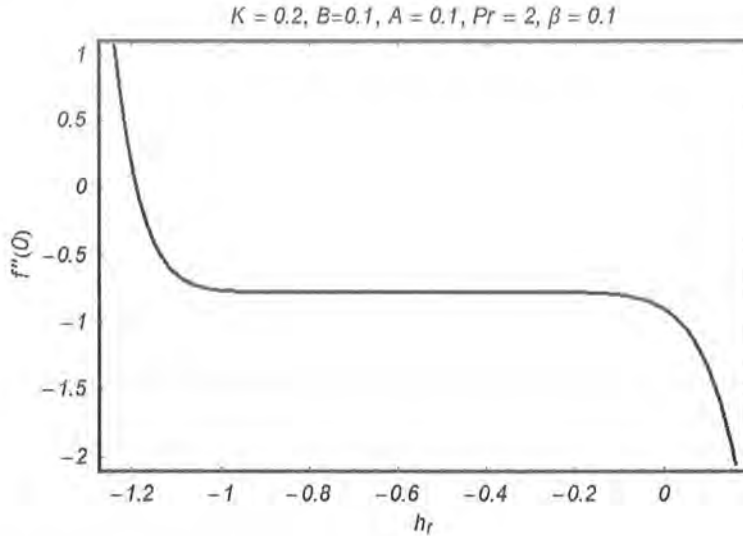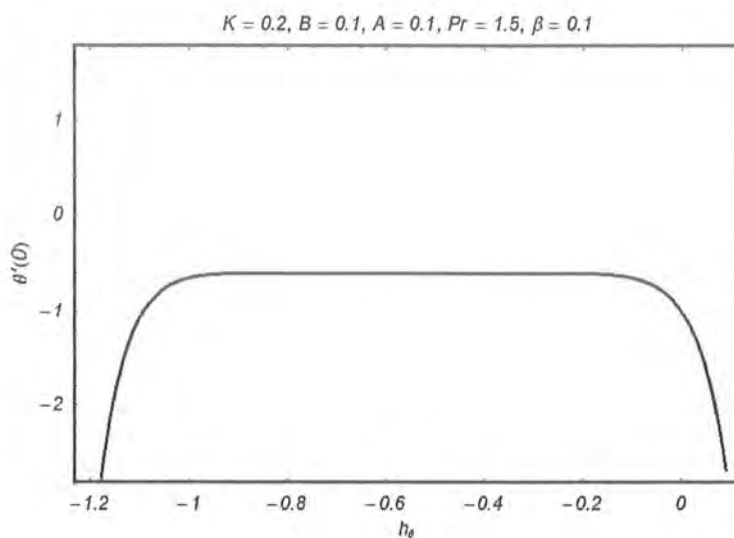


Fig 6.1: $\hbar_f$ for velocity profile.

73

Fig 6.2: $\hbar_\theta$ for temperature profile.

| Order of approximations | $-f''(0)$ | $-\theta'(0)$ |
|---|---|---|
| 1 | 0.79025 | 0.65000 |
| 5 | 0.75167 | 0.57333 |
| 7 | 0.75148 | 0.57762 |
| 8 | 0.75147 | 0.57884 |
| 9 | 0.75147 | 0.57947 |
| 12 | 0.75147 | 0.57946 |
| 13 | 0.75147 | 0.57945 |
| 14 | 0.75147 | 0.57944 |
| 15 | 0.75147 | 0.57944 |

Table 6.1. Convergence table for $K = 0.2$, $\beta = 0.1$, $A = 0.1$, $B = 0.1$ and Pr $= 2.0$.

## 6.5 Shooting method

For the numerical solution by Shooting method the given nonlinear ordinary differential equations are converted to a system of first order ordinary differential equations. The system is transformed to initial value problems by replacing missing initial conditions with slopes.

74

Using end conditions (i.e. when $\eta \to \infty$) initial conditions are computed through Newton-Raphson method which meets the given target. We can rewrite the dimensionless governing Eqs. (6.9) − (6.10) in the following form:

$$f''' = \frac{1}{(2+2K\eta)(1-B\theta)}[-2(1-B\theta)Kf'' + (1-B\theta)(2+2K\eta)Bf''\theta' - ff'' + (f')^2 - A^2], \quad (6.42)$$

$$\theta'' = -\frac{1}{(2+2K\eta)}(2K\theta' + \Pr f\theta' + \Pr \beta\theta). \quad (6.43)$$

Now, we can define the equations with new variables as

$$f_1 = f, \quad f_2 = f', \quad f_3 = f'', \quad f_4 = \theta, \quad f_5 = \theta'. \quad (6.44)$$

The two higher order differential equations and the boundary conditions may be converted to five equivalent first order differential equations. Using above equations

$$\begin{pmatrix} f_1 \\ f_2 \\ f_3 \\ f_4 \\ f_5 \end{pmatrix} = \begin{pmatrix} f_2 \\ f_3 \\ \frac{1}{(1+2K\eta)(1-Bf_4)}[-2(1-Bf_4)Kf_2 + (1-Bf_4)(1+2K\eta)Bf_3f_5 - f_1f_2 + (f_2)^2 - A^2] \\ f_5 \\ -\frac{1}{(1+2K\eta)}(2Kf_5 + \Pr f_1f_5 + \Pr \beta f_4) \end{pmatrix}. \quad (6.45)$$

Here prime denotes the differentiation with respect to $\eta$ and the initial conditions are

$$\begin{pmatrix} f_1 \\ f_2 \\ f_3 \\ f_4 \\ f_5 \end{pmatrix} = \begin{pmatrix} 0 \\ 1 \\ \alpha \\ 1 \\ \beta \end{pmatrix}. \quad (6.46)$$

In the above system there are five ordinary differential equations with three initial conditions

and two end conditions. To solve this system by Runge-Kutta-Fehlberg method five initial conditions are required to solve five unknowns that appears in the solution. Three of them are given while two initial guesses are still required. The other two conditions are given for $\eta \to \infty$. An important step is to find the value of $\eta$ at $\infty$ (i.e. $\eta_\infty$) where end conditions are satisfied. The solution procedure starts with initial guess (e.g. $f'(0) = s$) and solve the system of ordinary differential equations to determine the appropriate value of $f''(0)$ and $\theta'(0)$. The process is continued (using Newton-Raphson method) with revised value of $s$ until two successive values of $f''(0)$ and $\theta'(0)$ differ only after the specific number of significant digits. The final value of $\eta$ is considered as $\eta_\infty$ that can be used to calculate the fluid velocity $f'$ and the temperature field $\theta$ in the boundary layer for a set of physical parameters. Numerical solution is getting by employing the fifth order Runge-Kutta-Fehlberg method with shooting technique using MATLAB software.

## 6.6 Comparison of HAM and Shooting method

Comparison between numerical solutions obtained through homotopy analysis method and shooting method are presented in Fig. 6.3. For shooting method solution is obtained in conjunction with Fehlberg method.
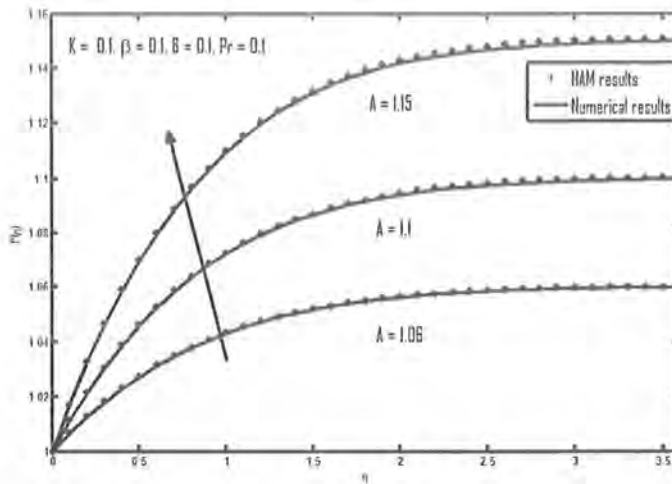


**Fig 6.3**: Comparison of velocity profile obtained through HAM and Shooting Method for different value $A$
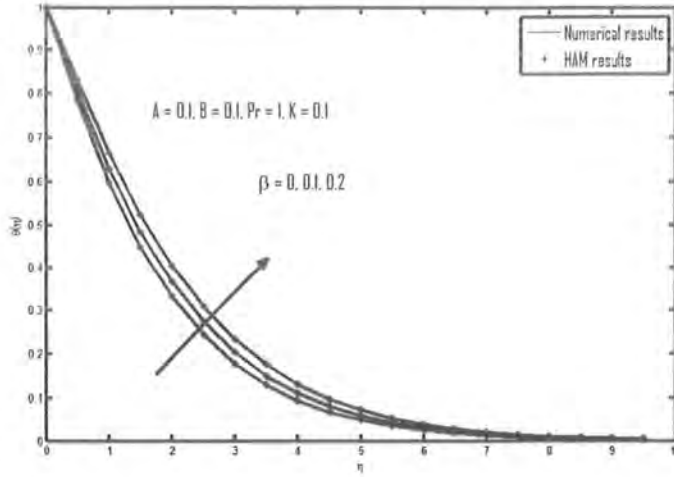
**Fig 6.4**: Comparison of temperature profile obtained through HAM and Shooting method for different value $\beta$.

| | $A = 1.1$ | | $A = 1.2$ | | $A = 1.3$ | | $A = 1.4$ | |
|---|---|---|---|---|---|---|---|---|
| $B$ | $HAM$ | $SM$ | $HAM$ | $SM$ | $HAM$ | $SM$ | $HAM$ | $SM$ |
| 0.1 | 0.1191 | 0.1194 | 0.2439 | 0.2445 | 0.3751 | 0.3753 | 0.5112 | 0.5114 |
| 0.2 | 0.1165 | 0.1169 | 0.2387 | 0.2393 | 0.3667 | 0.3670 | 0.4997 | 0.4999 |
| 0.3 | 0.1364 | 0.1370 | 0.2321 | 0.2325 | 0.3560 | 0.3563 | 0.4848 | 0.4851 |
| 0.4 | 0.1091 | 0.1098 | 0.2428 | 0.2434 | 0.3432 | 0.3436 | 0.4670 | 0.4675 |

**Table 6.2** Comparison of HAM and shooting method (SM) results.

| | $\beta = 0.1$ | | $\beta = 0.2$ | | $\beta = 0.3$ | | $\beta = 0.4$ | |
|---|---|---|---|---|---|---|---|---|
| Pr | $HAM$ | $SM$ | $HAM$ | $SM$ | $HAM$ | $SM$ | $HAM$ | $SM$ |
| 0.1 | -0.5562 | -0.5564 | -0.5531 | -0.5533 | -0.5496 | -0.5500 | -0.5465 | -0.5468 |
| 0.2 | -0.5641 | -0.5644 | -0.5811 | -0.5816 | -0.5513 | -0.5518 | -0.5449 | -0.5454 |
| 0.3 | -0.5723 | -0.5726 | -0.5626 | -0.5631 | -0.5531 | -0.5537 | -0.5433 | -0.5440 |
| 0.4 | -0.5805 | -0.5809 | -0.5676 | -0.5683 | -0.5560 | -0.5567 | -0.5419 | -0.5427 |

**Table 6.3** Comparison of HAM and shooting method (SM) results.

## 6.7 Results and discussion

The outcome of velocity and temperature field on varying different physical parameters are presented graphically in Figs. $(6.5 - 6.10)$. Comparison of results obtained through two different solution techniques that is HAM and shooting method is presented in Figs. $(6.3 - 6.4)$ and in Tables $(6.1 - 6.2)$. It is observed that the results obtained through HAM and shooting method compares well. Variation in curvature parameter $K$ on velocity field is in Fig 6.5 and we can see that velocity decreases on increasing curvature parameter $K$, this causes less resistance to be offered by the cylinder and hence velocity of the fluid increases. Furthermore, boundary layer is thicker for higher values of curvature parameter $K$, so we can see that velocity of the fluid increases by increasing mixed convection parameter. The characteristics of curvature parameter $K$ on temperature field is shown in Fig. 6.6. It is observed that temperature increases with an increase in curvature parameter $K$. Fig. 6.7 is plotted for the influence of stretching ratio parameter $A$ upon temperature field. In this case we can see that temperature field decreases with an increase in stretching ratio parameter $A$. The behavior of velocity profile due to variation in small parameter $B$ in Fig. 6.8. It is observed that velocity decreases as we increase the small parameter $B$. Fig. 6.9 represent the behavior of temperature field after increasing Prandtl number Pr. Temperature decrease with an increase in Prandtl number. Fig. 6.10 is plotted for temperature field when heat generation/absorption parameter $\beta$ increases. It is clear from the figure that with an increase in heat generation/absorption $\beta$ temperature and thermal boundary layer increases.
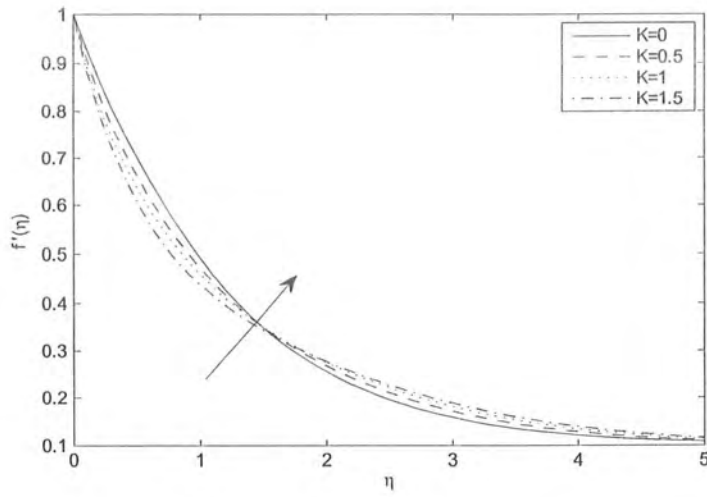
**Fig 6.5**: Effect of $K$ for velocity profile where $B = 0.1$, $\mathrm{Pr} = 1$, $A = 0.1$, $\beta = 0.1$.
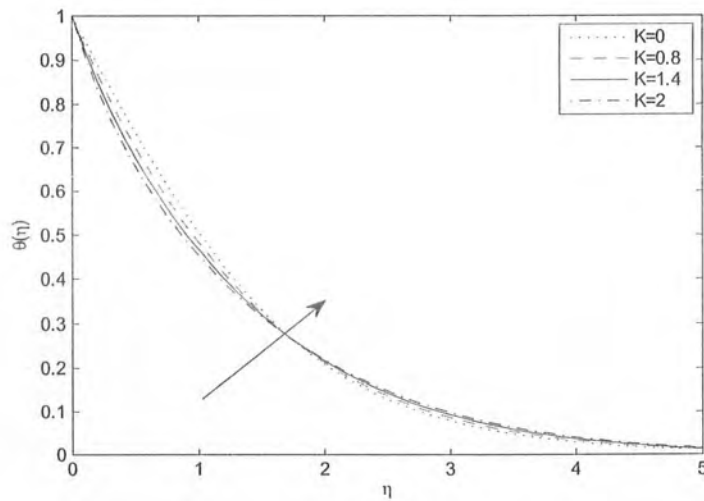


**Fig 6.6**: Effect of $K$ on temperature profile where $B = 0.1, \mathrm{Pr} = 1, A = 0.1, \beta = 0.1$.
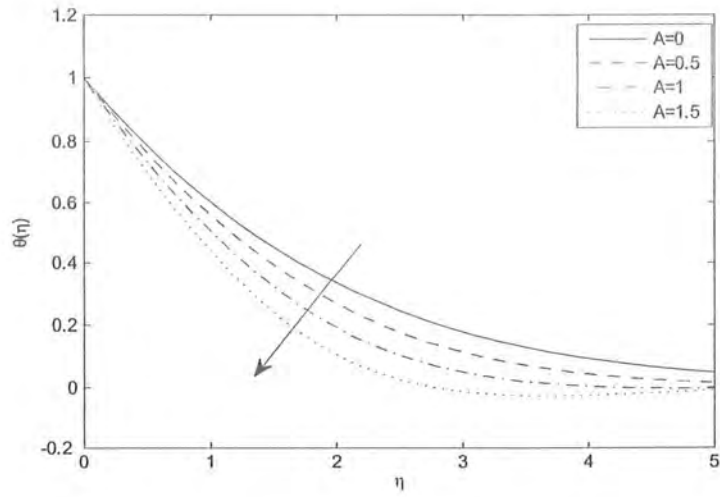
**Fig 6.7**: Effect of $A$ for temperature profile where $B = 0.1$, $\mathrm{Pr} = 1, K = 0.1, \beta = 0.1$.
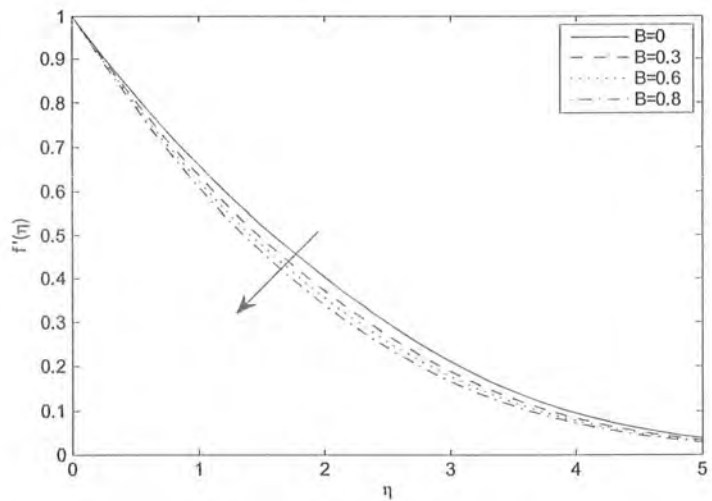


**Fig 6.8**: Effect of $B$ for velocity profile where $K = 0.1, \mathrm{Pr} = 1, A = 0.1, \beta = 0.1$.
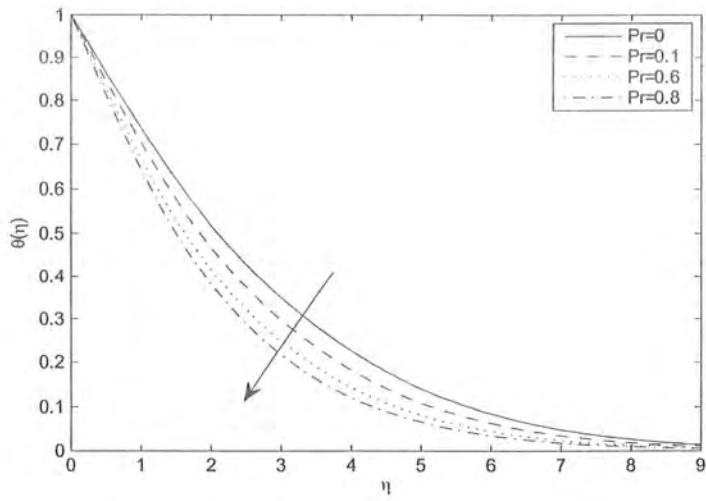
**Fig 6.9**: Effect of Pr for temperature profile where $B = 0.1, K = 0.1, A = 0.1, \beta = 0.1$.
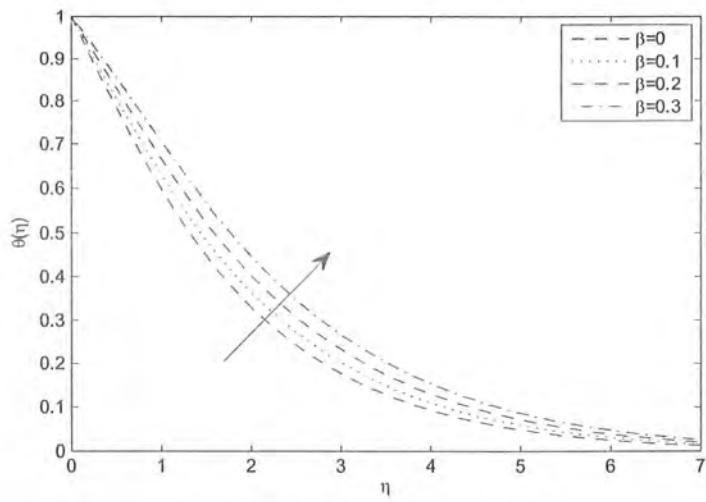


**Fig 6.10**: Effect of $\beta$ for temperature profile when $B = 0.1, \mathrm{Pr} = 1, A = 0.1, K = 0.1$.

| $K$ | $B$ | $A$ | $-f''(0)$ |
|---|---|---|---|
| 0.1 | 0.1 | 0.1 | 0.6763 |
| 0.2 | | | 0.6930 |
| 0.3 | | | 0.7094 |
| 0.1 | 0.2 | | 0.7277 |
| | 0.3 | | 0.7904 |
| | 0.4 | | 0.8690 |
| | 0.1 | 0.2 | 0.5693 |
| | | 0.3 | 0.4606 |
| | | 0.4 | 0.3556 |

**Table 6.4:** The values of Skin friction $\frac{1}{\sqrt{2}}C_f\sqrt{\text{Re}_x}$ on varying $K$, $B$ and $A$.

| Pr | $\beta$ | $-\theta'(0)$ |
|---|---|---|
| 1.2 | 0.1 | 0.4371 |
| 1.3 | | 0.4596 |
| 1.4 | | 0.4813 |
| 1.1 | 0.2 | 0.3979 |
| | 0.3 | 0.2960 |
| | 0.4 | 0.1576 |

**Table 6.5:** The effects of Pr and $\beta$ on temperature gradient $-\theta'(0)$ at the outer surface of cylinder.

Since $C_f \propto Re_x^{-\frac{1}{2}}$ we can see that as Reynold number increases, $|C_f|$ decreases (see **Table 6.4**). Clearly we can see that when $Re_x$ increases the viscous forces start reducing, in turn $|C_f|$ reduces. Here as we increase the variable viscosity parameter $B$, $|C_f \, Re_x|$ decreases. Also when

we increase the stretching ratio parameter $A$, $|C_f \operatorname{Re}_x|$ decreases. But in the case of curvature parameter $K$, $|C_f \operatorname{Re}_x|$ increases.

From **Table 6.5**, we know that $Nu_x^2 \propto Re_x$. We can say that on increasing $Re_x = \frac{Ux}{v}$ viscosity decreases in turn increase in magnitude of rate of convectional heat transfer for stretching cylinder. Also, Prandtle number Pr is responsible for the coefficient of convectional heat and heat generation/absorption parameter $\beta$.

## 6.8 Concluding remarks

The important findings of this work are as follows

- Influence curvature parameter $K$ upon velocity and temperature fields are same i.e both velocity and temperature fields increases with increasing curvature parameter.

- On increasing the values of Prandtl number Pr and heat generation/absorption parameter $\beta$ temperature field increases.

- With the increase of small parameter $B$ velocity field decreases.

- Temperature field decreases on increasing stretching ratio parameter $A$.

# Chapter 7

# MHD Stagnation Point Flow over a Stretching Cylinder with Variable Viscosity and Joule Heating Effect

## 7.1 Introduction

In this chapter stagnation point flow upon stretching cylinder having variable viscosity with MHD is discussed. The effects of joule heating are also encountered. The problem is solved through HAM with Shooting method, and the computed results are compared graphically. Skin friction coefficient and local Nusselt number are calculated to see the effects of fluid flow due to the surface of cylinder. Also, attitude of velocity profile and temperature profile on varying values of physical parameters are studied graphically.

## 7.2 Mathematical Formulation

Here we are taking steady, incompressible and two-dimensional flow with variable viscosity over a stretching cylinder in the region of stagnation point with Joule heating effect. The governing equations are

$$\frac{\partial (ru)}{\partial x} + \frac{\partial (rv)}{\partial r} = 0, \tag{7.1}$$

$$u\frac{\partial u}{\partial x} + v\frac{\partial u}{\partial r} = U_e\frac{\partial U_e}{\partial x} + \frac{1}{r\rho_0}\frac{\partial}{\partial r}(\mu r\frac{\partial u}{\partial r}) - \frac{\sigma B_0^2}{\rho}(U_e - u), \tag{7.2}$$

$$u\frac{\partial T}{\partial x} + v\frac{\partial T}{\partial r} = \frac{\alpha}{r\rho c_p}\frac{\partial}{\partial r}\left(r\frac{\partial T}{\partial r}\right) + \frac{\sigma B_0^2}{\rho c_p}u^2, \tag{7.3}$$

inserting boundary conditions

$$u = U_w = ax, \quad v = 0, \quad T = T_w \quad \text{at } r = R, \tag{7.4}$$

$$u \to U_e = bx, \quad T \to T_\infty \quad \text{as } r \to \infty. \tag{7.5}$$

In the above equations $\nu$ represent kinematic viscosity, $\sigma$ represent electric charge density, $B_0$ represent magnitude of magnetic field, $\rho$ represent density, $c_p$ represent specific heat, $T$ and $T_\infty$ are the temperature of the fluid and surroundings respectively, $U_w$ is the stretching velocity, $U_e$ is the free stream velocity.

Variation of the viscosity are assumed to be in the form:

$$\mu = \mu_0 e^{-\xi(T-T_0)}, \tag{7.6}$$

where $\mu_0$ is viscosity at slit temperature $T_0$.

Using the transformations of the form

$$\eta = \sqrt{\frac{a}{\nu}}\left(\frac{r^2 - R^2}{2R}\right), \quad \psi = \sqrt{\nu a}xRf(\eta), \tag{7.7}$$

$$u = axf'(\eta), \quad v = -\sqrt{\nu a}\frac{R}{r}f(\eta), \quad \theta(\eta) = \frac{T - T_\infty}{T_w - T_\infty}. \tag{7.8}$$

Equation (7.1) is identically satisfied while Eqs. (7.2 − 7.5) are reduced to

$$(1 - B\theta)[(1 + 2K\eta)f''' + 2Kf'' - (1 + 2K\eta)Bf''\theta'] + ff'' - (f')^2 - M^2(f' - A) + A^2 = 0, \tag{7.9}$$

$$(1 + 2K\eta)\theta'' + 2K\theta' + \Pr(f\theta' + M^2 Ec f'^2) = 0, \tag{7.10}$$

$$f(0) = 0, \quad f'(0) = 1, \quad f'(\infty) = A, \tag{7.11}$$

85

$$\theta\left(0\right) = 1, \ \theta\left(\infty\right) = 0, \tag{7.12}$$

where $K$ represent curvature parameter, $M$ represent Hartmann number, $A$ represent stretching ratio parameter, $B$ represent variable viscosity, $Ec$ represent Eckert number and $Pr$ represent Prandtl number which are given by

$$K = \frac{1}{R}\sqrt{\frac{2\nu}{a}}, \quad M^2 = \frac{\sigma B_0^2}{\rho a}, \quad \Pr = \frac{\mu c_p}{\alpha}, \tag{7.13}$$

$$A = \frac{b}{a}, \qquad Ec = \frac{U_w^2}{c_p\left(T_w - T_\infty\right)}, \tag{7.14}$$

$C_f$ Skin friction and $Nu_x$ local Nusselt number can be defined as

$$C_f = \frac{\tau_w}{\rho U_w^2}, \qquad Nu_x = \frac{xq_w}{k(T_f - T_\infty)}, \tag{7.15}$$

$$\tau_w = \mu\left(\frac{\partial u}{\partial r}\right)_{r=R}, \qquad q_w = -k\left(\frac{\partial T}{\partial r}\right)_{r=R}, \tag{7.16}$$

$$C_f\,\mathrm{Re}_x^{1/2} = (1 - A\theta)f''\left(0\right), \qquad Nu_x\,\mathrm{Re}_x^{-1/2} = -\theta'\left(0\right). \tag{7.17}$$

Where $\mathrm{Re}_x = x\sqrt{\frac{a}{\nu}}$.

## 7.3  Homotopic solutions

Homotopy analysis method depends upon the initial guesses $(f_0, \theta_0)$ and linear operators $(L_f, L_\theta)$ which are given in the forms

$$f_0\left(\eta\right) = A\eta + (1 - A)(1 - \exp\left(-\eta\right)), \quad \theta_0\left(\eta\right) = \exp\left(-\eta\right), \tag{7.18}$$

$$L_f\left(\eta\right) = \frac{d^3 f}{d\eta^3} - \frac{df}{d\eta}, \quad L_\theta\left(\eta\right) = \frac{d^2\theta}{d\eta^2} - \theta, \tag{7.19}$$

with

$$L_f\left[C_1 + C_2\exp(-\eta)\right] = 0, \tag{7.20}$$

86

$$L_\theta \left[ C_3 \exp(-\eta) \right] = 0, \tag{7.21}$$

where $C_i$ $(i = 1, 2, 3)$ are the arbitrary constants.

### 7.3.1 Zeroth-order problem

$$(1 - p) L_f \left[ \widehat{f}(\eta; p) - f_0(\eta) \right] = p\hbar_f N_f \left[ \widehat{f}(\eta; p) \right], \tag{7.22}$$

$$(1 - p) L_f \left[ \widehat{\theta}(\eta; p) - \theta_0(\eta) \right] = p\hbar_\theta N_\theta \left[ \widehat{\theta}(\eta; p), \widehat{f}(\eta; p) \right], \tag{7.23}$$

$$\widehat{f}(0; p) = 0, \quad \widehat{f}'(0; p) = 1, \quad \widehat{f}'(\infty; p) = A, \tag{7.24}$$

$$\widehat{\theta}(0; p) = 1, \quad \widehat{\theta}(\infty; p) = 0, \tag{7.25}$$

$$
\begin{aligned}
N_f \left[ \widehat{f}(\eta, p) \right] &= (1 - B\widehat{\theta}(\eta; p))[(1 + 2K\eta) \frac{\partial^3 \widehat{f}(\eta; p)}{\partial \eta^3} + 2K \frac{\partial^2 \widehat{f}(\eta; p)}{\partial \eta^2} \\
&\quad - (1 + 2K\eta) B \frac{\partial^2 \widehat{f}(\eta; p)}{\partial \eta^2} \frac{\partial \widehat{\theta}(\eta, p)}{\partial \eta}] + \widehat{f}(\eta; p) \frac{\partial^2 \widehat{f}(\eta; p)}{\partial \eta^2} \\
&\quad - \left( \frac{\partial \widehat{f}(\eta; p)}{\partial \eta} \right)^2 + A^2 - M^2 \frac{\partial \widehat{f}(\eta; p)}{\partial \eta} + M^2 A, \tag{7.26}
\end{aligned}
$$

$$
\begin{aligned}
N_\theta \left[ \widehat{\theta}(\eta; p), \widehat{f}(\eta; p) \right] &= (1 + 2K\eta) \frac{\partial^2 \widehat{\theta}(\eta, p)}{\partial \eta^2} + 2K \frac{\partial \widehat{\theta}(\eta, p)}{\partial \eta} \\
&\quad + \Pr \left( \widehat{f}(\eta; p) \frac{\partial \widehat{\theta}(\eta; p)}{\partial \eta} + M^2 Ec \left( \frac{\partial \widehat{f}(\eta; p)}{\partial \eta} \right)^2 \right), \tag{7.27}
\end{aligned}
$$

where $p \in [0, 1]$.

### 7.3.2 mth-order deformation problems

$$L_f \left[ f_m(\eta) - \chi_m f_{m-1}(\eta) \right] = \hbar_f \mathcal{R}_m^f(\eta), \tag{7.28}$$

$$L_\theta \left[ \theta_m(\eta) - \chi_m \theta_{m-1}(\eta) \right] = \hbar_\theta \mathcal{R}_m^\theta(\eta), \tag{7.29}$$

$$f_m(0) = f_m'(0) = f_m'(\infty) = 0, \tag{7.30}$$

87

$$\theta_m(0) = \theta_m(\infty) = 0, \tag{7.31}$$

$$M^2 f'_{m-1} + \left(M^2 A + A^2\right)(1 - \chi_m), \tag{7.32}$$

$$
\begin{aligned}
\mathcal{R}_m^f(\eta) = {} & (1 + 2K\eta) f'''_{m-1}(\eta) + 2K f''_{m-1} - (1 + 2K\eta)B \sum_{k=0}^{m-1} f''_{m-1-k} g'_k - B(1 + 2Kx) \\
& \sum_{k=0}^{m-1} f'''_{m-1-k} g_k - 2KB \sum_{k=0}^{m-1} f''_{m-1-k} g_k + (1 + 2Kx)B^2 \sum_{k=0}^{m-1} f''_{m-1-k} g'_{m-1-k} g_k \\
& + \sum_{k=0}^{m-1} \left[ f_{m-1-k} f''_k - f'_{m-1-k} f'_k \right] + A^2(1 - \chi_m) + M^2 f'_{m-1} \\
& + \left(M^2 A + A^2\right)(1 - \chi_m), \tag{7.33}
\end{aligned}
$$

$$
\begin{aligned}
\mathcal{R}_m^\theta(\eta) = {} & (1 + 2K\eta)\left( \theta''_{m-1} + \epsilon \sum_{k=0}^{m-1} \theta_{m-1-k} \theta''_k \right) + 2k\theta'_{m-1} \\
& + \Pr\left( \sum_{k=0}^{m-1} f_{m-1-k} \theta'_k + M^2 Ec \sum_{k=0}^{m-1} f'_{m-1-k} f'_k \right), \tag{7.34}
\end{aligned}
$$

$$\chi_m = \begin{cases} 0, & m \le 1 \\ 1, & m > 1 \end{cases}. \tag{7.35}$$

For $p = 0,1$, we can write

$$\widehat{f}(\eta; 0) = f_0(\eta), \quad \widehat{f}(\eta; 1) = f(\eta), \tag{7.36}$$

$$\widehat{\theta}(\eta; 0) = \theta_0(\eta), \quad \widehat{\theta}(\eta; 1) = \theta(\eta). \tag{7.37}$$

By Taylor's series we have

$$\widehat{f}(\eta; p) = f_0(\eta) + \sum_{m=1}^{\infty} f_m(\eta) p^m, \quad f_m(\eta) = \frac{1}{m!} \frac{\partial^m \widehat{f}(\eta; p)}{\partial p^m}\bigg|_{p=0} \tag{7.38}$$

88

$$\widehat{\theta}(\eta; p) = \theta_0(\eta) + \sum_{m=1}^{\infty} \theta_m(\eta) p^m, \qquad \theta_m(\eta) = \frac{1}{m!} \frac{\partial^m \widehat{\theta}(\eta; p)}{\partial p^m}\bigg|_{p=0}. \qquad (7.39)$$

Auxiliary parameter is chosen such that the series (7.38) and (7.39) converge at $p = 1$ i.e.

$$f(\eta) = f_0(\eta) + \sum_{m=1}^{\infty} f_m(\eta), \qquad (7.40)$$

$$\theta(\eta) = \theta_0(\eta) + \sum_{m=1}^{\infty} \theta_m(\eta). \qquad (7.41)$$

The general solutions are given by

$$f_m(\eta) = f_m^{\star}(\eta) + C_1 + C_2 e^{-\eta}, \qquad (7.42)$$

$$\theta_m(\eta) = \theta_m^{\star}(\eta) + C_3 e^{-\eta}. \qquad (7.43)$$

## 7.4   Convergence of HAM solutions

Homotopy analysis method is applied to find the convergence of required equations. The convergence of the series solution depends upon the auxiliary parameter $\hbar$.

| Orders of approximation | $-f''(0)$ | $-\theta'(0)$ |
|---|---|---|
| 1 | 0.7925 | 0.5679 |
| 5 | 0.7512 | 0.3600 |
| 10 | 0.7500 | 0.3148 |
| 15 | 0.7496 | 0.2986 |
| 20 | 0.7496 | 0.2909 |
| 25 | 0.7496 | 0.2866 |
| 30 | 0.7496 | 0.2842 |
| 34 | 0.7496 | 0.2829 |
| 35 | 0.7496 | 0.2827 |
| 36 | 0.7496 | 0.2826 |
| 37 | 0.7496 | 0.2826 |

89

Table **7.1.** Convergence table of series solution for different orders of approximation when $K = 0.2$, $M = 0.1$, $A = 0.1$, $B = 0.1$, $Ec = 0.1$ and $\Pr = 2.0$.

## 7.5   Shooting method

To apply Shooting method first the given nonlinear ordinary differential equations are reduced to a system of first order ordinary differential equations. This system is transformed to initial value problems by replacing missing initial conditions with assumed slopes. Using end conditions (i.e. when $\eta \to \infty$) initial conditions are computed through Newton-Raphson method that meet the given target. We can rewrite the dimensionless governing *Eqn.* $(7.9) - (7.10)$ in the following form:

$$f''' = \frac{1}{(1+2K\eta)}\left[\frac{1}{(1-B\theta)}[(f')^2 - ff'' - 2Kf'' - A^2 - H_a^2(A - f')] - 2Kf'' + (1+2K\eta)\,Bf''\theta'\right],$$
$$(7.45)$$

$$\theta'' = \frac{-1}{(1+2K\eta)}\left[2K\theta' + \Pr\left(f\theta' + M^2Ecf'^2\right)\right].$$
$$(7.46)$$

Define a set of new variables

$$y_1 = f, \ y_2 = f', y_3 = f'', y_4 = \theta \ \text{ and } \ y_5 = \theta'.$$
$$(7.47)$$

By assuming these variables:

$$y_1' = y_2,$$
$$(7.48)$$

$$y_2' = y_3,$$
$$(7.49)$$

$$y_3' = \frac{1}{(1+2K\eta)}\left[\begin{array}{c}\frac{1}{(1-By_4)}[(y_2)^2 - y_1y_3 - 2Ky_3 - A^2 - H_a^2(A - y_2)] \\ -2Ky_3 + (1+2K\eta)\,By_3y_5\end{array}\right],$$
$$(7.50)$$

90

$$y_4' = y_5, \tag{7.51}$$

$$y_5' = \frac{-1}{(1 + 2K\eta)} \left[ 2Ky_5 + \Pr\left( fy_5 + M^2 Ecy_2^2 \right) \right]. \tag{7.52}$$

In this system of ordinary differential equations prime denotes derivatives w.r.t. $\eta$. The initial conditions are modified to

$y_1(0) = 0, \quad y_2(0) = 1, \quad y_4(0) = 1,$

and the end conditions takes the form $y_2(\eta) \to A, \quad y_4(\eta) \to 0$ when $\eta \to \infty$.

In the above system there are five ordinary differential equations with three initial conditions and two end conditions. To solve this system of ODE by Runge-Kutta-Fehlberg method five initial conditions are required to find the value of five unknowns that appear in the solution. Three of them are given while two initial guesses are still required. The other two conditions are given for $\eta \to \infty$. An important step is to find the value of $\eta$ at $\infty$ (i.e. $\eta_\infty$) where end conditions are satisfied. The solution procedure starts with initial guess (e.g. $f'(0) = s$) and solve the system of ordinary differential equations to determine the appropriate value of $f''(0)$ and $\theta'(0)$. The process is continued (using Newton-Raphson method) with revised value of $s$ until two success values of $f''(0)$ and $\theta'(0)$ differ only after the specific number of significant digits. The final value of $\eta$ is considered as $\eta_\infty$ that can be used to calculate the fluid velocity $f'$ and the temperature field $\theta$ in the boundary layer for a given set of physical parameters. Numerical solution is getting by employing the fifth order Runge-Kutta-Fehlberg method with shooting technique using MATLAB software.

## 7.6 Comparison of HAM and Shooting method

Comparison between numerical solutions obtained through homotopy analysis method and shooting method are presented in Fig. 7.1. For shooting method solution is obtained in conjunction with Fehlberg method.
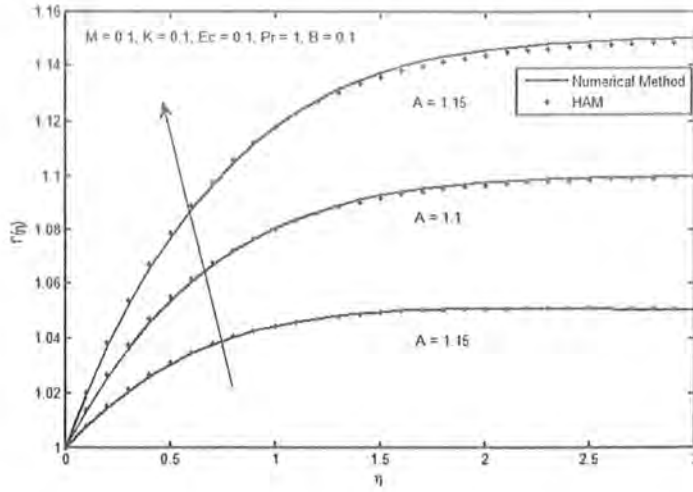
Fig 7.1: Comparison of HAM and Shooting method.

| $Ec$ | 0.1 | | 0.2 | | 0.3 | | 0.4 | |
|------|-----|-----|-----|-----|-----|-----|-----|-----|
| Pr | $HAM$ | $SM$ | $HAM$ | $SM$ | $HAM$ | $SM$ | $HAM$ | $SM$ |
| 0.1 | 0.5562 | 0.5562 | 0.5531 | 0.5533 | 0.5496 | 0.5500 | 0.5465 | 0.5468 |
| 0.2 | 0.5641 | 0.5644 | 0.5811 | 0.5816 | 0.5513 | 0.5518 | 0.5449 | 0.5454 |
| 0.3 | 0.5723 | 0.5726 | 0.5626 | 0.5631 | 0.5531 | 0.5537 | 0.5433 | 0.5440 |
| 0.4 | 0.5805 | 0.5809 | 0.5676 | 0.5683 | 0.5560 | 0.5567 | 0.5419 | 0.5427 |

Table 7.2: Comparison of $-\theta'(0)$ obtained through HAM and shooting method for Prandtl number Pr and Eckert number $Ec$ when $K = 0.1$, $A = 0.1$ and $M = 0.1$.

## 7.7 Results and discussion

Fig. 7.1 shows the comparison of HAM and shooting method for different values of stretching ratio parameter $A$. Table 7.1 reflects the values of $-\theta'(0)$ for different values of Prandtl and Eckert number. On comparing the results obtained by using HAM and shooting method and we can say that the results are in good agreement. Fig. 7.2 is the influence of curvature parameter $K$ on velocity field. It is analyzed that velocity decreases with the increase of curvature

parameter $K$ near the plate while increases far away from the plate. Because as we increase the curvature parameter $K$, radius of curvature decreases which implies that contact area of the cylinder with fluid decreases. Thus less resistance is offered by the cylinder therefore, velocity of the fluid increases. Further boundary layer is thickener for higher values of curvature parameter $K$. The effect of Hartmann number $M$ on velocity field is displayed in Fig. 7.3. From the figure we can see that velocity of the fluid decreases with an increase in Hartmann number. As with the increase of magnetic field, Lorentz force increases which effect the fluid motion in return reduces the velocity of the fluid. Fig. 7.4 is plotted for the curvature parameter $K$ on temperature profile. Fig. 7.5 is plotted for the influence of stretching ratio parameter $A$ on temperature field. Increase in stretching ratio parameter $A$ temperature field decreases. Further, thermal boundary layer thickness is thinner for higher values of stretching ratio parameter. Fig. 7.6 is plotted for the influence of Eckert number $Ec$ on temperature field. It is analyzed that temperature and thermal boundary layer increases with an increase in Eckert number. The influence of Hartmann number $M$ on temperature profile is displayed in Fig. 7.7. It is observed that temperature field and thermal boundary layer increases with an increase in Hartmann number. Fig.7.8 is plotted for the behavior of variable viscosity $B$ on velocity profile. It is observed that velocity profile decreases with an increase in variable viscosity $B$.
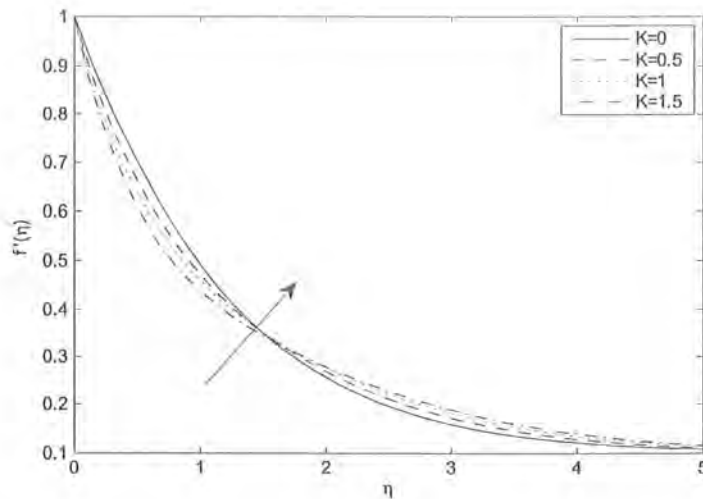


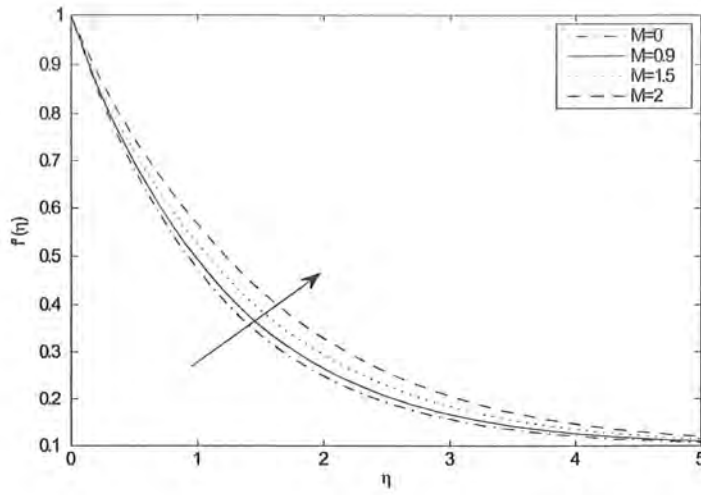**Fig 7.2**: Effect of $K$ on velocity field where $M = 0.1$, $A = 0.1$, $B = 0.1, Ec = 0.1$ and $\text{Pr} = 2.0$.

**Fig 7.3:** Effect of $M$ on velocity field where $K = 0.1$, $A = 0.1$, $B = 0.1, Ec = 0.1$ and $\Pr = 2.0$.
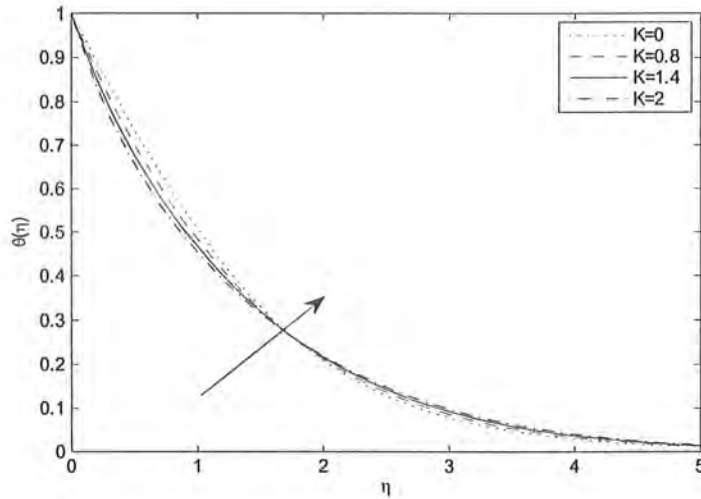


**Fig 7.4:** Effect of $K$ on temperature field where $M = 0.1$, $A = 0.1$, $B = 0.1, Ec = 0.1$ and $\Pr = 2.0$
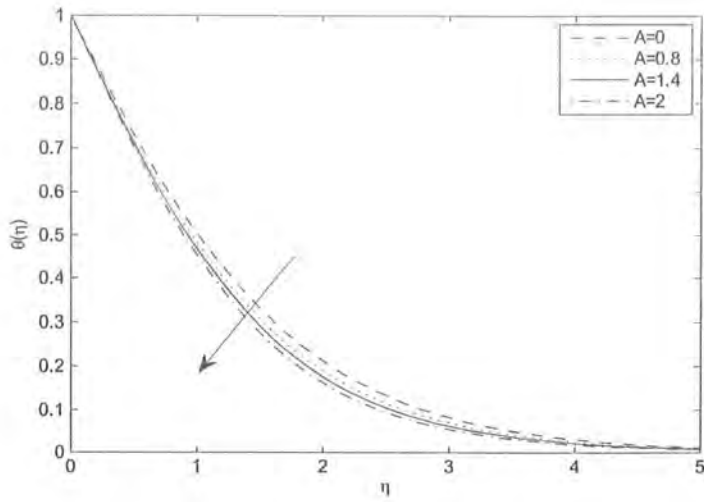
**Fig 7.5**: Effect of $A$ on temperature field where $M = 0.1$, $K = 0.1$, $B = 0.1$, $Ec = 0.1$ and $\Pr = 2.0$
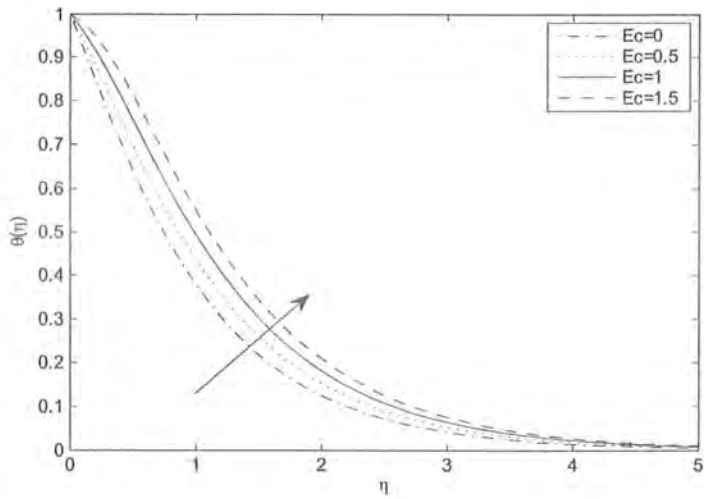


**Fig 7.6**: Effect of $Ec$ on temperature field where $M = 0.1$, $A = 0.1$, $B = 0.1$, $K = 0.1$ and
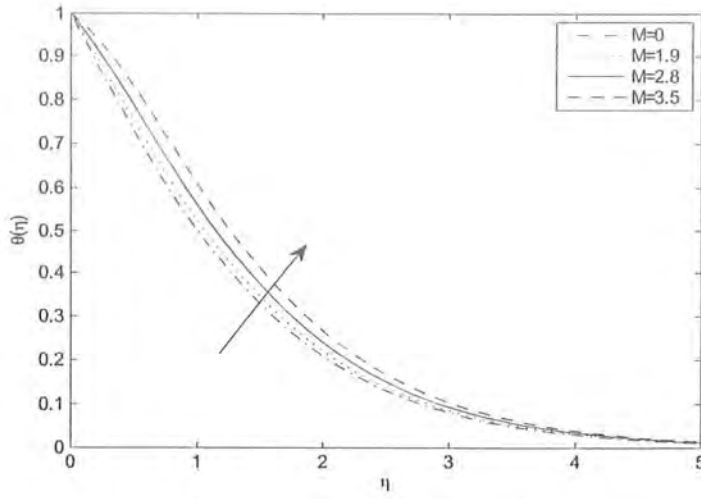
Pr = 2.0



**Fig 7.7**: Effect of $M$ on temperature field where $K = 0.1$, $A = 0.1$, $B = 0.1$, $Ec = 0.1$ and Pr = 2.0
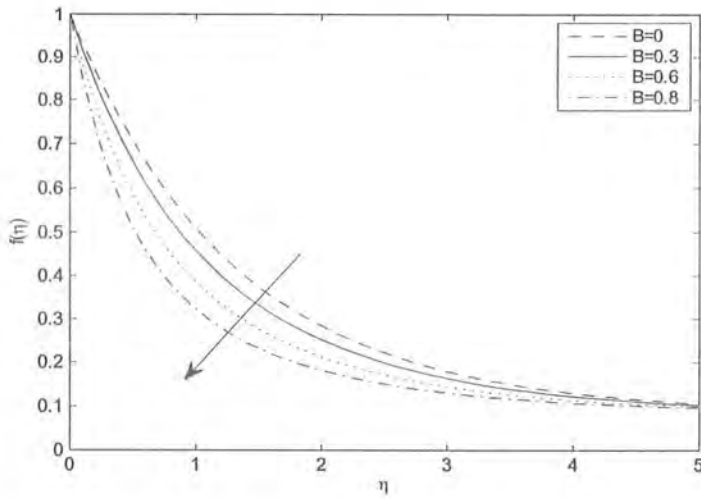


**Fig 7.8**: Effect of $B$ on velocity field where $M = 0.1$, $A = 0.1$, $K = 0.1$, $Ec = 0.1$ and Pr = 2.0.

| $A$ | $B$ | $K$ | $M$ | $-f''(0)$ |
|---|---|---|---|---|
| 0.1 | 0.1 | 0.1 | 0.1 | 0.7578 |
| 0.2 | | | | 0.7549 |
| 0.3 | | | | 0.7526 |
| 0.1 | 0.1 | | | 0.7578 |
| | 0.2 | | | 0.8071 |
| | 0.3 | | | 0.8674 |
| | | 0.1 | | 0.8071 |
| | | 0.2 | | 0.8268 |
| | | 0.3 | | 0.8462 |
| | | | 0.1 | 0.8071 |
| | | | 0.2 | 0.8026 |
| | | | 0.3 | 0.7948 |

**Table 7.3:** The variation of $\frac{1}{2}C_f\sqrt{\mathrm{Re}_x}$ with respect to $K$, $B$, $M$ and $A$ .

| $Ec$ | $\mathrm{Pr}$ | $M$ | $-\theta'(0)$ |
|---|---|---|---|
| 0.1 | 1.5 | 0.1 | 0.5464 |
| 0.3 | | | 0.5453 |
| 0.5 | | | 0.5438 |
| 0.1 | 1.6 | | 0.5689 |
| | 1.7 | | 0.5913 |
| | 1.8 | | 0.6114 |
| | 1.6 | 0.2 | 0.5698 |
| | | 0.3 | 0.5693 |
| | | 0.5 | 0.5656 |

**Table 7.4:** Temperature gradient $-\theta'(0)$ at the outer surface of cylinder for different values of $Pr$, $M$ and $Ec$.

Table 7.3 and Table 7.4 shows the behavior of skin friction coefficient and local Nusselt number for different values of physical parameters. From **Table 7.3** we see that on increasing $A$ and $M$, skin friction decreases while for higher values of $B$ and $K$ skin friction increases which is due to the inverse proportionality relation $C_f \propto Re_x^{-\frac{1}{2}}$. Here as Reynold number increase, $|C_f|$ decreases. This means that viscous forces start decreasing. For the stretching ratio parameter $A$, when it increases, $|C_f \, Re_x|$ decreases. When we think about curvature parameter $K$, $|C_f \, Re_x|$ increases. In **Table 7.4** increase in Eckert number $Ec$ or Hartmann number $M$ reduces local Nussult number but for increase in Prandtl number Pr, increases the value of $-\theta'(0)$. Since $Nu_x^2 \propto Re_x$ this means that increase in Reynold number $Re_x = \frac{Ux}{v}$ will increase the viscosity.

## 7.8 Concluding remarks

We have investigated the characteristics of MHD and ohmic dissipation of viscous fluid close to stagnation point over a stretching cylinder. The main observations are

- The behavior of velocity and temperature field is same on increasing curvature parameter $K$ i.e both velocity and temperature field increases with increasing curvature parameter $K$.

- By increasing Hartmann number $M$ both velocity and temperature increases.

- Temperature field increases by increasing Eckert number $Ec$.

- On increasing stretching ratio parameter $A$ temperature field decreases .

- Also the increase in variable viscosity $B$ will reduce the fluid velocity.

# Chapter 8

# Mixed Convection Stagnation Point Flow over a Stretching Cylinder with Variable Thermal Conductivity and Heat Generation/absorption

This chapter addresses the mixed convection stagnation point flow of Casson nanofluid past an impermeable vertical stretching cylinder. Buongiorno model is used to explore the characteristics of nanofluid with velocity, thermal and solutal slip phenomena. Stratification process due to temperature and concentration is considered. An analysis of constructive and destructive chemical reaction processes is also made. A system of highly coupled nonlinear equations is solved. Homotopy analysis method and shooting method are used to find numerical solutions for comparison. Impacts of various pertinent parameters on the velocity, temperature and concentration distributions are discussed. Characteristics of Skin friction coefficient, Nusselt and Sherwood numbers corresponding to different physical parameters are computed.

## 8.1 Mathematical formulation

Consider a steady, incompressible and two-dimensional boundary layer mixed convection flow of a viscous fluid over a stretched cylinder in the region of stagnation point with heat generation/absorption. Here we assume that thermal conductivity varies linearly with temperature. The governing equations are

$$\frac{\partial\left(ru\right)}{\partial x} + \frac{\partial\left(rv\right)}{\partial r} = 0, \tag{8.1}$$

$$u\frac{\partial u}{\partial x} + v\frac{\partial u}{\partial r} = U_e\frac{\partial U_e}{\partial x} + \nu\left(\frac{\partial^2 u}{\partial r^2} + \frac{1}{r}\frac{\partial u}{\partial r}\right) + g\beta_T(T - T_\infty), \tag{8.2}$$

$$u\frac{\partial T}{\partial x} + v\frac{\partial T}{\partial r} = \frac{1}{\rho c_p}\frac{\partial}{\partial r}\left(k\left(T\right)r\frac{\partial T}{\partial r}\right) + \frac{Q}{\rho c_p}(T - T_\infty), \tag{8.3}$$

subjected to the boundary layer conditions

$$u = U_w = ax, \quad v = 0, \quad T = T_w \quad \text{at } r = R, \tag{8.4}$$

$$u \to U_e = bx, \quad T \to T_\infty \quad \text{as } r \to \infty. \tag{8.5}$$

In the above expressions, $u$ and $v$ are the velocity components in $x$ and $r$ directions respectively, $\beta_T$ is the thermal expansion coefficient, $Q$ is the heat added or removed from the fluid, $\nu$ is the kinematic viscosity, $\rho$ is the density, $c_p$ is the specific heat, $k\left(T\right)$ is the variable thermal conductivity, $T$ and $T_\infty$ are the temperatures of the fluid and surroundings respectively, $U_w$ is the stretching velocity and $U_e$ is the free stream velocity.

Using the similarity transformations

$$\eta = \sqrt{\frac{a}{\nu}}\left(\frac{r^2 - R^2}{2R}\right), \quad \psi = \sqrt{\nu a}xRf\left(\eta\right), \tag{8.6}$$

$$u = axf'\left(\eta\right), \quad v = -\sqrt{\nu a}\frac{R}{r}f\left(\eta\right), \quad \theta\left(\eta\right) = \frac{T - T_\infty}{T_w - T_\infty}. \tag{8.7}$$

Equation (8.1) is identically satisfied while Eqs. (8.2) to (8.4) takes the form

$$(1 + 2K\eta)f''' + ff'' - \left(f'\right)^2 + 2Kf'' + \lambda\theta + A^2 = 0, \tag{8.8}$$

$$(1 + \epsilon\theta)(1 + 2K\eta)\,\theta'' + \epsilon(1 + 2K\eta)\,\theta'^2 + 2(1 + \epsilon\theta)\,K\theta' + \Pr f\theta' + \beta\theta = 0, \tag{8.9}$$

$$f(0) = 0, \quad f'(0) = 1, \quad f'(\infty) = A, \tag{8.10}$$

$$\theta(0) = 1, \quad \theta(\infty) = 0, \tag{8.11}$$

where $K$, $A$, $\beta$, $\epsilon$, $\lambda$ and $\Pr$ denotes the curvature parameter, stretching ratio parameter, heat generation/absorption, small temperature parameter, mixed convection and Prandtl number which are given by

$$K = \frac{1}{R}\sqrt{\frac{2\nu}{a}}, \quad \Pr = \frac{\mu c_p}{k_\infty}, \quad A = \frac{b}{a}, \tag{8.12}$$

$$\lambda = \frac{g\beta_T(T - T_\infty)}{a^2 x}, \quad \beta = \frac{Q}{\rho c_p a}. \tag{8.13}$$

## 8.2  Homotopic solutions

Homotopy analysis method depends upon the initial guesses $(f_0(\eta),\ \theta_0(\eta))$ and linear operators $(L_f,\ L_\theta)$ which are given in the forms

$$f_0(\eta) = A\eta + (1 - A)(1 - \exp(-\eta)), \quad \theta_0(\eta) = \exp(-\eta), \tag{8.14}$$

$$L_f(\eta) = \frac{d^3 f}{d\eta^3} - \frac{df}{d\eta}, \quad L_\theta(\eta) = \frac{d^2\theta}{d\eta^2} - \theta, \tag{8.15}$$

$$L_f\left[C_1 + C_2\exp(-\eta)\right] = 0, \tag{8.16}$$

$$L_\theta\left[C_3\exp(-\eta)\right] = 0, \tag{8.17}$$

where $C_i$ $(i = 1 - 3)$ are the arbitrary constants.

### 8.2.1 Zeroth-order problem

$$(1-p) L_f \left[ \widehat{f}(\eta;p) - f_0(\eta) \right] = p\hbar_f N_f \left[ \widehat{f}(\eta;p) \right], \tag{8.18}$$

$$(1-p) L_\theta \left[ \widehat{\theta}(\eta;p) - \theta_0(\eta) \right] = p\hbar_\theta N_f \left[ \widehat{\theta}(\eta;p), \widehat{f}(\eta;p) \right], \tag{8.19}$$

$$\widehat{f}(0;p) = 0, \quad \widehat{f}'(0;p) = 1, \quad \widehat{f}'(\infty;p) = A, \tag{8.20}$$

$$\widehat{\theta}(0;p) = 1, \quad \widehat{\theta}(\infty;p) = 0, \tag{8.21}$$

$$
\begin{aligned}
N_f \left[ \widehat{f}(\eta,p) \right] &= (1+2K\eta) \frac{\partial^3 \widehat{f}(\eta;p)}{\partial \eta^3} + \widehat{f}(\eta;p) \frac{\partial^2 \widehat{f}(\eta;p)}{\partial \eta^2} - \left( \frac{\partial \widehat{f}(\eta;p)}{\partial \eta} \right)^2 \\
&\quad + 2K \frac{\partial^2 \widehat{f}(\eta;p)}{\partial \eta^2} + \lambda \widehat{\theta}(\eta;p) + A^2,
\end{aligned} \tag{8.22}
$$

$$
\begin{aligned}
N_\theta \left[ \widehat{\theta}(\eta;p), \widehat{f}(\eta;p) \right] &= \left( 1 + \epsilon \widehat{\theta}(\eta,p) \right) (1+2K\eta) \frac{\partial^2 \widehat{\theta}(\eta,p)}{\partial \eta^2} \\
&\quad + \epsilon (1+2K\eta) \left( \frac{\partial \widehat{\theta}(\eta,p)}{\partial \eta} \right)^2 + 2 \left( 1 + \epsilon \widehat{\theta}(\eta,p) \right) K \frac{\partial \widehat{\theta}(\eta,p)}{\partial \eta} \\
&\quad + \Pr \left( \widehat{f}(\eta;p) \frac{\partial \widehat{\theta}(\eta;p)}{\partial \eta} + \beta \widehat{\theta}(\eta,p) \right),
\end{aligned} \tag{8.23}
$$

where $p \in [0,1]$ is embedding parameter and $\hbar_f$ and $\hbar_\theta$ are the non-zero auxiliary parameters.

### 8.2.2 mth-order deformation problems

$$L_f \left[ f_m(\eta) - \chi_m f_{m-1}(\eta) \right] = \hbar_f \mathcal{R}_m^f(\eta), \tag{8.24}$$

$$L_\theta \left[ \theta_m(\eta) - \chi_m \theta_{m-1}(\eta) \right] = \hbar_\theta \mathcal{R}_m^\theta(\eta), \tag{8.25}$$

$$f_m(0) = f_m'(0) = f_m'(\infty) = 0, \tag{8.26}$$

$$\theta_m(0) = \theta_m(\infty) = 0, \tag{8.27}$$

$$\mathcal{R}_m^f(\eta) = (1+2K\eta) f_{m-1}'''(\eta) + 2K f_{m-1}'' + \sum_{k=0}^{m-1} \left[ f_{m-1-k} f_k'' - f_{m-1-k}' f_k' \right] + \lambda \theta_{m-1} + A^2 (1-\chi_m), \tag{8.28}$$

$$\mathcal{R}_m^\theta(\eta) = (1+2K\eta)\left(\theta_{m-1}'' + \epsilon \sum_{k=0}^{m-1}\theta_{m-1-k}\theta_k''\right) + \epsilon(1+2K\eta)\sum_{k=0}^{m-1}\theta_{m-1-k}'\theta_k'$$

$$+2k\left(\theta_{m-1}' + \epsilon\sum_{k=0}^{m-1}\theta_{m-1-k}\theta_k'\right) + \Pr\left(\sum_{k=0}^{m-1}f_{m-1-k}\theta_k' + \beta\theta_{m-1}\right), \quad (8.29)$$

$$\chi_m = \begin{cases} 0, & m \le 1 \\ 1, & m > 1 \end{cases}. \qquad (8.30)$$

For $p = 0, 1$, we can write

$$\widehat{f}(\eta; 0) = f_0(\eta), \quad \widehat{f}(\eta; 1) = f(\eta), \qquad (8.31)$$

$$\widehat{\theta}(\eta; 0) = \theta_0(\eta), \quad \widehat{\theta}(\eta; 1) = \theta(\eta). \qquad (8.32)$$

Using Taylor's series we have

$$\widehat{f}(\eta; p) = f_0(\eta) + \sum_{m=1}^{\infty} f_m(\eta)\, p^m, \quad f_m(\eta) = \frac{1}{m!}\frac{\partial^m \widehat{f}(\eta; p)}{\partial p^m}\bigg|_{p=0} \qquad (8.33)$$

$$\widehat{\theta}(\eta; p) = \theta_0(\eta) + \sum_{m=1}^{\infty} \theta_m(\eta)\, p^m, \quad \theta_m(\eta) = \frac{1}{m!}\frac{\partial^m \widehat{\theta}(\eta; p)}{\partial p^m}\bigg|_{p=0}. \qquad (8.34)$$

The value of auxiliary parameter is selected so properly that the series (8.33) and (8.34) converges at $p = 1$ i.e,

$$f(\eta) = f_0(\eta) + \sum_{m=1}^{\infty} f_m(\eta), \qquad (8.35)$$

$$\theta(\eta) = \theta_0(\eta) + \sum_{m=1}^{\infty} \theta_m(\eta). \qquad (8.36)$$

The general solutions $(f_m, \theta_m)$ of Eqs. (8.24) and (8.25) in terms of special solutions $(f_m^*, \theta_m^*)$ are given by

$$f_m(\eta) = f_m^*(\eta) + C_1 + C_2 e^{-\eta}, \qquad (8.37)$$

$$\theta_m(\eta) = \theta_m^*(\eta) + C_3 e^{-\eta}, \qquad (8.38)$$

Skin friction, local Nusselt number, shear stress at the surface and the surface heat flux can be defined as

$$C_f = \frac{\tau_w}{\rho u_w^2}, \qquad Nu_x = \frac{x q_w}{k(T_f - T_\infty)}, \tag{8.39}$$

$$\tau_w = \mu \left(\frac{\partial u}{\partial r}\right)_{r=R}, \qquad q_w = -k \left(\frac{\partial T}{\partial r}\right)_{r=R}. \tag{8.40}$$

While the dimensionless forms of skin friction and local Nusselt number are

$$C_f \, \mathrm{Re}_x^{1/2} = f''(0), \qquad Nu_x \, \mathrm{Re}_x^{-1/2} = -\theta'(0), \tag{8.41}$$

where $\mathrm{Re}_x = x\sqrt{\frac{a}{\nu}}$.

## 8.3 Convergence of HAM solutions

Homotopy analysis method is applied to obtain criteria of convergence for desired solution of given equations. The convergence control parameter $\hbar$ is involved in the series solution. HAM solution depends upon this parameter which basically control the convergence region and rate of approximation. Therefore, we have plotted the $\hbar$-curves for $f''(0)$ and $\theta'(0)$ in Figs. $(8.1 - 8.2)$. The admissible ranges of the auxiliary parameters $\hbar_f$ and $\hbar_\theta$ are $-1 \leq \hbar_f \leq -0.2$ and $-0.8 \leq \hbar_\theta \leq -0.2$.

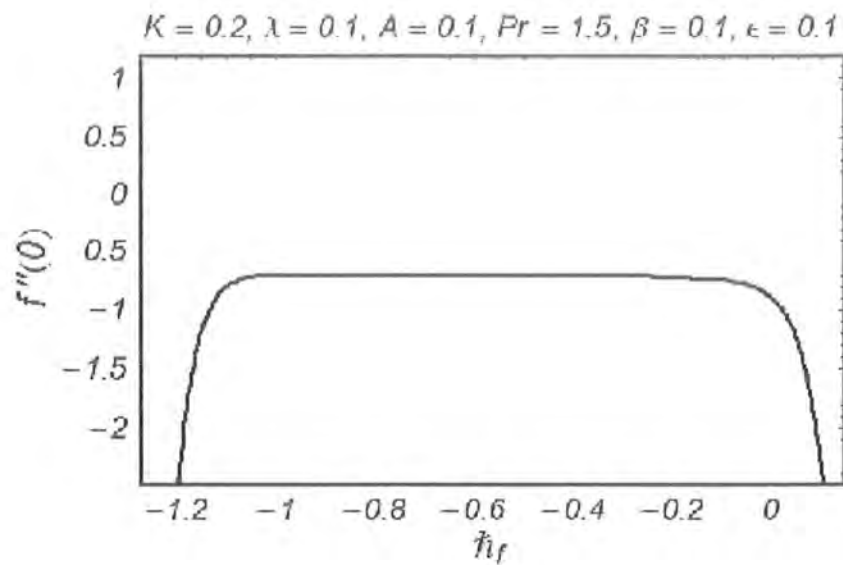| Order of approximations | $-f''(0)$ | $-\theta'(0)$ |
|---|---|---|
| 1 | 0.7287 | 0.5259 |
| 5 | 0.6825 | 0.4174 |
| 7 | 0.6813 | 0.4102 |
| 10 | 0.6808 | 0.4075 |
| 11 | 0.6808 | 0.4073 |
| 12 | 0.6808 | 0.4072 |
| 14 | 0.6808 | 0.4072 |
| 15 | 0.6808 | 0.4073 |
| 16 | 0.6808 | 0.4073 |

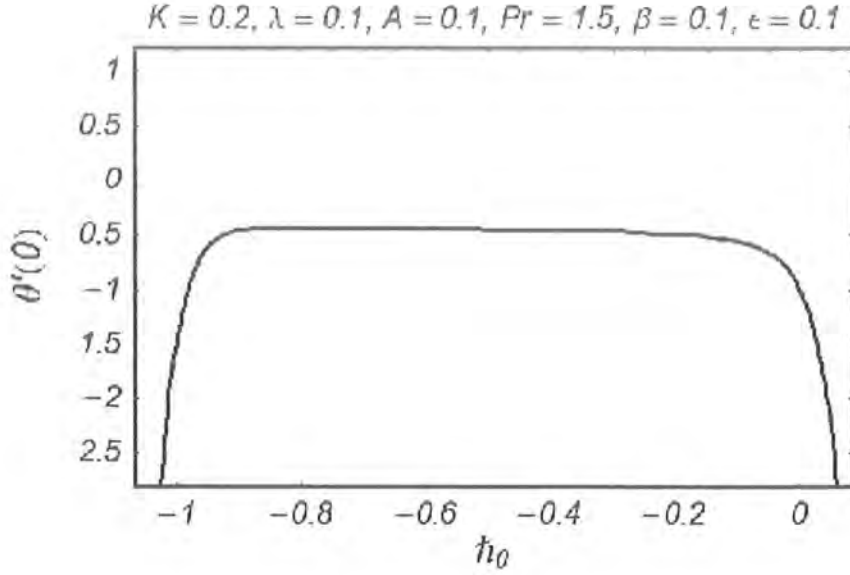Fig 8.1: $\hbar_f$ for velocity profile.

Fig 8.2: $\hbar_\theta$ for temperature profile.

## 8.4   Shooting method

To apply Shooting method first the given nonlinear ordinary differential equation is reduced to a system of first order ordinary differential equations. This system is transformed to initial value problems by replacing missing initial conditions with assumed slopes. Using end conditions (i.e. when $\eta \to \infty$) initial conditions are computed through Newton-Raphson method which meet the given target. We can rewrite the dimensionless governing $Eqn.\ (8.8)-(8.9)$ in the following form:

$$f''' = \frac{1}{(1+2K\eta)} \left[ \left(f'\right)^2 - ff'' - 2Kf'' - A^2 - \lambda\theta \right], \qquad (8.43)$$

$$\theta'' = \frac{1}{(1+\epsilon\theta)(1+2K\eta)} \left[ -\epsilon(1+2K\eta)\theta'^2 - 2(1+\epsilon\theta)K\theta' - \Pr f\theta' - \beta\theta \right]. \qquad (8.44)$$

106

We define a set of new variables

$$y_1 = f, \ y_2 = f', y_3 = f'', y_4 = \theta \ \text{and} \ y_5 = \theta'. \tag{8.45}$$

By assuming these variables above ordinary differential equations are modified to the following system of first order ordinary differential equations:

$$y_1' = y_2, \tag{8.46}$$

$$y_2' = y_3, \tag{8.47}$$

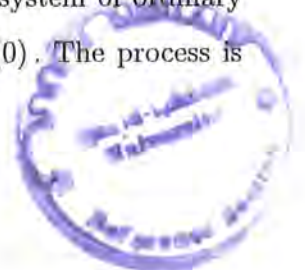$$y_3' = \frac{1}{(1+2K\eta)}[(y_2)^2 - y_1 y_3 - 2K y_3 - A^2 - \lambda y_4], \tag{8.48}$$

$$y_4' = y_5, \tag{8.49}$$

$$y_5' = \frac{1}{(1+\epsilon y_4)(1+2K\eta)} \left[ -\epsilon (1+2K\eta) y_4^2 - 2(1+\epsilon y_4) K y_5 - \Pr y_1 y_5 - \beta y_4 \right]. \tag{8.50}$$

In this system of ordinary differential equations prime denotes derivatives w.r.t. $\eta$. The initial conditions are modified to

$y_1(0) = 0, \quad y_2(0) = 1, \quad y_4(0) = 1,$

and the end conditions takes the form $y_2(\eta) \to A, \quad y_4(\eta) \to 0$ when $\eta \to \infty$.

In the above system there are five ordinary differential equations with three initial conditions and two end conditions. To solve this system by Runge-Kutta-Fehlberg method five initial conditions are required to solve five unknowns that appears in the solution. Three of them are given while two initial guesses are still required. The other two conditions are given for $\eta \to \infty$. An important step is to find the value of $\eta$ at $\infty$ (i.e. $\eta_\infty$) where end conditions are satisfied. The solution procedure starts with initial guess (e.g. $f'(0) = s$) and solve the system of ordinary differential equations to determine the appropriate value of $f''(0)$ and $\theta'(0)$. The process is

107

continued (using Newton-Raphson method) with revised value of $s$ until two success values of $f''(0)$ and $\theta'(0)$ differ only after the specific number of significant digits. The final value of $\eta$ is considered as $\eta_\infty$ that can be used to calculate the fluid velocity $f'$ and the temperature field $\theta$ in the boundary layer for set of physical parameters. Numerical solution is getting by employing the fifth order Runge-Kutta-Fehlberg method with shooting technique using MATLAB software.

## 8.5    Comparison of HAM and Shooting method

Comparison between numerical solutions obtained through homotopy analysis method and shooting method is presented in Fig. 8.3. For shooting method solution is obtained in conjunction with Fehlberg method.
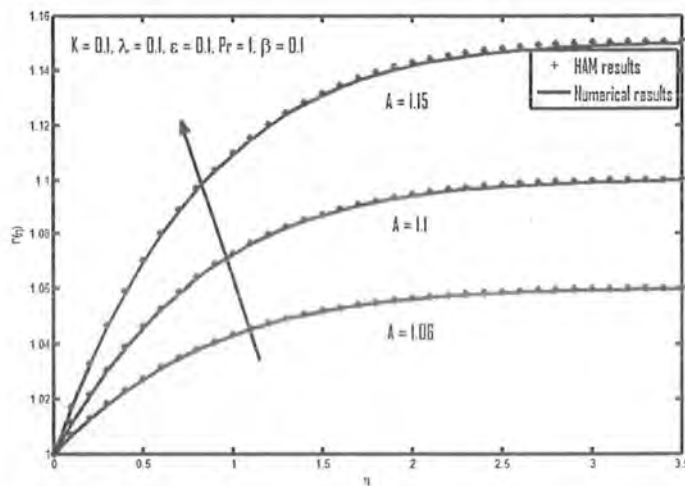


**Fig 8.3**: Comparison between numerical solutions obtained through HAM and Shooting method for different values of A.

| λ | A =0.4 | | A =0.5 | | A =0.6 | |
|---|---|---|---|---|---|---|
| | HAM | SM | HAM | SM | HAM | SM |
| 0.1 | 0.5199 | 0.5211 | 0.4485 | 0.4500 | 0.3684 | 0.3699 |
| 0.2 | 0.4856 | 0.4863 | 0.4148 | 0.4161 | 0.3353 | 0.3378 |
| 0.3 | 0.2514 | 0.2519 | 0.3812 | 0.3826 | 0.3024 | 0.3039 |
| 0.4 | 0.4174 | 0.4171 | 0.3478 | 0.3493 | 0.2696 | 0.2712 |

**Table 8.2** Comparison of HAM and shooting method at $-f''(0)$ for mixed convection parameter $\lambda$ and stretching ratio parameter $A$ when $K = 0.2$, $\beta = 0.2$, $\epsilon = 0.1$ and $Pr = 1.0$.

| Pr | β =0.1 | | β =0.2 | | β =0.3 | | β = 0.4 | |
|---|---|---|---|---|---|---|---|---|
| | HAM | SM | HAM | SM | HAM | SM | HAM | SM |
| 0.1 | 0.2934 | 0.2938 | 0.2805 | 0.2814 | 0.2811 | 0.2838 | 0.2769 | 0.2781 |
| 0.5 | 0.3454 | 0.3459 | 0.3135 | 0.3144 | 0.2892 | 0.2901 | 0.2584 | 0.2609 |
| 2.0 | 0.5616 | 0.5625 | 0.4803 | 0.4821 | 0.3913 | 0.3930 | 0.2847 | 0.2879 |
| 2.5 | 0.6348 | 0.6359 | 0.5432 | 0.5447 | 0.4465 | 0.4480 | 0.3205 | 0.3205 |

**Table 8.3:** Comparison of HAM and SM(Shooting method) with $-\theta'(0)$ for Prandtl number Pr and heat generation/absorption parameter $\beta$ when $K = 0.1$, $A = 0.1$, $\epsilon = 0.1$ and $\lambda = 0.1$.

## 8.6  Results and discussion

Fig. 8.3 shows the comparison of numerical solutions obtained through HAM and shooting method. Tables 8.2 and 8.3 also reflect the comparison of numerical solutions obtained by using HAM and shooting method for $f''(0)$ and $\theta'(0)$. From Fig. 8.3 and tables (8.2 − 8.3) it is observed that the results obtained by using HAM and shooting method compares well. Fig. 8.4 is plotted to show the effects of curvature parameter $K$ on velocity field. It is observed that with the increase of curvature parameter $K$ velocity decreases near the plate while increases on moving away from the plate. Because by increasing curvature parameter $K$, radius of curvature decreases which implies that surface area of the cylinder incontact with fluid decreases. Thus

less resistance is offered by the cylinder. Therefore, velocity of the fluid increases. Further boundary layer is thicker for higher values of curvature parameter $K$. Variation of stretching ratio parameter $A$ on velocity is sketched in Fig. 8.5. Fig. 8.6 shows the graphical behaivour of curvature parameter $K$. From the figure we can see that by increasing $K$ temperature increases.. Fig. 8.7 is plotted for the influence of stretching ratio parameter $A$ upon temperature field. It is depicted that temperature field decreases with an increase in stretching ratio parameter $A$. The influence on temperature field by small parameter $\epsilon$ is shown in Fig. 8.8. we can say that temperature increases as we increase the small parameter $\epsilon$. The behavior of Prandtl number $\Pr$ upon temperature field is sketched in Fig. 8.9. Basically by increasing Prandtl number temperature and thermal boundary layer decreases. Fig. 8.10 is the influence on temperature field by the positive values of heat generation/absorption parameter $\beta$. It is analyzed that increasing heat generation/absorption parameter $\beta$ increases temperature and thermal boundary layer. Fig. 8.11 is the influence on temperature field by the negative values of heat generation/absorption parameter $\beta$. It is analyzed that temperature and thermal boundary layer decreases with an increase in heat generation/absorption parameter $\beta$. Fig. 8.12 is sketched to check the behavior of mixed convection parameter $\lambda$ upon velocity field. From the figure we can say that on increasing mixed convection parameter velocity of the fluid increases.
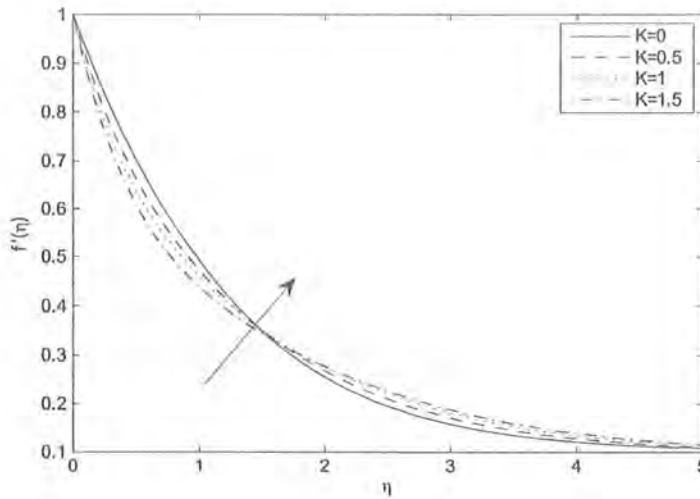


**Fig 8.4:** Effect of $K$ on velocity profile when $\beta = 0.1$, $A = 0.1$, $\epsilon = 0.1$, $\lambda = 0.1$ and $\Pr = 2.0$.
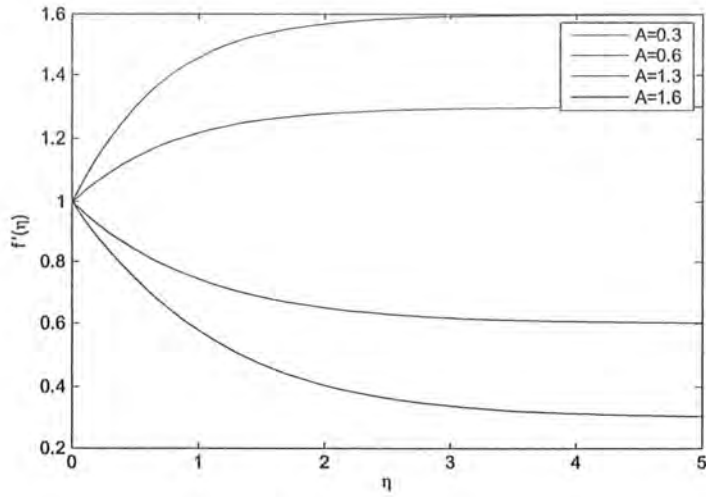
**Fig 8.5:** Effect of $A$ on velocity profile when $\beta = 0.1$, $A = 0.1$, $\epsilon = 0.1, K = 0.1$ and $\Pr = 2.0$.
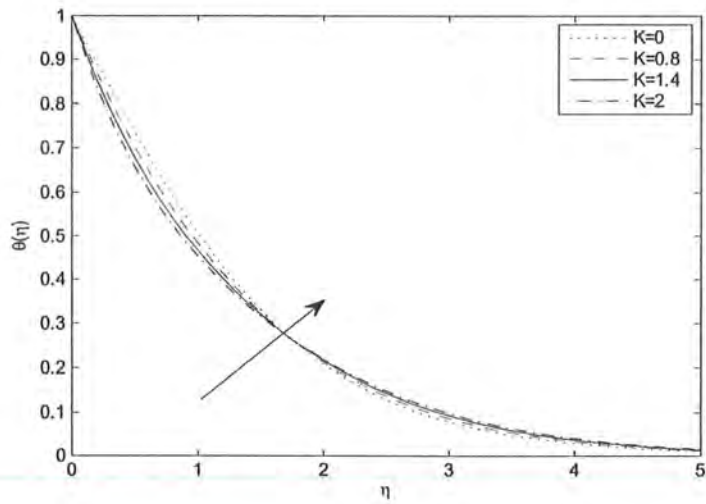


**Fig 8.6:** Effect of $K$ on temperature when $\beta = 0.1$, $K = 0.1$, $\epsilon = 0.1, \lambda = 0.1$ and $\Pr = 2.0$.
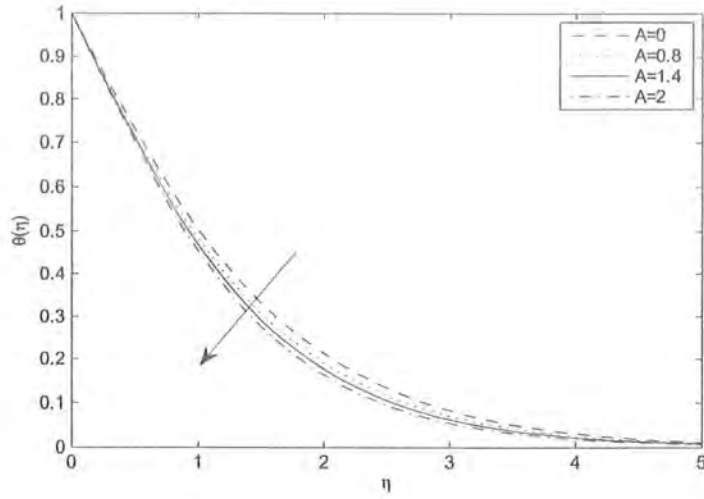
111

**Fig 8.7**: Effect of $A$ on temperature when $\beta = 0.1$, $A = 0.1$, $\epsilon = 0.1$, $\lambda = 0.1$ and $\Pr = 2.0$.
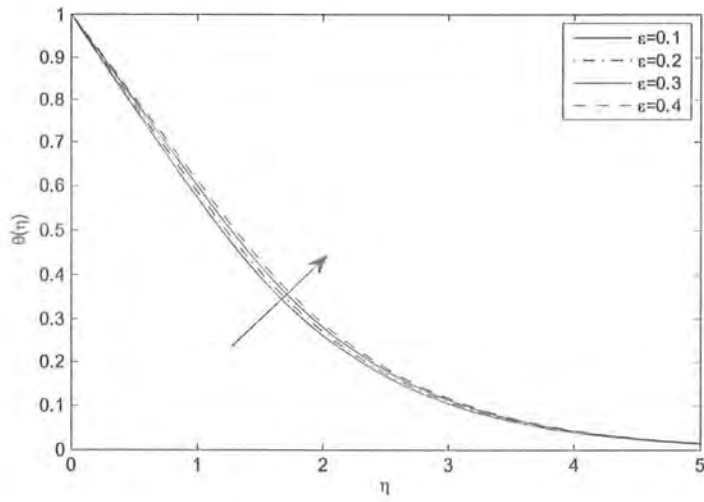


**Fig 8.8**: Effect of $\epsilon$ on temperature when $K = 0.1, \beta = 0.1$, $A = 0.1$, $\epsilon = 0.1, \lambda = 0.1$ and $\Pr = 2.0$.
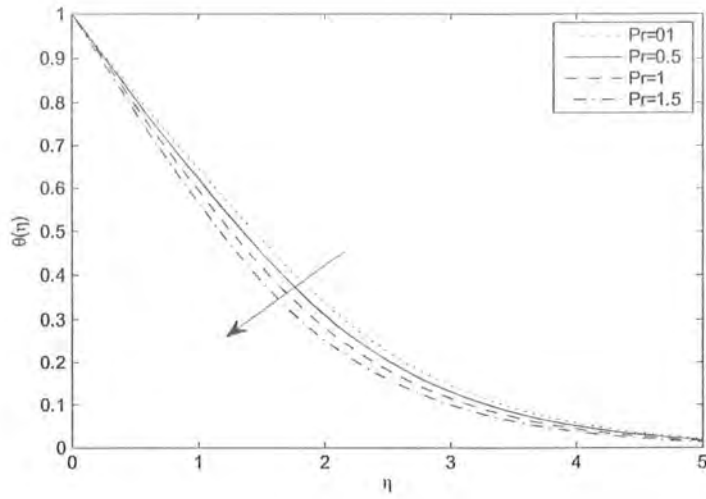
112

**Fig 8.9**: Effect of Pr on temperature when $K = 0.1, \beta = 0.1$, $A = 0.1$, $\epsilon = 0.1, \lambda = 0.1$ and $\epsilon = 2.0$.
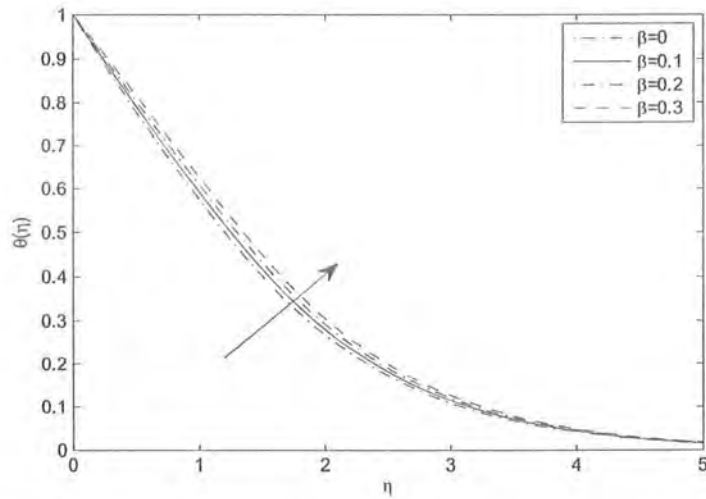


**Fig 8.10**: Effect of $\beta > 0$ on temperature when $K = 0.1, \text{Pr} = 0.1$, $A = 0.1$, $\epsilon = 0.1, \lambda = 0.1$ and $\epsilon = 2.0$.

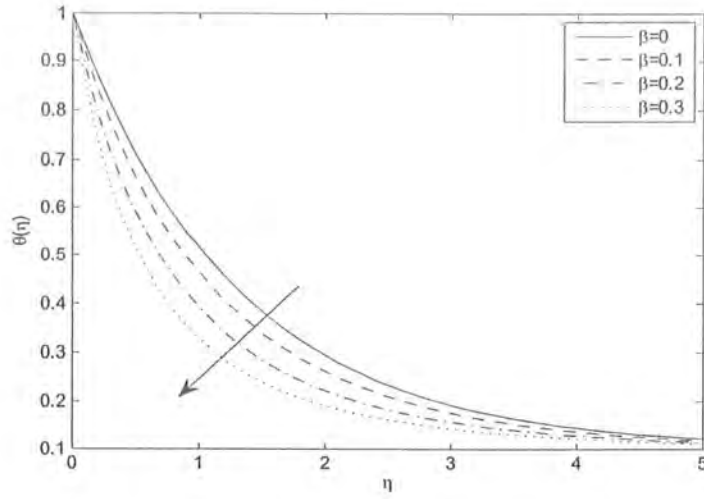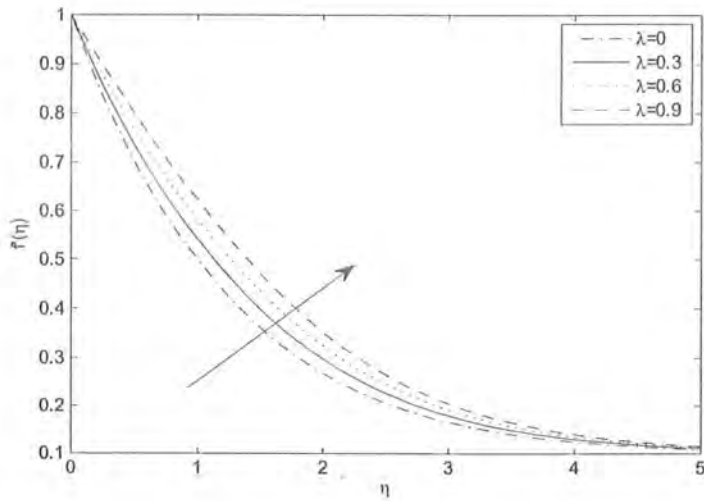**Fig 8.11:** Effect of $\beta < 0$ on temperature when $K = 0.1, \epsilon = 0.1, A = 0.1, \epsilon = 0.1, \lambda = 0.1$ and $\mathrm{Pr} = 2.0$.



**Fig 8.12:** Effect of $\lambda$ on velocity when $\beta = 0.1$, $K = 0.1$, $\epsilon = 0.1$, $A = 0.1$ and $\mathrm{Pr} = 2.0$.

| $\lambda$ | $A$ | $K$ | $-f''(0)$ |
|---|---|---|---|
| 0.1 | 0.1 | 0.1 | 0.6584 |
| 0.5 | | | 0.4953 |
| 1 | | | 0.3165 |
| 0.5 | 0.2 | | 0.4675 |
| | 0.5 | | 0.3082 |
| | 0.7 | | 0.1510 |
| | 0.5 | 0.2 | 0.3137 |
| | | 0.4 | 0.3246 |
| | | 0.6 | 0.3355 |

Table 8.4: The variation of $-f''(0) = \frac{1}{2}C_f\sqrt{\mathrm{Re}_x}$ with respect to $K$, $A$ and $\lambda$ .

| Pr | $\beta$ | $\epsilon$ | $-\theta'(0)$ |
|---|---|---|---|
| 1 | 0.1 | 0.1 | 0.4044 |
| 1.5 | | | 0.5077 |
| 1.7 | | | 0.5444 |
| 1 | 0.2 | | 0.3523 |
| | 0.4 | | 0.2292 |
| | 0.5 | | 0.1539 |
| | 0.1 | 0.2 | 0.3806 |
| | | 0.4 | 0.3425 |
| | | 0.5 | 0.3267 |

Table 8.5: Temperature gradient $-\theta'(0)$ at the cylinder outer surface at different points of $\epsilon$, Pr and $\beta$.

Reading the Table 8.4, we see that $C_f \propto Re_x^{-\frac{1}{2}}$. Thus, as Reynold number increases $|C_f|$ decreases. We know that as $Re_x$ enhanced viscous forces start reducing, in turn $|C_f|$ reduces. Here as we increase the mixed convection parameter $\lambda$, $|C_f\,\mathrm{Re}_x|$ decreases. As we increase the

stretching ratio parameter $A$, $|C_f \operatorname{Re}_x|$ decreases. But in the case of curvature parameter $K$, $|C_f \operatorname{Re}_x|$ increases.

On reading Table 8.5, as $Nu_x^2 \propto Re_x$ so we can say that decrease in viscocity is due to increase in Reynolds number, $Re_x = \frac{Ux}{v}$ , which enhances magnitude of rate of convectional heat transfer in case of stretching cylinder. Also, the coefficient of convectional heat depends on Prandtl number Pr, curvature parameter $K$, thermal variable parameter $\epsilon$ and heat generation/absorption parameter $\beta$. Behavior of the coefficient of convectional heat transfer is studied in Table 8.5, showing that on increasing Prandtl number Pr, $-\theta'(0)$ increases while for increasing thermal variable parameter $\epsilon$ and heat generation/absorption parameter $\beta$, $-\theta'(0)$ decreases.

## 8.7  Concluding remarks

The main observations are:

- It is observed that the thermal slip parameters reduce the velocity distribution.

- Temperature distribution is enhanced by the Brownian motion and thermophoresis.

  Behavior of velocity and temperature fields on varying curvature parameter $K$ is same i.e both velocity and temperature field increases with increasing curvature parameter $K$.

- Temperature field increases for positive $\beta$ and decreases for the negative values of $\beta$.

- Temperature field increases on increasing small parameter $\epsilon$.

- The effects of stretching ratio parameter $A$ upon velocity and temperature fields are opposite.

116

# Bibliography

[1] M. Sajid and T. Hayat, Influence of thermal radiation on the boundary layer flow due to an exponentially stretching sheet, International Communications in Heat and Mass Transfer, $35(2008)347 - 356$

[2] Sohail Nadeem, Rizwan Ul Haq and Noreen Sher Akber, MHD three dimensional boundary layer flow of Casson nanofluid past a linearly stretching sheet with convective boundary condition, Nanotechnology, IEEE Transactions on 13(1)109-115.

[3] M. Naseer, M. Y. Malik, S. Nadeem, The boundary layer flow of hyperbolic tangent fluid over a vertical exponentially stretching cylinder, Alexandria Engg. J. (AEJ), $53(2014)52 - 67.$

[4] S. Nadeem, A.U. Rehman and R. Mehmood, Boundary layer flow of rotating two phase nanofluid over a stretching surface, Alexandria Engineering Journal, $53(2014)747 - 750.$

[5] Sadia Siddiqa, Mixed convection boundary layer flow over a vertical flat plate with radiative heat transfer, Applied Mathematics, $3(2012)705 - 716.$

[6] M. Erfanian Nakhchi, M. R. H. Nobari and H. Basirat Tabrizi, Non-Similarity thermal boundary layer flow over a stretching flat plate, Chinese Physics Letters, $29(2012)357 - 392.$

[7] Dennis P. M. van Gils and Gert-Wim Bruggert, Daniel P. Lathrop, Chao Sun and Detlef Lohse, The Twente turbulent Taylor-Couette ($T^3C$) facility: Strongly turbulent (multiphase) flow between two independently rotating cylinders. Rev. Sci. Inst., $82(2011)517 - 534.$

[8] Avila K. and Hof B., High-precision Taylor-Couette experiment to study subcritical transitions and the role of boundary conditions and size effects, Rev. Sci. Inst., **84**(2013)112−129.

[9] Collins C., Clark M., Cooper C.M., Flanagan K., Khalzov I.V., Nornberg M.D., Seidlitz B., Wallace J. and Forest C.B., Taylor-Couette flow of unmagnetized plasma, Phys. Plasmas, **21**(2014)52 − 67.

[10] Youd A. J., Willis A. P. and Barenghi C. F., Non-reversing modulated Taylor-Couette flows, Fluid Dyn. Res., **36**(2005)61 − 73.

[11] Watanabe T. and Toya Y., Vertical Taylor-Couette flow with free surface at small aspect ratio, Acta Mech., **223**(2012)347 − 353.

[12] Shi L., Rampp M., Hof B. and Avila M., A hybrid MPI-OpenMP parallel implementation for pseudospectral simulations with application to Taylor-Couette flow, Comp. Fluids, **106**(2015)1 − 11.

[13] Pomeau Y., Manneville P., Stability and fluctuations of a spatially periodic convective flow, J. Phys. Paris, **40**(1979)609 − 612.

[14] Kramer L., Ben-Jacob E., Brand H. and Cross M. C, Wavelength selection in systems far from equilibrium, Phys. Rev. Lett., **49**(1982)1891 − 1894.

[15] Riecke H. and Paap H. G., Perfect wave-number selection and drifting patterns in ramped Taylor vortex flow, Phys. Rev. Lett., **59**(1987)2570 − 2573.

[16] Chomaz J. M., Global instabilities in spatially developing flows: Non-normality and nonlinearity, Ann. Rev. Fluid Mech., **37**(2005)357 − 392.

[17] Cannell D.S., Dominguez-Lerma M.A., Ahlers G., Experiments on wave number selection in rotating Couette-Taylor flow, Phys. Rev. Lett., **50**(1983)1365 − 1368.

[18] Dominguez-Lerma M.A., Cannell D.S. and Ahlers G., Eckhaus boundary and wave-number selection in rotating Couette-Taylor flow, Phys. Rev. A, **34**(1986)4956 − 4970.

[19] Ning L., Ahlers G. and Cannell D.S., Wave-number selection and traveling vortex waves in spatially ramped Taylor-Couette flow, Phys. Rev. Lett., **64**(1990)1235 − 1238.

[31] P. D. Ariel, T. Hayat and S. Asghar, Homotopy perturbation method and axisymmetric flow over a stretching sheet, Int. J. Nonlinear Sciences and Numerical Simulation, 7(4)(2006)399 − 406.

[32] T. Hayat, S. A. Shehzad, Ansa Rafique and M. Y. Malik, Mixed convection unsteady stagnation point flow over a stretching sheet with heat transfer in the presence of variable free stream, International Journal for Numerical Methods in Fluids, 68(4)(2012)483 − 493.

[33] M.Y. Malik, Azad Hussain, Sohail Nadeem and Tasawar Hayat, Flow of a third grade fluid between coaxial cylinders with variable viscosity, Zeitschrift für Naturforschung A., 64(2008)588 − 596.

[34] P.S. Gupta and A.S. Gupta, Heat and mass transfer on a stretching sheet with suction or blowing, Can. J. Chem. Eng., 55(1977)744 − 746.

[35] C.K. Chen and M.I. Char, Heat transfer of a continuous stretching surface with suction or blowing, J. Math. Anal. Appl., 135(1988)568 − 580.

[36] P.D. Ariel, Extended homotopy perturbation method and computation of flow past a stretching sheet, Comput. Math. Appl., 58(2009)2402 − 2409.

[37] J. Gary, D.R. Kassoy, H. Tadjeran and A. Zebib, The effects of significant viscosity variation on convective heat transport in water saturated porous medium, J. Fluid Mech., 117(1982)233 − 249.

[38] K.N. Mehta and S. Sood, Transient free convection flow with temperature dependent viscosity in a fluid saturated porous medium, Int. J. Eng. Sci., 30(1992)1083 − 1087.

[39] S. Mukhopadhyay, G.C. Layek and S.A. Samad, Study of MHD boundary layer flow over a heated stretching sheet with variable viscosity, Int. J. Heat Mass Transfer, 48(2005)4460 − 4466.

[40] T.R. Mahapatra and A.G. Gupta, Heat transfer in stagnation point flow towards a stretching sheet, Heat Mass Transfer, 38(2002)517 − 521.

[41] C.Y. Wang, Stagnation point flow towards a shrinking sheet, Int. J. Non-Linear Mech., 43(2008)377 − 382.

[42] K. Vajravelu and J. Nayfeh, Hydromagnetic convection at a cone and a wedge, Int. Commun. Heat Mass Transfer, 19(1992)701 − 710.

[43] E. M. Sparrow and R. D. Cess, Temperature dependent heat sources or sinks in a stagnation point flow, App. Sci, Res., A10(1961)185 − 197.

[44] A. J. Chamkha, Non-darcy hydromagnetic free convection from a cone and a wedge in porous media, Int. Commun. Heat Mass Transfer, 23(1996)875 − 887.

[45] B. C. Sakiadis, Boundary-layer behavior on continuous solid surfaces: I. Boundary-layer equations for two-dimensional and axisymmetric flow, American Institute of Chemical Engineers, 7(1961)26 − 28.

[46] L. J. Crane, Flow past a stretching plate, Z. Angew. Math., 21(1970)645 − 647.

[47] S. Manjunatha, B. J. Gireesha1 and C. S. Bagewadi, Effect of thermal radiation on boundary layer flow and heat transfer of dusty fluid over an unsteady stretching sheet, International Journal of Engineering, Science and Technology, 4(2012)36 − 48 .

[48] B.K. Datta, P. Roy and A.S. Gupta, Temperature field in the flow over a stretching sheet with uniform heat flux, Int. J. Heat and Mass Transfer, 12(1)(1985)89 − 94.

[49] E. M. A. Elbashebeshy, Heat transfer over a stretching surface with variable surface heat flux, Int. J. Appl. Phys, 31(1998)1951 − 1954.

[50] E. M. A. Elbashebeshy and M. A. Bazid, Heat transfer over a unsteady stretching surface, Int. J. Heat and Mass Transfer, 411(2004)1 − 4.

[51] S. S. Wang and I. Choi, Boundary-layer effects in composite laminates free-edge stress solutions and basic characteristics, J. Appl. Mech, 49(1982)549 − 560.

[52] L. J. Grubka and K. M. Bobba, Heat transfer characteristic of a continuous stretching surface with variable temperature, Int. J. Heat Transfer, 107(1985)248 − 250.

[53] I. Pop and T. Y. Na, Unsteady flow past a stretching sheet, Int. J. Acta Mechanica, 4(1996)413 − 422.

[54] L. J. Grubka and K. M. Bobba, Heat transfer characteristic of a continuous stretching surface with variable temperature, Int. J. Heat Transfer, 107(1985)248 − 250.

[55] M. F. EI-Amin, I. Abbas and R. S. R. Gorla, Effect of thermal radiation on a natural convection in a porous medium, Int. J. Fluid Mechanics, 2(2007)129 − 144.

[56] T.C. Chiam, Heat transfer in a fluid with variable thermal conductivity over a linearly stretching sheet, Int. J. Acta Mech., 129(1998)63 − 72.

[57] M. A. Seddeek and F.A. Salama, The effects of temperature dependent viscosity and thermal conductivity on unsteady MHD convective heat transfer past a semi-infinite vertical porous moving plate with variable suction, Int. Comp. Mater, 40(2007)186 − 192.